



**NAM**

# **Induced seismicity in the Groningen field second statistical assessment of tremors along faults in a compacting reservoir**

---

**H.M. Wentinck, Shell Global Solutions International B.V.**

Date May 2016

Editors Jan van Elk & Dirk Doornhof



## General Introduction

This report presents the results of two phenomenological statistical models for the prediction of tremor rates from gas producing reservoirs from trends in the past in regions of several tens of square kilometers. This report is an extension of the study presented in 2015 (Ref. 1).

Focus is on the rate of the earthquakes and inter-event times for several regions of the Groningen field. As such the study complements the studies into the seismological model (Ref. 2 and 3). Seismicity in selected smaller fields in The Netherlands (Annerveen, Eleveld and Emmen) is also analysed in the study.

## References

1. Induced seismicity in the Groningen field - statistical assessment of tremors along faults in a compacting reservoir, Rick Wentinck, July 2015.
2. An activity rate model of induced seismicity within the Groningen Field, (Part 1), Stephen Bourne and Steve Oates, February 2015.
3. An activity rate model of induced seismicity within the Groningen Field, (Part 2), Stephen Bourne and Steve Oates, June 2015.



**NAM**

<b>Title</b>	<b>Induced seismicity in the Groningen field second statistical assessment of tremors along faults in a compacting reservoir</b>		<b>Date</b>	May 2016
			<b>Initiator</b>	NAM
<b>Autor(s)</b>	<b>H.M. Wentinck</b>	<b>Editors</b>	Jan van Elk, Dirk Doornhof	
<b>Organisation</b>	Shell Global Solutions International B.V.	<b>Organisation</b>	NAM	
<b>Place in the Study and Data Acquisition Plan</b>	<p><u>Study Theme:</u> Seismological Model</p> <p><u>Comment:</u>  This report presents the results of two phenomenological statistical models for the prediction of tremor rates from gas producing reservoirs from trends in the past in regions of several tens of square kilometers. This report is an extension of the study presented in 2015 (Ref. 1).</p> <p>Focus is on the rate of the earthquakes and inter-event times for several regions of the Groningen field. As such the study complements the studies into the seismological model (Ref. 2 and 3). Seismicity in selected smaller fields in The Netherlands (Annerveen, Eleveld and Emmen) is also analysed in the study.</p>			
<b>Directly linked research</b>	(1) Seismological Model Groningen (2) Hazard Studies			
<b>Used data</b>	KNMI Earthquake catalogue			
<b>Associated organisation</b>	NAM			
<b>Assurance</b>	Shell Global Solutions International B.V.			

report for NAM 2016

**Induced seismicity in the Groningen field**

**second statistical assessment of tremors along faults in a compacting  
reservoir**

by

**H.M. Wentinck**

Copyright Shell Global Solutions International B.V., Rijswijk International, B.V., 2016.

Neither the whole nor any part of this document may be reproduced, stored in any retrieval system or transmitted in any form or by any means (electronic, mechanical, reprographic, recording or otherwise) without the prior written consent of the copyright owner.

## Executive Summary

This report presents the results of two phenomenological statistical models for the prediction of tremor rates from gas producing reservoirs from trends in the past in regions of several tens of square kilometers. The models assume that tremors are generated along faults when parts of these faults become critically stressed and slip seismically due to reservoir pressure decline and related reservoir compaction.

The models are executed as Monte Carlo simulations where the relative likelihood of a tremor depends on the Weibull distribution function. The two models use two different state variables to normalise the calculated tremor rates to the observed tremor rates. In the first model M1, the state variable is the reservoir pressure reduction rate. In the second model M2, the state variable is the reservoir pressure itself. Both state variables determine the stress changes on the faults.

The seismic moments of the tremors follow from a Pareto distribution function, as is frequently done when modelling natural and manmade induced seismicity. The models ignore a-seismic fault slip.

The modified models have been applied to various regions in the Groningen field and to surrounding gas fields. These are the Annerveen and Eleveld fields south of the Groningen field and two other small gas fields near Emmen and Roswinkel. Like the Annerveen and Eleveld fields, gas production and reservoir pressure drop in the Emmen and Roswinkel fields have been marginal for almost ten years. Modelling these long periods of low pressure drop helps us to evaluate the robustness of these models when they would be applied to various gas production scenarios for the Groningen field.

It could be considered to predict tremor rates in regions of interest using the presented models. Parameters for these regions can be derived from fits to the observed tremor rates in these regions. The models reproduce reasonably well the tremor rates and the distribution of periods between subsequent tremors, i.e. the interevent time distribution, for the regions in the Groningen field, the entire Groningen field and for the Annerveen, Eleveld and Emmen fields. However, the tremor rate in the Roswinkel field cannot be reproduced by these models. In this field, tremors occur in a period in which the reservoir pressure hardly changes.

We have not been successful to reproduce the spatial distribution of the tremors over the Groningen field using the spatial variation in the reservoir compaction. The tremor rate is overpredicted in regions south-west and north-east of Loppersum. Other field or fault properties must contribute to the spatial distribution of the tremors. In this respect, the presented models will not improve the current activity rate model used in the seismological model for the Groningen field and used for the seismic hazard and risk analysis.

# Table of Contents

<b>1</b>	<b>Introduction</b>	<b>4</b>
<b>2</b>	<b>Model</b>	<b>6</b>
2.1	Summary of the original model . . . . .	6
2.2	Normalisation of the tremor rate by a Poisson process . . . . .	9
2.2.1	Original model . . . . .	10
2.2.2	Modified models . . . . .	10
<b>3</b>	<b>Application of the models to the seismic activity in the Groningen field and other fields</b>	<b>13</b>
3.1	Groningen field . . . . .	18
3.2	Other fields . . . . .	25
<b>4</b>	<b>Discussion</b>	<b>31</b>
<b>5</b>	<b>Acknowledgements</b>	<b>33</b>
	<b>APPENDICES</b>	<b>36</b>
<b>A</b>	<b>Additional simulation results</b>	<b>37</b>
A.1	Original model using a better proxy for the reservoir pressure . . . . .	37
A.2	Modified models M1 and M2 . . . . .	43
A.3	Modified model M2 applied to the entire Groningen field . . . . .	52
A.4	Fit function for $c_{PS}$ . . . . .	57
A.5	Additional simulations for the Roswinkel field . . . . .	60
<b>B</b>	<b>Reservoir pressure interval and time step</b>	<b>63</b>
<b>C</b>	<b>Field data</b>	<b>66</b>
C.1	Detailed maps . . . . .	66
C.2	Cumulative fault slip area of the observed tremors . . . . .	80

<b>D Reservoir pressures, gas production and tremors</b>	<b>85</b>
D.1 Reservoir pressure . . . . .	85
D.2 Gas production and tremors . . . . .	93
<b>E Tremor data</b>	<b>96</b>

Table 0.1 : List of frequently used symbols

Symbol .....	Property .....	Unit .....
$b$	b-value of the Gutenberg-Richter frequency-magnitude law	-
$c_{M_0}$	geometric constant relating seismic moment to stress reduction	Pa/J
$c_{\sigma_v}$	geometric constant relating vertical stress to mean shear stress	Pa
$C_m$	uniaxial compaction coefficient	Pa <sup>-1</sup>
$D$	seismic slip length or relative displacement in fault plane	m
$IT$	interevent time	s
$k_W$	shape parameter of Weibull distribution	-
$n_{step}$	number of steps taken in simulation	-
$L$	length of fault along strike or length of slip plane	m
$M_0$	seismic moment	J
$M$	seismic moment magnitude	Richter
$M_L$	local magnitude	Richter
$M_{llm}$	lower limiting seismic moment magnitude	Richter
$n$	integer to identify loading step	-
$N$	total number of tremors observed or modelled	-
$p$	fluid pressure in reservoir	Pa
$R$	radius of the area or seismic slip plane	m
$S$	slip area	m <sup>2</sup>
$t$	time	s
$t_{step}$	time steps taken in simulation	s
$W$	width of slip plane	m
$x$	value of stochastic variable $X$	-
$x$	location in the field in terms of coordinates	m
$X$	stochastic variable	-
$X_{cen}, Y_{cen}$	easting and northing coordinates of the centre of the selected region	m
$X, Y$	easting and northing coordinates	m

Table 0.2 : List of frequently used symbols, continued

Symbol	Property	Unit
.....	.....	.....
$\alpha$	Biot constant	-
$\beta$	shape parameter of the Pareto distribution	-
$\delta$	dip angle of fault	degree
$\delta p_{int}$	pressure interval used for modified model M2	Pa
$\delta p_{fail}$	typical change in reservoir pressure for seismic fault failure	Pa
$\eta$	failure criterion variable	-
$\lambda$	shape parameter of probability distribution functions	-
$\lambda_{PS}$	shape parameter of the Poisson probability distribution function	-
$\mu$	shear modulus or Lamé constant	Pa
$\nu$	Poisson ratio	-
$\sigma_h, \sigma_H$	minimum and maximum horizontal field stresses	Pa
$\sigma_n$	normal stress on fault plane	Pa
$\sigma_v$	vertical field stress	Pa
$\tau$	shear stress on a fault plane	Pa
$\tau_{fail}$	typical mean shear stress on faults for seismic fault failure	Pa
$\delta$	difference	
$\sim$	about, roughly	
$\approx$	approximately	
$\propto$	proportional to	

Table 0.3 : List of frequently used symbols, continued

Symbol	Refers to
.....	
subscripts	
area	selected region or area
cen	centre of selected area or region
cum	cumulative
n	time step $n$
v	vertical field stress
fail	rock failure leading to a tremor
min	minimum value
max	maximum value
obs	observed value
P	Pareto probability distribution function
PS	Poisson probability distribution function
res	reservoir
W	Weibull probability distribution function
x, y, z	rectangular coordinate component in x, y and z direction
abbreviations	
cdf	cumulative distribution function
CBS	Centraal Bureau voor Statistiek
KNMI	Koninklijk Nederlands Meteorologisch Instituut
NAM	Nederlandse Aardolie Maatschappij
PSHA	Probabilistic Seismic Hazard Analysis
pdf	probability distribution or density function

# Chapter 1

## Introduction

In Wentinck (2015), we have presented a statistical model to reproduce the observed tremor rates and tremor magnitudes in the Groningen field and in the smaller Annerveen and Eleveld gas fields south of the Groningen field. This phenomenological model assumes that the tremors originate from fault failure, likely at reservoir offsets. When the gas pressure in the reservoir declines during gas production, the reservoir rock surrounding the fault compacts and the shear stress on the fault increases.

The relative likelihood for a tremor follows from the Weibull probability distribution function. According to this distribution function, the tremor rate quickly increases when the mean stress condition on the faults approaches a critical value. The model ignores a-seismic fault slip. The Pareto probability distribution function is used to determine the so-called frequency seismic moment distribution of the tremors<sup>1</sup>.

The model reasonably performed using a simple linear reservoir pressure proxy. However, it was not applied using a realistic proxy for the reservoir pressure. Further, it could well be that other models are better to reproduce the observed reduction in tremor rates over long periods as in the smaller Annerveen and Eleveld fields.

In this report, we show that the original model performs better if we use a more realistic reservoir pressure proxy. To reproduce the observed reduction in tremor rates over long periods, we have improved this model by the following modifications

- in modified model M1, the Poisson shape parameter  $\lambda_{PS}$  is proportional to the rate of change in the reservoir pressure.
- in modified model M2, the evaluation of the relative likelihood of tremors is done for fixed reservoir pressure intervals.

The models have been applied to the same regions and fields as in Wentinck (2015). Also, they have been applied to two other regions in the Groningen field, one around Meed-

---

<sup>1</sup>Note that the Pareto distribution pertains to the seismic moment itself and not the moment magnitude. The frequency versus moment magnitude relation, or the Gutenberg-Richter frequency-magnitude relation, is exponential.

huizen and the other around Hellum and to two other small gas fields, one near Emmen and the other near Roswinkel. As for the Annerveen and Eleveld fields, the reservoir pressure decline in the Emmen and Roswinkel fields has been marginal over a period of about 10 years<sup>2</sup>.

Further, we have investigated whether these modified models can reproduce the observed interevent time distribution, i.e. the distribution of periods between subsequent tremors. To highlight the difference between the original model and the two modified models M1 and M2, we neglect that tremors can reduce the mean stress on the faults in contrast with what we have done in the aforementioned reference.

The modified models are explained in Chapter 2. The results of the modified models are presented in Chapter 3. In Chapter 4, we discuss the main results.

---

<sup>2</sup>In the period between 1995 and 2007, the Roswinkel field shows a stable pressure level or even a small increase while gas was produced. The gas production in the Roswinkel field has been stopped in 2007.

# Chapter 2

## Model

### 2.1 Summary of the original model

For convenience, we repeat the main assumptions and equations of the original model from Wentinck (2015), Chapter 2. We assume

- Regions in the Groningen gas field of 10 - 70 square kilometres contain a considerable number of faults or fault segments<sup>1</sup>. These fault segments have different orientations, dips and throws (or reservoir offsets). They are loaded by field stresses and by reservoir compaction induced stress changes. The latter are driven by a change in the reservoir pressure. The change in the reservoir pressure is supposed to be uniform in the region of interest.
- In relation to the generation of tremors, the rock behaves as a pure ‘elastic-brittle’ medium. Relaxation of stress by a-seismic plastic deformation along the fault segments is ignored. Also, stress relaxations following from salt creep in the overlying Zechstein formation are ignored.
- Changes in the mean stress on the fault segments are driven by changes in the reservoir pressure and by energy released by the tremors. The latter is proportional to the total seismic moment of the tremors in the region of interest.
- The relative likelihood of seismic failure along a fault or a tremor is given by a Weibull probability distribution function. This phenomenological probability distribution function has been found to be useful to describe rock failure. The related state variable is the change in the mean stress on the fault segments which linearly depends on a change in the reservoir pressure.
- The fault segments respond independently to the mean stress change. There is no triggering of tremors by preceding tremors.

---

<sup>1</sup>A fault segment is bounded by a significant local change in fault azimuth angle.

- The relation between the frequency and the seismic moment of the tremors follows from a Pareto probability distribution function. The Pareto distribution shape parameter  $\beta$  is matched to the b-value of the observed exponential frequency-magnitude relationship using  $\beta = 2/3b$ .

Discretising the time  $t$  in small equal time steps  $\delta t$ , the uniaxial effective vertical stress  $\sigma'_v$  in the reservoir away from faults changes during a time step  $n$  as

$$\delta\sigma'_{v,n} = -\alpha\delta p_n. \quad (2.1)$$

$\delta p_n = p(t_n) - p(t_{n-1})$  [Pa] is a change in the reservoir pressure during time step  $n$ .  $\alpha$  [-] is the Biot constant of the reservoir rock. The mean shear stress on faults in the region of interest  $\bar{\tau}$  changes during time step  $n$  as<sup>2</sup>

$$\delta\bar{\tau}_n = c_{\sigma_v}\delta\sigma'_{v,n} - \delta\bar{\tau}_{rup,n}. \quad (2.2)$$

$c_{\sigma_v}$  [-] is a geometrical constant of order 1 which relates the effective vertical stress away from the faults to the mean shear stress on the faults. It depends on geometrical factors, such as the fault throw and fault dip. The last term in Eq. (2.2) accounts for the mean shear stress reduction in the region due to tremors during time step  $n$ .  $\delta\bar{\tau}_{rup,n}$  is proportional to the total seismic moment released by the tremors during this time step,

$$\delta\bar{\tau}_{rup,n} = c_{M_0} \sum_{i=1}^{N(n)} M_{0,i}. \quad (2.3)$$

The summation is over the  $N(n)$  tremors during time step  $n$ .  $M_{0,i}$  [J] is the seismic moment of tremor  $i$ .  $c_{M_0}$  [Pa/J] is a poorly constrained constant which relates a reduction in the mean shear stress on the faults to the released energy by the tremors. An extensive explanation about the values taken for this constant is given in the aforementioned reference<sup>3</sup>. After time step  $n$ , the mean shear stress on the faults is given by

$$\bar{\tau}_n = \bar{\tau}_0 + c_{\sigma_v}\sigma'_{v,n} - \bar{\tau}_{rup,n}. \quad (2.4)$$

$\bar{\tau}_0$  [Pa] is the mean initial shear stress on the faults before gas production and reservoir compaction and which is usually unknown.  $\sigma'_{v,n} = -\alpha(p_n - p_0)$  is the effective uniaxial

---

<sup>2</sup>In the reservoir at a reservoir offset, the shear stress varies strongly along the fault and even changes sign. For this reason we regard the mean of the absolute shear stress as a measure of the stress state of the fault instead of the mean of the shear stress. To simplify notations, we omit the  $||$  symbol to denote the absolute value of a property where it does not lead to confusion. When determining the mean value, we consider in the region of interest the surface  $S$  of all faults with at least on one side reservoir rock. The mean value of a property  $x$ ,  $\bar{x}$  is calculated from integrating  $x$  over  $S$  and dividing this value by the area of  $S$ .

<sup>3</sup>A theoretical underlimit for the constant is  $c_{M_0} = 1/V$  [Pa/J] where  $V$  [m<sup>3</sup>] is the volume of the reservoir in the region of interest.

vertical stress change due to the reduction of the reservoir pressure from  $p_0$  to  $p_n$ .  $\bar{\tau}_{rup,n}$  is the mean stress reduction due to tremors up to time step  $n$ , i.e.

$$\bar{\tau}_{rup,n} = c_{M_0} \sum_{i=1}^{N_n} M_{0,i}. \quad (2.5)$$

$N_n$  is the total number of tremors in the region up to time step  $n$ .

We assume that the relative likelihood of a tremor can be described by a Weibull probability distribution function. In this case the relative likelihood of a tremor depends on the following evaluation<sup>4</sup>,

$$X > 1 - \exp(-\eta^{k_W}). \quad (2.6)$$

The dimensionless variable  $\eta$  [-] is a loading parameter leading to rock failure and a tremor. It is also called a failure criterion variable.  $k_W$  [-] is the Weibull distribution shape parameter. The value of the stochastic variable  $X$  follows from a random sample taken from a uniform probability distribution in the interval [0,1] at each time step  $n$ . A tremor occurs if  $X$  is larger than the value of the expression on the right hand side of Eq. (2.6).  $\eta$  is at timestep  $n$

$$\eta_n = \frac{\bar{\tau}_n - \bar{\tau}_0}{\tau_{fail}}. \quad (2.7)$$

$\tau_{fail}$  [Pa] is called the typical stress for seismic failure. This fit constant must be derived from the observed tremors. Herewith, the variable  $\eta$  concerns only a change in the conditions, as is usually done when using the Weibull distribution function to determine the relative likelihood of failure. If stress reduction by tremors can be neglected, we could use equally well  $\eta_n = (p_n - p_0)/\delta p_{fail}$  where  $\delta p_{fail} = \tau_{fail}/(\alpha c_{\sigma_v})$  [Pa] is a typical change in the reservoir pressure for seismic failure.

The model generates the number of observed tremors in the region of interest by multiplying the relative likelihood of a tremor with a probability following from the Poisson probability distribution function, see below<sup>5</sup>. We use the Pareto probability distribution function to generate the seismic moments  $M_0$  [J] of the tremors and the related tremor magnitudes  $M$  [-]<sup>6</sup>. The b-value of the model is fitted to the observed data.

<sup>4</sup>One can also call and use this distribution function directly in Python and other software for statistical analysis.

<sup>5</sup>On forehand, one could also multiply the relative likelihood of a tremor with a constant factor to obtain the number of tremors in the region of interest. For the tremors in the Groningen field, this multiplication leads to a curve which quite well follows the observed number of tremors as a function of time. However, this multiplication cannot reproduce the histograms of the observed interevent times of the tremors. For small state intervals, multiplying the relative likelihood with the probability following from a uniform distribution or a Poisson distribution leads to a more ‘realistic’ histogram for the interevent times. This holds for the original and for the two modified models.

<sup>6</sup>We use  $M = (2/3) \log_{10} M_0 - 6.1$ , see for example Udias et al. (2014), §1.4 or Scholz (2002), §4.3.

## 2.2 Normalisation of the tremor rate by a Poisson process

The Poisson probability distribution is usually applied to stochastic variables which count the number of events in a certain time period, distance, area or volume. Examples are related to radioactive decay, the number of cars which pass a cross road, the number of typing errors in a page, the amount of telephone calls in a day, the number of dead animals on a road and the number of WEB server calls per day. The Poisson distribution is also used to explain the time sequence of earthquakes or tremors when a fault fails under a constant loading rate generated by far field tectonic motions. According to the Poisson distribution, the probability that exactly  $n$  events take place, where  $n$  is an integer  $(0,1,2,\dots)$ , is given by

$$P(X = n; \lambda_{PS}) = \frac{\lambda_{PS}^n}{n!} \exp(-\lambda_{PS}). \quad (2.1)$$

$X$  is the stochastic variable counting the number of events and  $\lambda_{PS}$  is a shape parameter with a value related to the subject to be analysed. The expected number of events in that same interval is where the probability has a maximum, i.e. where  $dP/dn = 0$ . At this maximum, also the logarithm of  $P$ ,  $\log P$  has a maximum. Using Stirling's approximation, for large  $n$ ,  $d \log P/dn \approx n \log \lambda_{PS} - n \log n$  and the expected value of  $n$  in the selected interval is equal to  $\lambda_{PS}$ .

For a steady process under constant conditions, the expected value of  $n$  (and herewith the Poisson distribution shape parameter  $\lambda_{PS}$ ) is proportional to the size or length of the interval selected.

For small intervals with a low probability for the occurrence of an event, the Poisson distribution shape parameter  $\lambda \ll 1$ , according to Eq. (2.1). In this case, only the first few terms of  $P(X = n; \lambda)$  in Eq. (2.1) do matter. They are

$$P(X = 0; \lambda) = \exp(-\lambda), \quad P(X = 1; \lambda) = \lambda \exp(-\lambda) \quad \text{and} \\ P(X = 2; \lambda) = \frac{\lambda^2}{2} \exp(-\lambda) \dots \quad (2.2)$$

Taking only the first two terms and using that for  $\lambda \ll 1$ ,  $\exp(-\lambda) \approx 1 - \lambda$ , we have in good approximation

$$P(X = 0; \lambda) \approx 1 - \lambda \quad \text{and} \quad P(X = 1; \lambda) \approx \lambda(1 - \lambda) \approx \lambda. \quad (2.3)$$

In this case, event rates are similar whether a sample is taken from the Poisson distribution function or from a uniform distribution function. The use of the latter can be compared with throwing a dice each time step and where throwing of e.g. number six leads to a failure.

### 2.2.1 Original model

We assume that the Poisson probability distribution function describes the number of events  $n$  in a time interval  $(0, t)$ , i.e.

$$P(X = n; \lambda_{PS}, t) = \frac{(\lambda_{PS}t)^n}{n!} \exp(-\lambda_{PS}t). \quad (2.4)$$

The Poisson distribution shape parameter  $\lambda_{PS}$  [1/s] refers now to a probability per unit time. Where conditions slowly vary over time, this expression is frequently generalised by letting  $\lambda_{PS} = \lambda_{PS}(t)$  be a function of time. Calling the stochastic variable  $X$  a ‘failure’, seismic event or tremor, the related time-to-failure follows or interevent time from inserting  $n = 1$  into Eq. (2.4). For  $t \geq 0$ ,

$$P(X = 1; \lambda_{PS}, t) = f_{PS}(x; \lambda_{PS}, t) = \lambda_{PS}t \exp(-\lambda_{PS}t). \quad (2.5)$$

Herewith, the probability for a tremor in a small time interval  $\delta t$  is approximately  $P(X = 1; \lambda_{PS}; t, t + \delta t) \approx \lambda_{PS}\delta t$ . Multiplying this with the relative likelihood for a tremor due to fault failure<sup>7</sup>

$$P_{X=1; \lambda_{PS}, \delta t} \approx (\lambda_{PS}\delta t) \times (1 - \exp(-\eta^{kw})). \quad (2.6)$$

The second term depends on the state variable  $\eta$ . Disregarding stress relaxation by tremors,  $\eta$  is proportional to the change in the reservoir pressure and herewith to the reservoir compaction  $c$ . The Poisson distribution shape parameter  $\lambda_{PS}$  is now a normalisation constant to match the number of modelled tremors to the number of observed tremors.

The result leads in a certain range of reservoir pressures to a steep increase in the probability of tremors when the reservoir pressure reduces at a constant rate. The latter condition is a reasonable proxy for the Groningen field.

Another essential feature of the original model is that when gas production stops the tremor rate only reduces by stress relaxation caused by the tremors itself according to Eq. (2.4). For the Groningen field, the reduction of the tremor rate by a relaxation of the mean stress can hardly be confirmed because the field has been produced at an almost constant reservoir pressure reduction rate, see also Wentinck (2015).

### 2.2.2 Modified models

Equivalent to the Poisson distribution shape parameter, Bourne and Oates (2014) use the conditional intensity or intensity function  $\lambda$ . This function depends on the reservoir

<sup>7</sup>Alternatively, the relative likelihood for a tremor is incorporated in the expression for  $\lambda_{PS}$ , i.e.  $\lambda_{PS} = \lambda_{PS}(1 - \exp(-\eta^{kw}))$  where  $\lambda_{PS}$  is now a normalisation constant and the time dependence is in the variable  $\eta = \eta(t)$ . In this case, we obtain the same expression for  $P(X = 1; \lambda_{PS}; t, t + \delta t)$  for small time intervals, i.e.

$$P(X = 1; \lambda_{PS}, \delta t) \approx \lambda_{PS}(1 - \exp(-\eta^{kw}))\delta t.$$

compaction, the reservoir compaction rate and a term from Ogata's aftershock model. Disregarding here the aftershock model term,  $\lambda$  is according to these authors<sup>8</sup>

$$\lambda = \beta_0 \dot{c}(1 + \beta_1 c) \exp(\beta_1 c). \quad (2.7)$$

$\beta_0$  [s/m] and  $\beta_1$  [1/m] are constants,  $c = c(t)$  [m] is the reservoir compaction and  $\dot{c} = \partial c(t)/\partial t$  [m/s] is the reservoir compaction rate. Since the compaction rate in the Groningen field has been approximately constant over the period of interest, the function  $\lambda$  can be approximated by

$$\lambda \approx \beta_2(1 + \beta_1 c) \exp(\beta_1 c), \quad (2.8)$$

where  $\beta_2$  [1/m] is a constant. For a small time interval  $\delta t$ , the tremor probability is approximately

$$P(X = 1, \delta t) = \lambda \delta t \approx \beta_2(1 + \beta_1 c) \exp(\beta_1 c) \delta t. \quad (2.9)$$

Comparing this expression with Eq. (2.6), we see that  $\lambda$  has been replaced in the original model by the Weibull probability distribution function for fault failure.

Extending this analogy, the first modified model M1 has a Poisson shape factor  $\lambda_{PS}$  which depends on the reservoir pressure reduction rate  $\dot{p}$ . The most simple function is

$$\lambda_{PS} = c_{PS}(x) \dot{p}. \quad (2.10)$$

Model M1 gives no tremors when there is no reservoir pressure reduction.  $c_{PS}(x)$  [Pa<sup>-1</sup>] is a fit function which may vary over the Groningen field or location  $x$ <sup>9</sup>. This spatial fit function can include the relation between compaction rate  $\dot{c}$  and reservoir pressure reduction rate  $\dot{p}$  but also other field attributes may play a role, such as fault density and fault properties. Indications for other factors are discussed in Appendix A, §A.4. In the following, we assume that  $c_{PS}$  is a local fit constant for the relatively small regions of interest.

The second modified model M2 follows from a Weibull probability distribution function which is based on equal stress intervals instead of equal time intervals. This transformation is illustrated in Figure 2.1. The probability for a tremor in a certain stress interval follows from multiplying the relative likelihood of a tremor in this stress interval with a probability following from the Poisson probability distribution function. Again, the

---

<sup>8</sup>The authors assume that the expected number of tremors  $\Lambda$  is given by  $\Lambda = Ac\beta_0 \exp(\beta_1 c)$  where  $A$  [m<sup>2</sup>] is the area of the reservoir,  $c$  [m] is the compaction of the reservoir and  $\beta_0$  [1/m<sup>3</sup>] and  $\beta_1$  [1/m] are fit constants.

Disregarding spatial variability, if  $c = c(t)$  [m] is a function of time,  $\Lambda$  is a function of time and  $\Lambda(t) = Ac(t)\beta_0 \exp(\beta_1 c(t))$  is the expected number of tremors in the time period  $(0, t)$ . Assuming that the tremors are distributed over this period according to a weighted Poisson distribution, the Poisson intensity function follows from  $\lambda(t) = d\Lambda(t)/dt$  [1/s] and is given by Eq. (2.7).

For a small time interval  $(t, t + \delta t)$ , the expected number of tremors in this time interval is given by  $\Lambda(t, t + \delta t) = \lambda(t)\delta t$ . If  $\lambda(t)$  or  $c(t)$  is practically constant in this time interval, the expected number of tremors is proportional to  $\delta t$ .

<sup>9</sup>If there would be evidence for a delay in the response of the pressure effect, the function could for example be replaced by a convolution integral over time function to include this effect.

Poisson probability distribution function matches the number of modelled tremors to the observed number and contributes to the stochastic nature of the tremor rate and the interevent times.

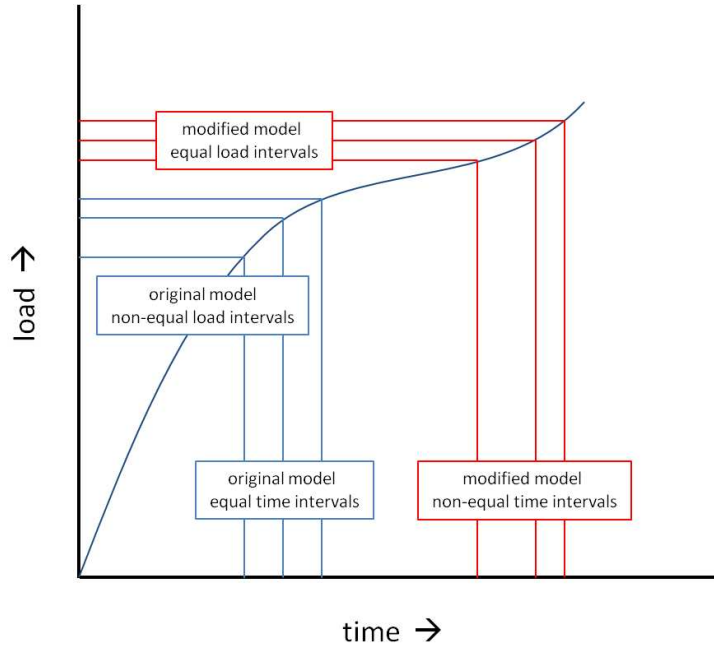


Figure 2.1 : The use of a modified state parameter for the relative likelihood of fault failure in modified model M2. The curve shows a load increasing with time. Selecting equal time intervals for the evaluation of the Poisson process, the load or stress intervals vary with the load function (blue lines). When the load curve flattens more evaluations per unit load or stress interval take place.

Selecting equal load or stress intervals for the evaluation of the Poisson process, the time interval per evaluation varies (red lines). In modified model M2, we use fixed load intervals to evaluate the probability of fault failure or a tremor.

Under a constant loading rate, the time and stress state are equivalent and this transformation is irrelevant<sup>10</sup>. However, under a non-constant loading rate, this transformation will make a difference. For example, the probability for a tremor will not increase with time in a period where the stress state does not change.

The stress interval chosen, or actually the reservoir pressure drop interval,  $\delta p_{int}$  should be small enough to allow for a gradual increase of the relative likelihood of a tremor according to the Weibull probability distribution function in subsequent intervals. In this case, the probability for the occurrence of a tremor is proportional to the size of the interval.

<sup>10</sup>This transformation would also be valid when the Weibull probability distribution function is used to model quasi-periodicity of natural earthquakes.

# Chapter 3

## Application of the models to the seismic activity in the Groningen field and other fields

In this chapter, we show the results of the modified models M1 and M2 using improved reservoir pressure proxy's. To highlight the importance of the tremor number normalisation methods, we exclude in these models the reduction of the mean stress on the faults by the tremors.

The number of simulations used to fit the model with the observed data is 20 although already 5 - 10 simulations are sufficient to make good fits to the observed data. From these simulations, we calculate the mean number of tremors as a function of time and the standard deviation and the interevent time distribution.

The Gutenberg-Richter b-values of the frequency-magnitude distribution of the tremors in the regions of interest are the same as those derived from the observed tremors in these regions<sup>1</sup>.

The models have been applied to analyse the tremors in the entire Groningen field, regions in this field and in the Annerveen, Eleveld, Emmen and Roswinkel fields. In all gas fields, no earthquakes have been recorded before gas production and it is accepted

---

<sup>1</sup>Using the same procedure as in Wentinck (2015), the values are obtained using the *curve\_fit* routine of Python which is based on the least square error method applied to the frequency lower limit magnitude relation. Note that they vary over the Groningen field and over the other fields.

The b-value is assumed to be constant during the whole period of gas production and reservoir compaction. We disregard a possible decrease of the b-value over time because a possible trend is hard to derive from the relative small number of tremors. According to Harris (2015), there is no statistical evidence for changing b-values over time, so far. On the other hand, there is no fundamental reason to expect a constant b-value for systems which deform non-steadily, such as a compacting reservoir. Since the modified models use the same expressions for the frequency-magnitude distribution and the same b-values as the original model, we don't present the modelled frequency-magnitude distributions in separate figures in this report.

that the tremors are due to gas production. As for the Annerveen and Eleveld fields, the reservoir pressure decline in the Emmen and Roswinkel fields was insignificant over a period of about 10 years. Fault data and tremor data for the Groningen field and other fields are given in Appendices C and E.

The reservoir pressure data used is explained in Appendix D. For the Groningen field, we use a realistic proxy for the reservoir pressure (at least until now) which follows from a reservoir simulation by NAM for a 33 Bcm/year scenario. Because of good pressure communication in the field and the gas production policy in the past years, the pressure drop has been practically uniform over a large part of the field and over an extended period of time. The 33 Bcm/year scenario reservoir pressure proxy includes the coming years. For the other fields we have constructed reservoir pressure curves from reservoir pressure data given by NAM.

As in the aforementioned report, the radius of the area of the regions,  $R_{area}$  is 5 km. The lower limit of the magnitude of the catalogue used is either  $M_{min} = 1$  or  $M_{min} = 1.5$ . Note that not all tremors of magnitudes below  $M = 1.5$  have been measured by at least three seismometers in the Groningen field because of seismic noise that varies over the seasons in the year. Further, possible aftershocks have not been eliminated.

The results are presented in the following sections. They show the observed and modelled number of tremors and the histograms of the interevent times of the tremors for the regions of interest. In general, the number of tremors follow trendlines as shown in Figure 3.1. There are small but significant ‘bumps’ in the number of tremors over time in the regions around Meedhuizen en Woudsbloem. These bumps occur at the onset of the occurrence of tremors and are followed by a relatively quiet period before the number of tremors strongly increases. They may be a natural consequence of a single realisation of a stochastic process or due to

- The installation of the network of geophones by KNMI in the Groningen field in 1995. Small tremors prior to this installation may have been undetected.
- Substantial local and temporal changes in the gas production.
- Different types of fault segments which respond differently on the increasing load from reservoir compaction.

So far, we have not found another correlation between changes in the gas production and changes in the tremor rate in a certain region other than one which follows from the relation between gas production and reservoir pressure. Further, more or less prominent deviations in the tremor rate from a smooth curve are hardly reflected in irregularities in the cumulative production, see Appendix D, §D.2.

Also, we have not found a significant trend over time in the properties of fault segments which are closest to the hypocentres of the tremors. From 1995 to 2015, values for the fault dip and fault throw scatter over the complete range of possible values without a

trend developing over time. For the Groningen field, we show this data in Appendix A, §A.3, Figure A.13 . Similar figures hold for the regions of interest.

Summarising, we have no explanation for irregularities in the tremor rates other than that it could be caused by the installation of the geophone network or that it is a natural consequence of a single realisation of a stochastic process in a relatively small region.

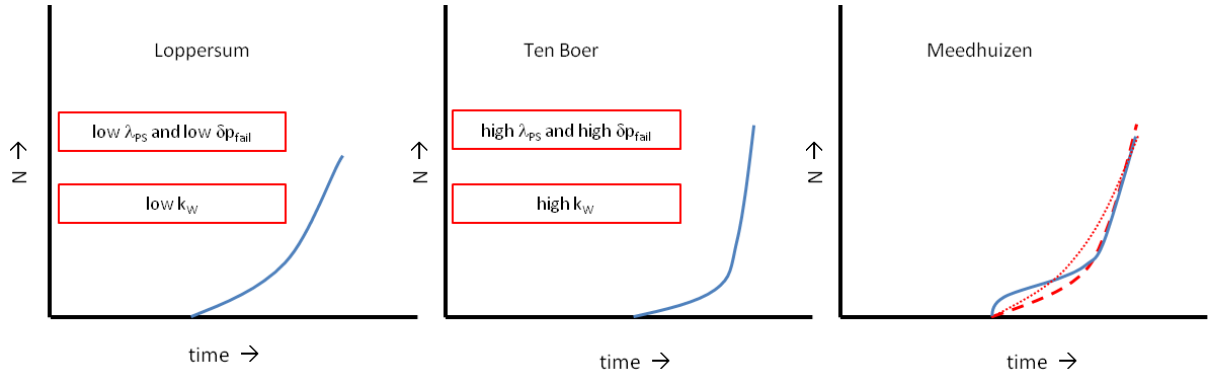


Figure 3.1 : Typical trends for the number of tremors as a function of time. The trends in the left and centre figures follow from models M1 and M2 when adjusting the fit parameters as indicated in the figures. For model M1, the parameter  $c_{PS}$  is adjusted in a similar direction as parameter  $\lambda_{PS}$ .

The trendlines in the right figure reproduce the tremor rate in the regions around Meedhuizen and Woudsbloem. It cannot be fitted well with these models using the improved reservoir pressure proxy for the Groningen field. Either, the fit disregards the bump of tremors in the period before the steep final rise (dashed red line) of the tremor rate or underestimates the number of tremors at the onset and overestimates the number of tremors just before the steep rise in the tremor rate (dotted red line).

Table 3.1 shows the coordinates of the centres of the regions of interest. Figure 3.2 shows the tremors and identified faults in and around the Groningen field and the tremors in the other gas fields of interest. Figures in Appendices C and D show also the location of the well clusters in the Groningen field and detailed maps for the regions of interest. The regions are the same as in Wentinck (2015) but include also the regions around Meedhuizen and Hellum in the Groningen field and the Emmen and Roswinkel fields.

Table 3.1 : Names and coordinates of the centres of the regions of interest and the names of a few nearby villages. The coordinates are based on the Dutch Rijksdriehoeksstelsel.

Field	Name region	Nearby Villages	$X_{cen}$ km	$Y_{cen}$ km
.....	.....	.....	.....	.....
Groningen	Loppersum	Loppersum	244	598
	Ten Boer	Garrelsweer Overschild Steendam	250	591
	Meedhuizen	Meedhuizen	257	590
	Lageland	Lageland	242	585
	Woudsbloem	Woudsbloem Hogezand Froombosch	248	578
	Hellum	Hellum	252	586
	Scheemda	Scheemda	258	577
	Usquert	Usquert	236	603
Annerveen	Annerveen	Annen	244	566
Eleveld	Eleveld	Eleveld	235	553
Emmen	Emmen	Emmen	257	532
Roswinkel	Roswinkel	Roswinkel	267	540

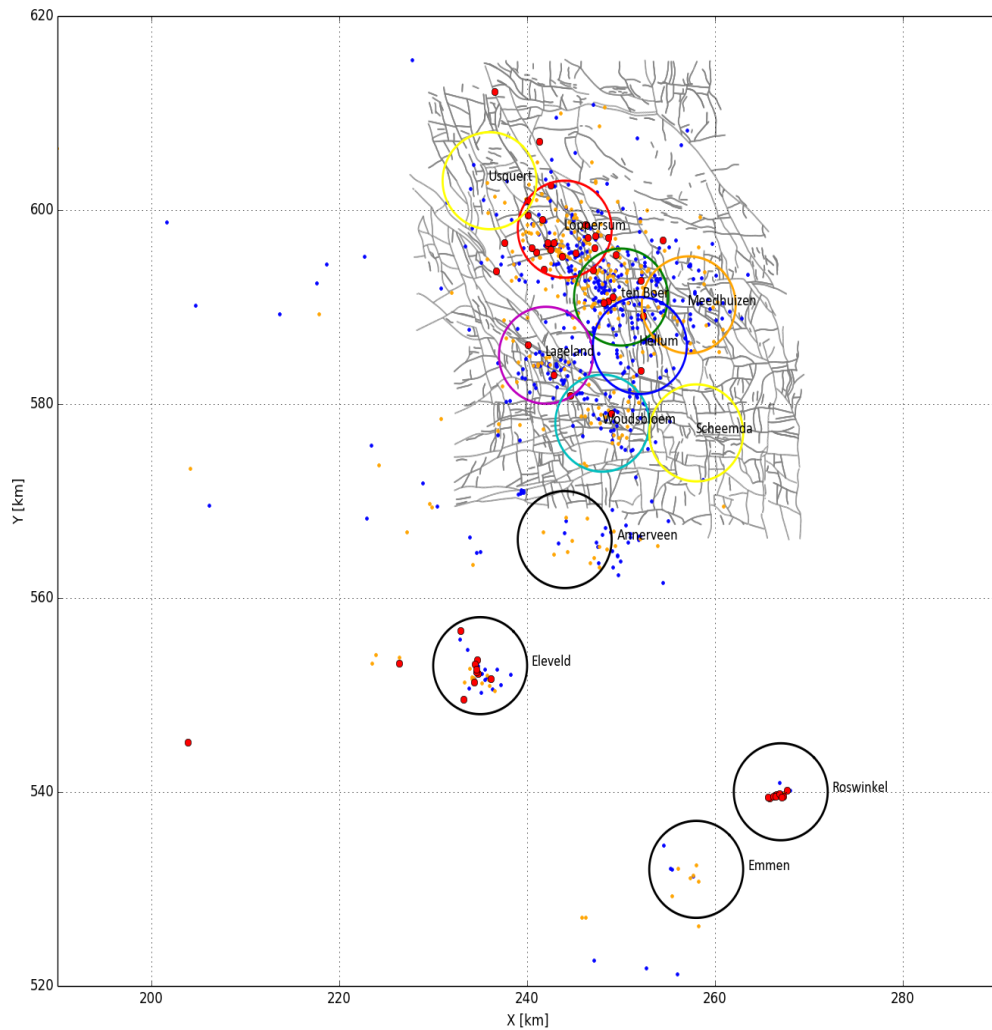


Figure 3.2 : Overview of faults and tremor hypocentres in the Groningen field and in the other gas fields according to KNMI and NAM data. The grey lines show the faults. The regions of interest are shown by circles of 5 km radius. In the Groningen field, they are around Loppersum (red), Ten Boer (green), Lageland (magenta), Woudsbloem (cyan), Meedhuizen (orange) and Hellum (blue). The regions around Scheemda and Usquert (yellow circles) with almost no tremors, and also shown in Wentinck (2015), have been added for convenience. The regions in the Annerveen, Eleveld, Emmen and Roswinkel fields are shown by black circles.

The hypocentres of the tremors are shown by the coloured dots. The colours correspond to the magnitude of the tremors in the following ranges on the scale of Richter: blue for  $1.0 \leq M < 1.5$ , orange for  $1.5 \leq M < 2.5$  and red for  $2.5 \leq M < 4$ . Not all faults with throws less than about 80 m and tremors below  $M = 1.5$  have been captured. Detailed maps are shown in Appendix C, §C.1.

### 3.1 Groningen field

Figure 3.3 shows the improved, and more realistic, reservoir pressure proxy used. Figures 3.4 and 3.5 show the results for modified model M2 using  $M_{min} = 1.0$ . Table 3.2 shows the fit parameters for the various regions for  $M_{min} = 1.0$ . Both models reproduce reasonably well the number of observed tremors and the observed interevent time distributions. The modelled interevent time distributions show a discontinuity around  $^{10} \log(IT) \sim 0.5$  where  $IT$  [s] is the interevent time or the time passed between two subsequent tremors. It is expressed in days. The discontinuity is a numerical artifact due to the time and pressure interval chosen. Taking more steps and smaller pressure intervals, this discontinuity becomes smaller.

Appendix A, §A.2 shows comparable results for modified model M1 and for  $M_{min} = 1.5$  and gives details about the simulations. For the Groningen field, both models give equivalent results.

Figure 3.6 shows the results of modified model M2 for the entire Groningen field. The tremor rate and the observed interevent time distribution are quite well reproduced, see further Appendix A, §A.3.

We found no systematic changes in the dip and throw of fault segments most close to the hypocentres of the tremors or in the distance between the subsequent tremors over time. Figure A.13 in Appendix A, §A.3 shows this for the entire Groningen field but this holds also for all regions of interest in the Groningen field.

For the regions around Loppersum and Ten Boer with most tremors, we have also used the original model but with the improved reservoir pressure proxy, see Appendix A, §A.1. Using this proxy, the fits of the original model improve. The values of the fit parameters somewhat differ for obvious reasons<sup>2</sup>. Figure 3.7 shows observed and modelled tremor rates for the region around Ten Boer using the linear and improved reservoir pressure proxy's.

Again, the Weibull distribution shape parameter  $k_W$  is high. We use for all simulations a single value  $k_W = 13$ . This value is about the lowest one needed to model the sharp onset of the observed tremors. Using the improved reservoir pressure proxy, the typical change in the reservoir pressure for failure  $\delta p_{fail}$  is higher than for the simple linear reservoir pressure proxy. This also holds for the original model, see Appendix A, §A.1.

---

<sup>2</sup>We have not repeated this exercise for the other regions and gas fields because the original model cannot reproduce the tremor poor periods unless tremors reduce the mean stress on the faults.

Table 3.2 : Fit parameters for the regions in the Groningen field for modified model M2 using the catalogue with  $M_{min} = 1.0$  using pressure intervals  $\delta p_{int} = 0.005$  MPa. The radius of regions is 5 km. The Weibull distribution shape parameter  $k_W = 13$ . The stress relaxation parameter  $c_{M_0} = 0$ .

The high b-value for the Meedhuizen region follows from the relative small seismic magnitude interval used to determine the b-value. Repeating the b-value fit for an interval  $1.1 \leq M \leq 2.2$  yields  $b = 1.7$ . This value is close to  $b = 1.6$  found by Chris Harris using sophisticated algorithms (recent, unpublished work). Regarding the low numbers of tremors in magnitude intervals of interest, we conclude that the b-value is in the range 1.6 - 2.1.

Property	Symbol	Unit			
.....	.....	.....	.....	.....	.....
region			Lop	TenB	Mee
number of observed tremors	$N_{obs}$	-	142	171	72
Gutenberg-Richter b-value	$b$	-	0.82	1.0	2.1
min. magn. to fit GR law	$M_{min,GR}$	Richter	1.5	1.5	1.5
max. magn. to fit GR law	$M_{max,GR}$	Richter	3.5	3.3	2.2
Poisson distr. shape parameter	$\lambda_{PS}$	Pa <sup>-1</sup>	0.11	0.18	0.10
typ. pressure change for fault failure	$\delta p_{fail}$	MPa	20	22	23
region			Lag	Wou	Hel
number of observed tremors	$N_{obs}$	-	74	69	80
Gutenberg-Richter b-value	$b$	-	1.2	1.2	0.9
min. magn. to fit GR law	$M_{min,GR}$	Richter	1.6	1.4	1.5
max. magn. to fit GR law	$M_{max,GR}$	Richter	2.8	2.8	3.2
Poisson distr. shape parameter	$\lambda_{PS}$	Pa <sup>-1</sup>	0.10	0.085	0.10
typ. pressure change for fault failure	$\delta p_{fail}$	MPa	21	23	23

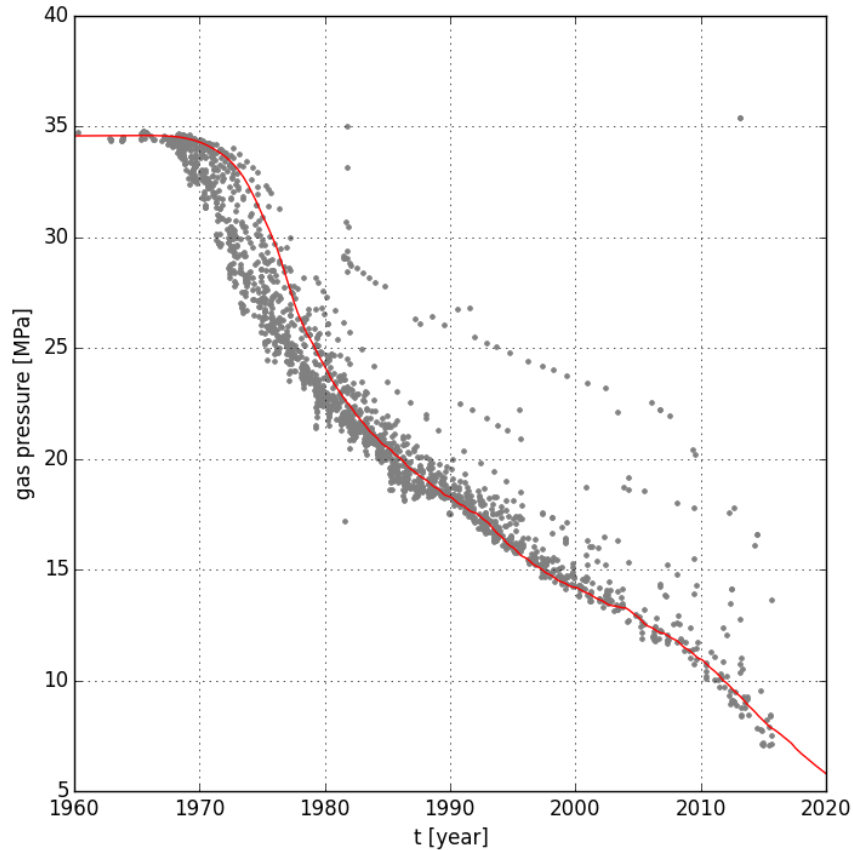


Figure 3.3 : Gas pressure in the reservoir of the Groningen field as measured at the gas production well clusters and observation wells (dots), see for more details Appendix D. The red line shows a moving average of the reservoir pressure in the Leermens gas production well cluster. The latter follows from reservoir simulations for a 33 Bcm/year scenario and holds for approximately most of the well cluster locations in the Groningen field, and in particular for the well clusters around Loppersum, see Appendix D, §D.1. For the period well before the onset of the tremors, local variations in the reservoir pressure hardly matter because the relative likelihood for fault failure is in this period negligible. Because of seasonal variations in the gas production, the reservoir pressure in the production well clusters show also a small seasonal variation. These pressure fluctuations smooth out in the surrounding area by pressure diffusion.

At this stage, it is not clear how much these fluctuations influence the tremor rate in the regions of interest. For this reason we have smoothed the reservoir pressure data in the Leermens gas production well cluster using a moving average filter. The moving average is over 20 data points taken each month, i.e. over a period of about 1.5 year. The effect of smoothing on the interevent time distribution is shown in Appendix B, Figure B.1 .

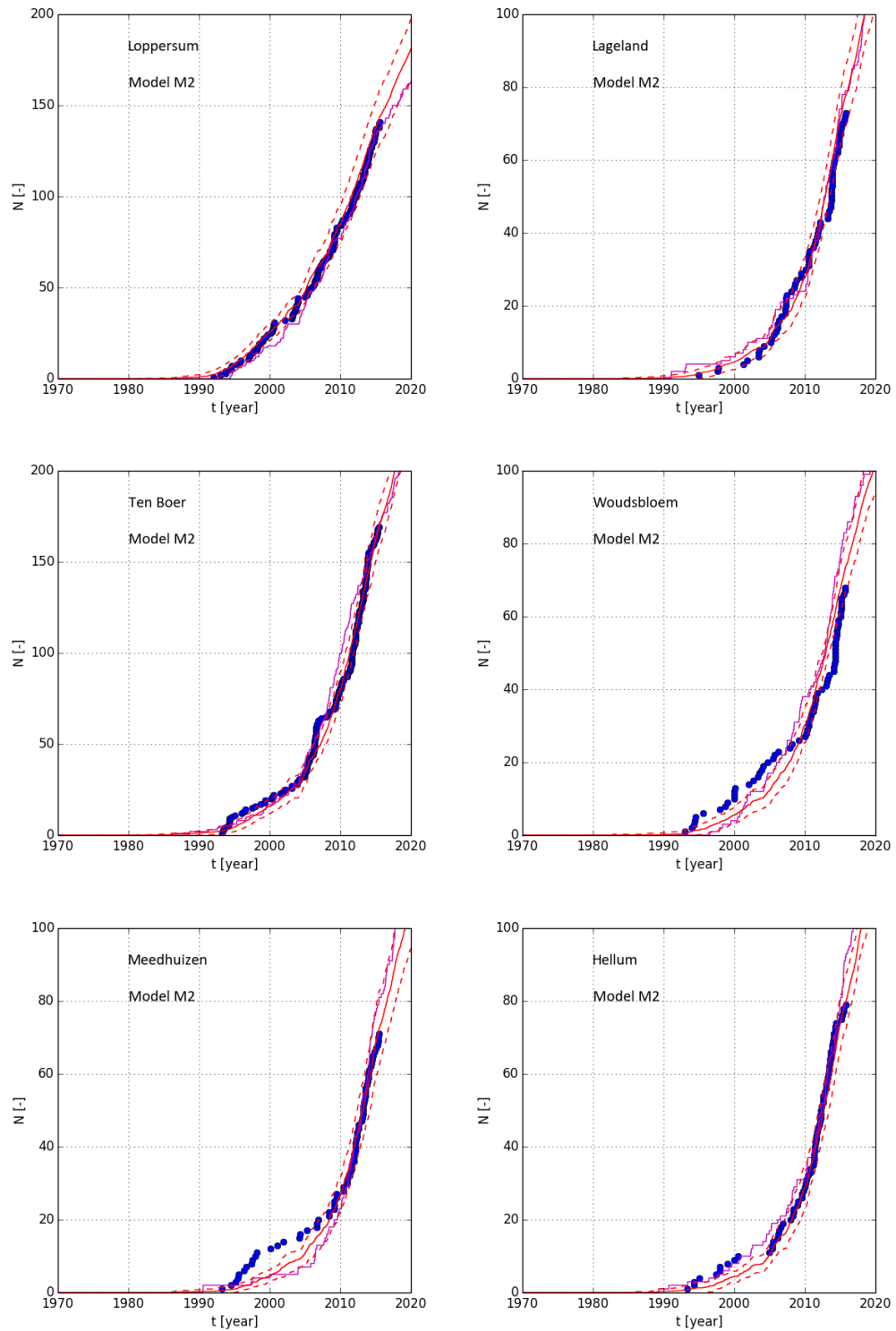


Figure 3.4 : Number of observed and modelled tremors in the various regions in the Groningen field, using model M2.  $M_{min} = 1.0$ ,  $c_{M_0} = 0$ . Period of simulation 1960 - 2020. The number of observed tremors are given by the blue dots. The red solid line shows the mean value of 20 simulations. The red dashed lines show  $\pm 1$  standard deviation from the mean value. The purple solid line shows one simulation. Note that the vertical scale of the top and centre left figures is twice as large than of the other figures.

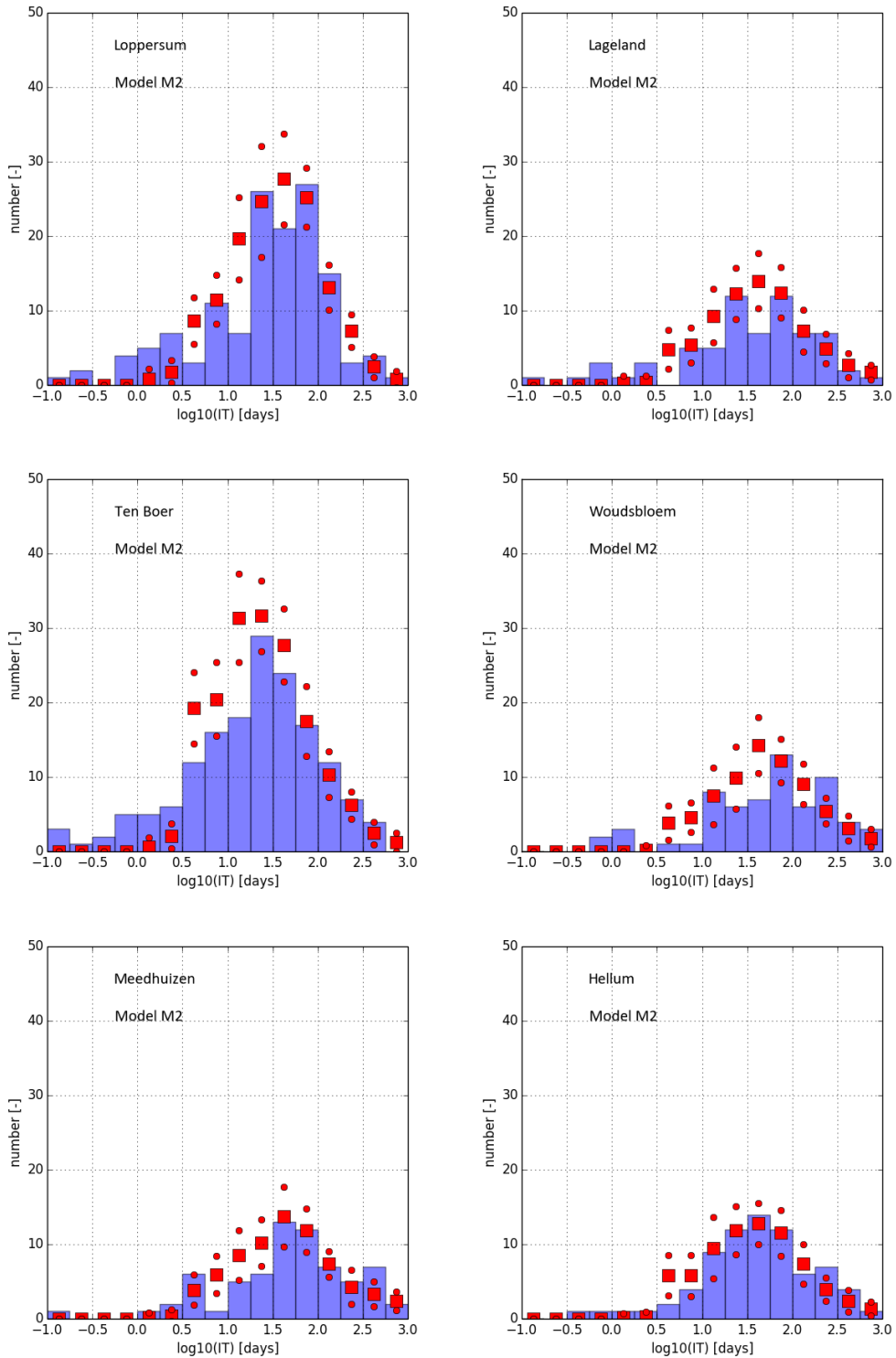


Figure 3.5 : Observed and modelled interevent time distributions in the various regions in the Groningen field, using model M2.  $M_{min} = 1.0$ ,  $c_{M_0} = 0$  in the period 1960 - 30 September 2015. Histograms of the logarithm of the interevent times of the observed tremors (blue bars) and the simulated tremors (red squares, mean value; red dots above and below  $\pm 1$  standard deviation from the mean value). The sum of the numbers in the 16 bins of the histograms is equal to the total number of tremors. The modelled distributions show a discontinuity around  $^{10}\log(IT) \sim 0.5$ . This is a numerical artifact due to the pressure interval chosen, see further Appendices A and B.

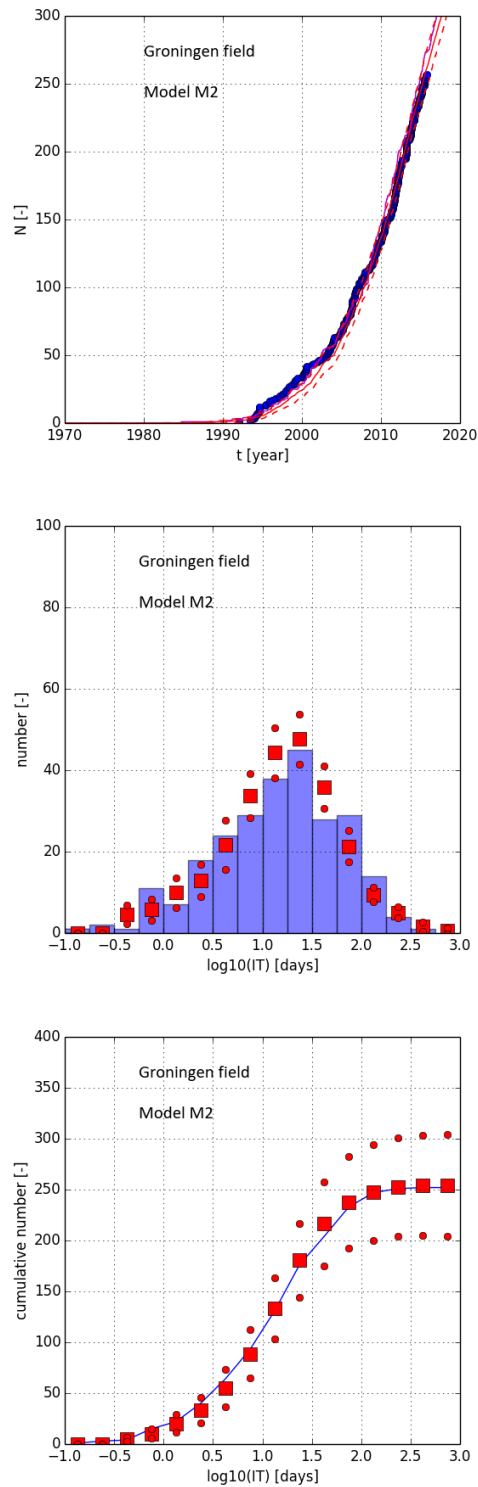


Figure 3.6 : Top figure: number of observed (blue dots) and modelled tremors in the entire Groningen field for  $M_{min} = 1.5$ . Period of simulation 1960 - 2020 in 100000 timesteps. The red solid line shows the mean value of 20 simulations. The red dashed lines show  $\pm 1$  standard deviation from the mean value. The purple solid line shows one simulation. Centre and bottom figures: observed and modelled interevent times of the observed tremors for  $M_{min} = 1.5$  in the period 1960 - 30 September 2015. Histograms of the logarithm of the interevent times of the observed tremors (blue bars) and the simulated tremors (red squares, mean value; red dots above and below  $\pm 1$  standard deviation from the mean value). The sum of the numbers in the 16 bins is equal to the total number of tremors.

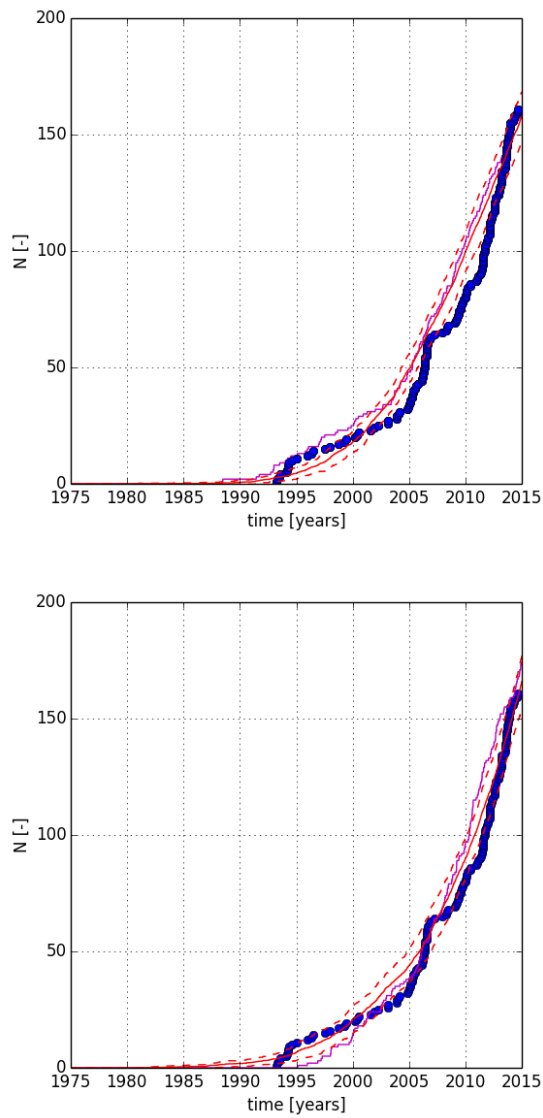


Figure 3.7 : Number of observed and modelled tremors in the Ten Boer region,  $M_{min} = 1.0$ ,  $c_{M_0} = 0$ . Top: The red solid line shows the mean value of 20 simulations. The red dashed lines show  $\pm 1$  standard deviation from the mean value. The purple solid line shows one simulation.

The top figure shows the fit using the simple reservoir pressure proxy. The bottom figure shows the fit using the improved, and more realistic, reservoir pressure proxy. For the period 2010 - 2015, the latter fit curves upwards and follows better the observed tremor rate.

## 3.2 Other fields

A natural consequence of modified models M1 and M2 is that the tremor rate reduces when the reservoir pressure reduction rate slows down. To validate if these models can also fit observed tremor rate reductions when this happens, we have analysed the tremors from the Annerveen, Eleveld, Emmen and Roswinkel fields. These smaller fields have a rather different gas production history than the Groningen field.

In the selected west part of the Annerveen field, the main reservoir pressure reduction from 35 MPa to 5 MPa took place in the period before 1995. In the Annerveen field the tremors started after the main gas production had taken place. Most tremors are observed in the period 1995 - 2014 when the reservoir pressure slowly declined from about 5 MPa to about 1 MPa<sup>3</sup>.

The Eleveld field has three blocks, from south to north B, B1 and B2 which have been depleted differently, see also Appendix D. In the Eleveld field, most of the reservoir pressure reduction took place before 2005. The reservoir pressure in the south and largest 4 × 3 km<sup>2</sup> B block decreased from about 38 MPa to about 3 MPa over the period 1975 - 2005, and initially at a somewhat higher rate. In June 2009, the reservoir pressure was about 2 MPa.

After 2005, the tremor rate substantially decreased in the Eleveld field after the reservoir pressure reduction rate in the largest south block B became insignificant although the smaller blocks B1 and B2 were still produced and the reservoir pressure in these blocks reduced substantially. In the south block region there are almost no tremors after 2005.

As for the Annerveen and Eleveld fields, gas production in the Emmen and Roswinkel fields became insignificant after 2005. The reservoir of the Emmen field is a carbonate rock. The reservoir complex of the Roswinkel field at 2 - 2.5 km depth is in the younger Buntersandstein with Zechstein salt quite below the reservoir. Under and above the reservoir complex are shales.

An interesting difference is that gas production in the Roswinkel field has been supported by an active aquifer. In the period between 1995 and 2007, the Roswinkel field shows a stable pressure level or even a small increase while gas was produced at a relative low production rate. Water infill from this aquifer leads to a small increase in the reservoir pressure after 2000. The gas production in the Roswinkel field has been stopped in 2007.

Another interesting aspect of the Roswinkel field is that the tremors concentrate along one or two faults in the field. From the relation between slip plane area and seismic moment, it is possible that the same area's in the fault have slipped a few times (provided that the stress reduction during rupture is only a few MPa) and that several tremors were triggered by others, see Appendix C, §C.2. Interesting is also that the tremor rate almost

---

<sup>3</sup>According to NAM data, this holds for the ANN, WTD, WVD and ZLV wells. The pressure drop in the ANS and ZLN wells is somewhat slower.

stopped after 2005 without a clear signal in the reservoir pressure. It is not clear if this may follow from stress relaxation due to the tremors before 2005.

A few  $M > 2.5$  tremors, but no smaller tremors, have been recorded by KNMI in the Roswinkel field before the completion of the network of geophones in Groningen in 1995. It could well be that a substantial number of smaller tremors have occurred before the completion of the network but not have been recorded.

Table 3.3 shows the fit parameters for the small fields using modified model M2 and using pressure interval of 0.01 MPa. Figures 3.8 - 3.10 show the reservoir pressure, the observed and modelled tremor rates and interevent time distributions using the catalogues with  $M_{min} = 1.0$ . The hypocentres of the tremors in these small fields are shown in Appendix C, §C.1, Figure C.8. Detailed reservoir pressure data for these fields is shown in Appendix D, §D.1.

In general, the typical change in the reservoir pressure for failure  $\delta p_{fail}$  is for the smaller fields considerably higher than for the Groningen field. It is not clear which field or fault attributes are important in this respect. The only observation is that the values for  $\delta p_{fail}$  are the highest for the Annerveen and Roswinkel fields. These fields have been depleted at the largest average reservoir pressure depletion rate.

While the fits for the Annerveen, Eleveld and Emmen fields are satisfactory, we cannot reproduce the observed tremors in the Roswinkel field with modified models M1 and M2. The fundamental problem is that most of the tremors occur during a period in which the reservoir pressure is approximately constant or even slightly rises because of water infill from a nearby aquifer. Modelled tremors cannot produce the right number of tremors as shown in Figure 3.9 or start years before the strong increase in the tremor rate, see Appendix A, §A.5.

In the Roswinkel field, the tremor rate cannot be explained from an elastic-brittle response where the stress on the fault elastically responds on the recorded reservoir pressure and this pressure is representative for the stress changes in the whole reservoir complex acting on the faults. Perhaps another slow process generates additional stress on the fault planes or deteriorates the stress barrier for seismic rupture during and after reservoir depletion. Since the tremors concentrate along one or two faults in a relatively small region (when compared to the other fields), tremors may have been triggered by others. Further, it cannot be excluded that a small reservoir pressure increase after the production stop had an effect on the tremor rate at the stress state after gas production.

Another possibility is that a large number of small tremors before 1995 have been missed by the limited geophone network before 1995 because it recorded only a few tremors  $M > 2.5$ . Another indication that tremors have been missed is a ‘kink’ in the frequency-magnitude relationship of the observed tremors in this field, see Appendix A, §A.5.

Table 3.3 : Fit parameters for the other gas fields for modified model M2 using the tremor catalogue with  $M_{min} = 1.0$ . The radius of regions is 5 km. The Weibull distribution shape parameter  $k_W = 13$ . The relaxation of the mean stress on the faults by tremors is disregarded. Hence, the stress relaxation parameter  $c_{M_0} = 0$ .

The small number of tremors results in more uncertainty in the derived fit parameters (about  $\pm 20\%$ ).

Property	Symbol	Unit		
.....	.....	.....	.....	.....
region			Ann	Ele
number of observed tremors	$N_{obs}$	-	21	39
Gutenberg-Richter b-value	$b$	-	1.2	0.7
min. magn. to fit GR law	$M_{min,GR}$	Richter	1.6	1.5
max. magn. to fit GR law	$M_{max,GR}$	Richter	2.8	3.0
Poisson distribution shape parameter	$\lambda_{PS}$	$\text{Pa}^{-1}$	0.050	0.0079
typ. pressure change for fault failure	$\delta p_{fail}$	MPa	37	29
region			Emm	Ros
number of observed tremors	$N_{obs}$	-	11	37
Gutenberg-Richter b-value	$b$	-	$\sim 0.9$	$\sim 1$
min. magn. to fit GR law	$M_{min,GR}$	Richter	1.3	2.0
max. magn. to fit GR law	$M_{max,GR}$	Richter	3.5	3.5
Poisson distribution shape parameter	$\lambda_{PS}$	$\text{Pa}^{-1}$	0.0015	0.07
typ. pressure change for fault failure	$\delta p_{fail}$	MPa	26	31

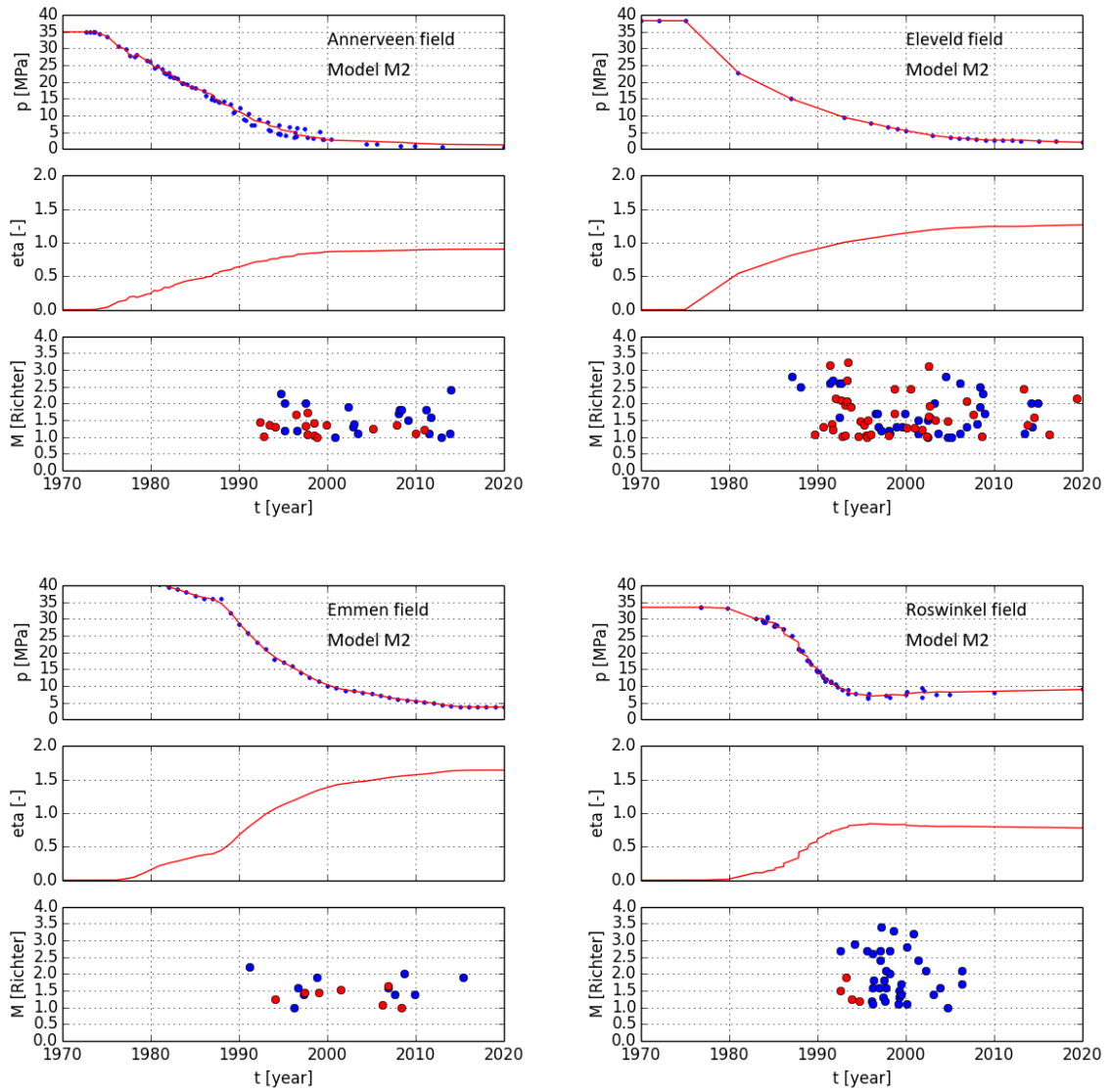


Figure 3.8 : Reservoir pressure (top), failure criterion variable  $\eta$  (centre figure) and observed and modelled tremors (bottom figure) in the Annerveen, Eleveld, Emmen and Roswinkel fields, using model M2.  $M_{min} = 1.0$ ,  $c_{M_0} = 0$ . Period of simulation 1960 - 2020. The observed reservoir pressures and used reservoir pressure proxy's are shown by the blue dots and the red lines, respectively. The observed and modelled tremors are given by the blue and red dots, respectively. Detailed reservoir pressure data for these fields is shown in Appendix D, §D.1.

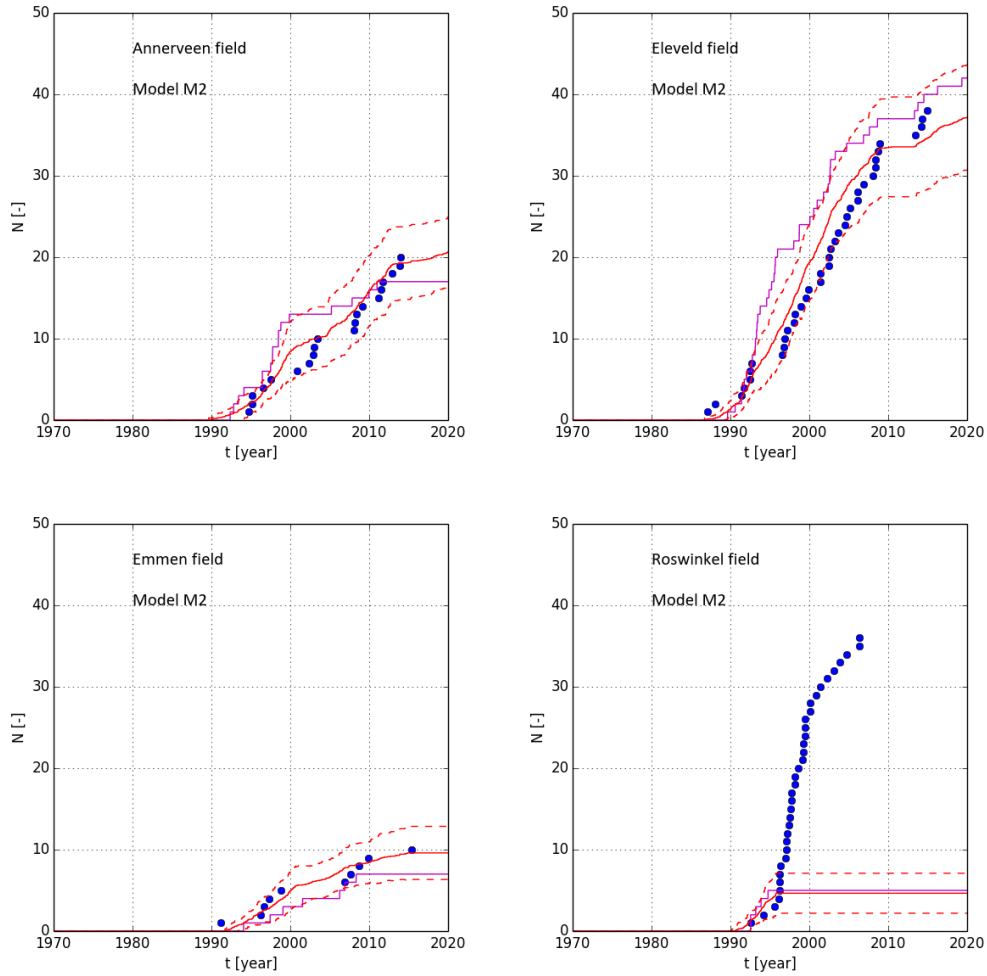


Figure 3.9 : Number of observed and modelled tremors in the Annerveen, Eleveld, Emmen and Roswinkel fields, using model M2.  $M_{min} = 1.0$ ,  $c_{M_0} = 0$ . Period of simulation 1960 - 2020. The number of observed tremors are given by the blue dots. The red solid line shows the mean value of 20 simulations. The red dashed lines show  $\pm 1$  standard deviation from the mean value. The purple solid line shows one simulation. One simulation curve can significantly deviate from the mean one.

The model is not able to reproduce the observed tremor rate in the Roswinkel field because tremors occur in a period where the reservoir pressure hardly changes.

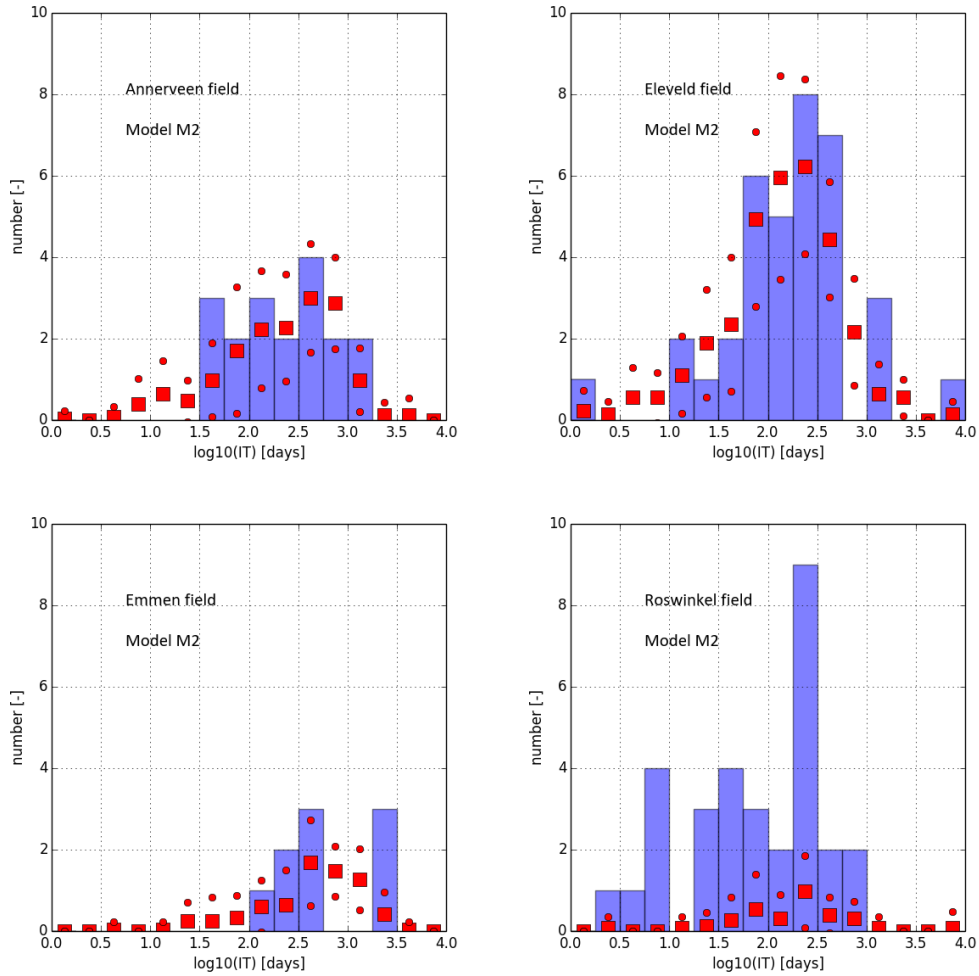


Figure 3.10 : Observed and modelled interevent time distributions in the Annerveen, Eleveld, Emmen and Roswinkel fields, using model M2.  $M_{min} = 1.0$ ,  $c_{M_0} = 0$  in the period 1960 - 30 September 2015. Histograms of the logarithm of the interevent times of the observed tremors (blue bars) and the simulated tremors (red squares, mean value; red dots above and below  $\pm 1$  standard deviation from the mean value). The sum of the numbers in the 16 bins of the histograms is equal to the total number of tremors.

The poor fit between the observed and modelled interevent time distribution for the Roswinkel field is a direct consequence of the clear misfit of the number of tremors as shown in Figure 3.9 . Note the relatively high number of observed short interevent times in the Roswinkel field when compared to the other fields and the Groningen field. It suggests that either the tremor catalogue of this field is far from complete or that aftershocks significantly contribute to the tremor catalogue.

# Chapter 4

## Discussion

The modified models M1 and M2 presented in this report reproduce quite well the tremor rates and the distribution of the periods between subsequent tremors, i.e. the interevent times in the regions of interest in the Groningen field, in the entire Groningen field and in the Annerveen, Eleveld and Emmen fields. In the latter fields, changes in the reservoir pressures were insignificant over a relatively long period of about 5 - 10 years. There is no need to use a mean field stress relaxation process to reduce the tremor rate in periods of low gas production as we have done for the original model.

Whether remaining differences between the observations and modelled results are statistically significant must still be sorted out. The present models have not been validated against changes in production over relatively short periods, such as seasonal changes in gas production and the stop of gas production from the well clusters near Loppersum since early 2014, see Bierman et al. (2015) and Paleja et al. (2015).

The tremor rate in the Roswinkel field cannot be reproduced with these models. Tremors appear in this field when the reservoir pressure hardly changes.

The high value of the Weibull distribution shape parameter  $k_W$  indicates that the transition to a stress state with tremors is sharper than would be expected from a normal Mohr-Coulomb failure criterion recognising the possible variations in fault properties over the field. This shape parameter determines the transition period from no tremors to a constant tremor rate in the case of a constant compaction rate.

We have found no significant trend over time in the properties of fault segments which are closest to the hypocentres of the tremors. From 1995 to 2015, values for the fault dip or fault throw scatter over the complete range of possible values. We have found no correlation between changes in the gas production and changes in the tremor rate in a certain region other than one resulting from a resulting change in the reservoir pressure. More or less prominent deviations in the tremor rate from a smooth curve are difficult to explain from changes in the gas production.

Significant deviations in the interevent time distribution from a distribution which follows from an independent Poisson process may indicate whether the tremor rate has become sensitive to small changes in the stress state or not. In this respect, a rapid change in the relative likelihood of a tremor, such as follows from the Weibull distribution for rock failure, may be regarded as approaching a critical condition for rock failure. So far, we have not identified other signatures of a sudden change in the tremor rate.

Over the period 1<sup>st</sup> May 1995 to 31<sup>st</sup> December 2014, there were 76 tremors of magnitude 1.5 and greater in the Loppersum region compared with 160 in the rest of the field. This is a ratio of 0.47 compared with a ratio of about 0.08 for the ratio of the area's of the Loppersum region and the rest of the field. In relation to the work of Harris (2015) on the b-values in the Loppersum region and the rest of the field, it would be interesting to calculate the spatial distribution for the entire Groningen field using a combination of two spatial Poisson processes to respect the actual numbers of tremors in the Loppersum region and the rest of the field.

We have not been successful to reproduce the spatial distribution of tremors over the Groningen field using only reservoir compaction data and keeping the other model input parameters constant. The tremor rate is systematically overpredicted in the regions south-west and north-east of Loppersum.

In this respect, the modified models do not improve the current activity rate model used in the seismological model for the Groningen field, which is used for the seismic hazard and risk analysis. Regarding the reasonable fits of the observed tremor rates using the modified models M1 and M2, it could be considered to improve predictions of tremor rates in regions of interest by using these local or regional models<sup>1</sup>. Local model parameters can be derived from the observed tremor rates in the region of interest.

At this stage, it's hard to say which other field or fault properties than the reservoir compaction or reservoir compaction rate are important for the spatial distributions of the tremors. Further research on field and fault properties in relation to tremor rates is recommended.

---

<sup>1</sup>These regions could be related to those defined in the so-called Groningen Meet and Regel Protocol under development by NAM.

# Chapter 5

## Acknowledgements

I heartily thank Chris Harris and Rob van Eijs for reviewing this work and for their comments. I thank Onno van der Wal, Henk van Oeveren and Leendert Geurtsen from NAM for providing me the reservoir pressure and gas production data.

# Bibliography

- Bierman, S. M., and Kraaijeveld, F., “Regularised Direct Inversion to Compaction in the Groningen Reservoir using Measurements from Optical Leveling Campaigns” ,, Technical Report SR.15.11194, Shell Global Solutions International B.V., 2015.
- Bierman, S., Paleja, R., and Jones, M., “Statistical Methodology for Investigating Seasonal Variation in Rates of Earthquake Occurrence in the Groningen Field” ,, Technical Report SR.15.13132, Shell Global Solutions International B.V., 2015.
- Bourne, S. J., and Oates, S., “An Activity Rate Model of Induced Seismicity within the Groningen Field” ,, Technical Report NAM report 2014, Nederlandse Aardolie Maatschappij B.V., The Netherlands, 2014.
- Bourne, S. J., and Oates, S., “An Activity Rate Model of Induced Seismicity within the Groningen Field (part 2)” ,, Technical Report NAM report 2015, Nederlandse Aardolie Maatschappij B.V., The Netherlands, 2015.
- Bourne, S. J., Oates, S., van Elk, J., and Doornhof, D., “A Seismological Model for Earthquakes Induced by Fluid Extraction from a Subsurface Reservoir”, *Geophys. Res. Solid Earth*, 119, 8991–9015, 2014.
- Dost, B., and Kraaijpoel, D., “The August 16, 2012 Earthquake near Huizinghe (Groningen)” ,, Technical Report KNMI report TR 16/1/2013, Koninklijke Nederlands Meteorologisch Instituut, the Netherlands, 2013.
- Dost, B., and Spetzler, J., “Probabilistic Seismic Hazard Analysis for Induced Earthquakes in Groningen; update 2015” ,, Technical Report KNMI report, Koninklijke Nederlands Meteorologisch Instituut, the Netherlands, 2015.
- Hanks, T. C., and Kanamori, H., “A Moment Magnitude Scale”, *J. of Geophys. Res. Solid Earth*, 84, 2348–2350, 1979.
- Harris, C. K., “Maximum Likelihood Estimates of b-Value for Induced Seismicity in the Groningen Field” ,, Technical Report SR.15.12673, Shell Global Solutions International B.V., 2015.

- Kraaijpoel, D., and Dost, B., “Implications of Salt-related Propagation and Mode Conversion Effects on the Analysis of Induced Seismicity”, *Journal of Seismology*, 17, 95–107, 2013.
- Leonard, M., “Earthquake Fault Scaling: Self-Consistent Relating of Rupture Length, Width, Average Displacement, and Moment Release”, *Bull. of the Seism. Soc. of America*, 100, 1971–1988, 2010.
- Mallik, J., “Map Based Fault Slip Risking for the Groningen Gas Field” ,, Technical Report EP201501207022, Nederlandse Aardolie Maatschappij B.V., The Netherlands, 2015.
- Paleja, R., Bierman, S., and Jones, M., “Impact of Production Shut-in on Inter-Event time in Groningen - A Statistical Perspective” ,, Technical Report SR.15.13107, Shell Global Solutions International B.V., 2015.
- Pijpers, F. P., “Significance of Trend Changes in Ground Subsidence in Groningen” ,, Technical Report Phase 0 Report 1, CBS Statistics Netherlands, the Netherlands, 2014.
- , “Significance of Trend Changes in Ground Subsidence in Groningen” ,, Technical Report Phase 0 Report 2, CBS Statistics Netherlands, the Netherlands, 2014.
- Pilkey, W. D., and Pilkey, D. F., “Peterson’s Stress Concentration Factors, 3<sup>rd</sup> edition”, John Wiley & Sons, 2008.
- Scholz, C. H., “The Mechanics of Earthquakes and Faulting, 2<sup>nd</sup> edition”, Cambridge University Press, 2002.
- Stein, S., and Wysession, M., “An Introduction to Seismology, Earthquakes, and Earth Structure”, Blackwell Publishing, 2003.
- Udias, A., Madariaga, R., and Buforn, E., “Source Mechanisms of Earthquakes - Theory and Practice”, Cambridge University Press, 2014.
- Wentinck, H. M., “Induced Seismicity in the Groningen Field - Statistical Assessment of Tremors along Faults in a Compacting Reservoir” ,, Technical Report SR.15.11335, Shell Global Solutions International B.V., 2015.



# Appendix A

## Additional simulation results

### Appendix A.1 Original model using a better proxy for the reservoir pressure

We apply the original model with the improved reservoir pressure proxy for the Loppersum and Ten Boer regions since they have a substantial number of tremors. The original model is explained in Wentinck (2015). Ignoring the gas production stop in the Loppersum region since early 2014, we use the tremor data until 1 January 2015. The improved reservoir proxy used is shown in Appendix D, §D.1, Figure D.1 .

We use the same constant values for the parameters  $\alpha$  and  $c_{\sigma_v}$  as in Wentinck (2015), i.e.  $\alpha = 0.7$  and  $c_{\sigma_v} = 0.5$ <sup>1</sup>. The mean stress relaxation by the tremors is disregarded. Hence, the stress relaxation parameter  $c_{M_0} = 0$ . As was discussed in the aforementioned report, a possible effect of tremors on the reduction of the mean stress is almost completely canceled by a small decrease of the shape parameter of the Poisson probability distribution function  $\lambda_{PS}$  under an almost steadily increasing load on the faults.

The number of time steps taken to simulate the period 1960 - 2015 is 20000 instead of 5000. This is needed to produce the histograms of the interevent times, i.e. the time between subsequent tremors<sup>2</sup>. This corresponds with a time step of about 1 day.

Figures A.1 and A.3 show the reservoir pressure and failure criterion variable  $\eta$  as a function of time for both regions. Figures A.2 and A.4 show the observed and modelled tremor rates for the improved and the linear reservoir pressure proxy's and the observed and modelled interevent time distributions. The minimum magnitude  $M_{min} = 1.0$ .

The observed interevent time distribution is quite well reproduced. There is a small difference between the observed and simulated interevent time distributions for interevent

---

<sup>1</sup>Vice-versa,  $\tau_{fail}$  can be calculated from the listed value  $\delta p_{fail}$  using  $\tau_{fail} = \alpha c_{\sigma_v} \delta p_{fail}$  using  $\alpha = 0.7$  and  $c_{\sigma_v} = 0.5$ .

<sup>2</sup>The simulated curves for the number of tremors over time are identical for both number of steps. For 5000 time steps, the minimum time step of about 4 days is too long to reproduce the short interevent times observed in these regions.

times of 0.5 - 5 days. This difference does not disappear by taking 100000 smaller time steps of about 0.25 day. If this difference is statistically significant, it may indicate that the catalogue with  $M_{min} = 1.0$  includes some aftershocks.

The fit parameters are given in Table A.1 . The values of these parameters differ for both reservoir pressure proxy's. The higher value for the Weibull distribution shape parameter  $k_W$  for the improved reservoir pressure proxy is a consequence of a lower reservoir pressure decline rate at the onset of the tremors than for the simple linear reservoir pressure proxy. The high value of  $k_W$  in both cases indicate a sharp stress related criterion for the onset of tremors.

$\lambda_{PS}$  and  $\delta p_{fail} = \tau_{fail}/(\alpha c_{\sigma_v})$  are different in the two regions due to differences in reservoir compaction and other factors, such as fault properties. For both regions, the fits for the number of tremors are better for the improved reservoir pressure proxy than for the simple linear reservoir pressure proxy.

Table A.1 : Fit parameters for the original model for the Loppersum and Ten Boer regions using the simple linear and improved reservoir pressure proxy's. The radius of the region is 5 km. The number of steps is 20000. The time step  $\delta t$  is about 1 day. The minimum magnitude is  $M = 1.0$  and the stress relaxation parameter is  $c_{M_0} = 0$ .

Property	Symbol	Unit	Lop	Lop	TenB	TenB
			simple proxy	improved proxy	simple proxy	improved proxy
.....	.....	.....	.....	.....	.....	.....
number of observed tremors until 1 January 2015	$N_{obs}$	-	137	137	162	162
Gutenberg-Richter b-value	$b$	-	0.82	0.82	1.0	1.0
Poisson distr. shape parameter	$\lambda_{PS}$	-	0.020	0.029	0.032	0.058
Weibull distr. shape parameter	$k_W$	-	6	9	7	9
typ. pressure change for failure	$\delta p_{fail}$	MPa	17	22	19	24

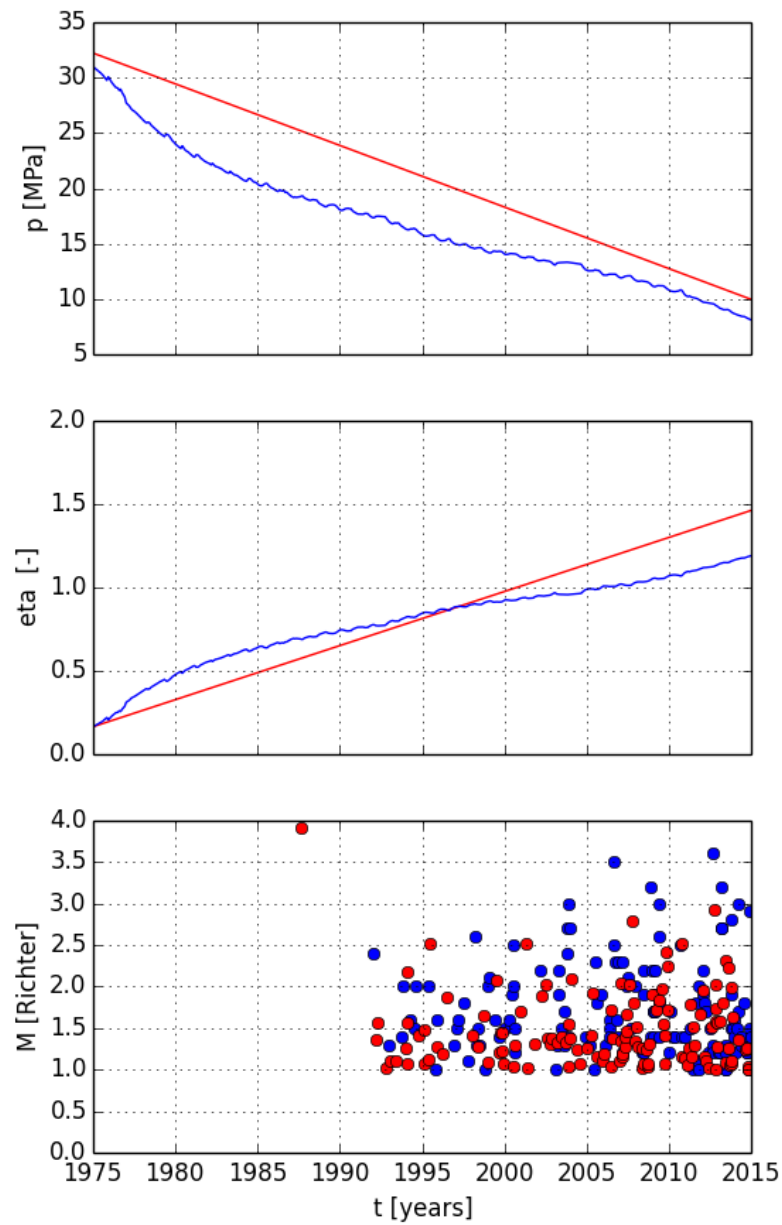


Figure A.1 : Reservoir pressure, failure criterion variable  $\eta$  and observed and modelled tremors in the Loppersum region.  $M_{min} = 1.0$ ,  $c_{M_0} = 0$ . The top and centre figures show the simple linear reservoir pressure proxy and resulting failure criterion variable  $\eta$  (red lines) used in Wentinck (2015) and the improved, more realistic, reservoir pressure proxy and failure criterion variable  $\eta$  (blue lines). The bottom figure shows the observed (blue dots) and modelled tremors (red dots) using the improved, and more realistic, reservoir pressure proxy.

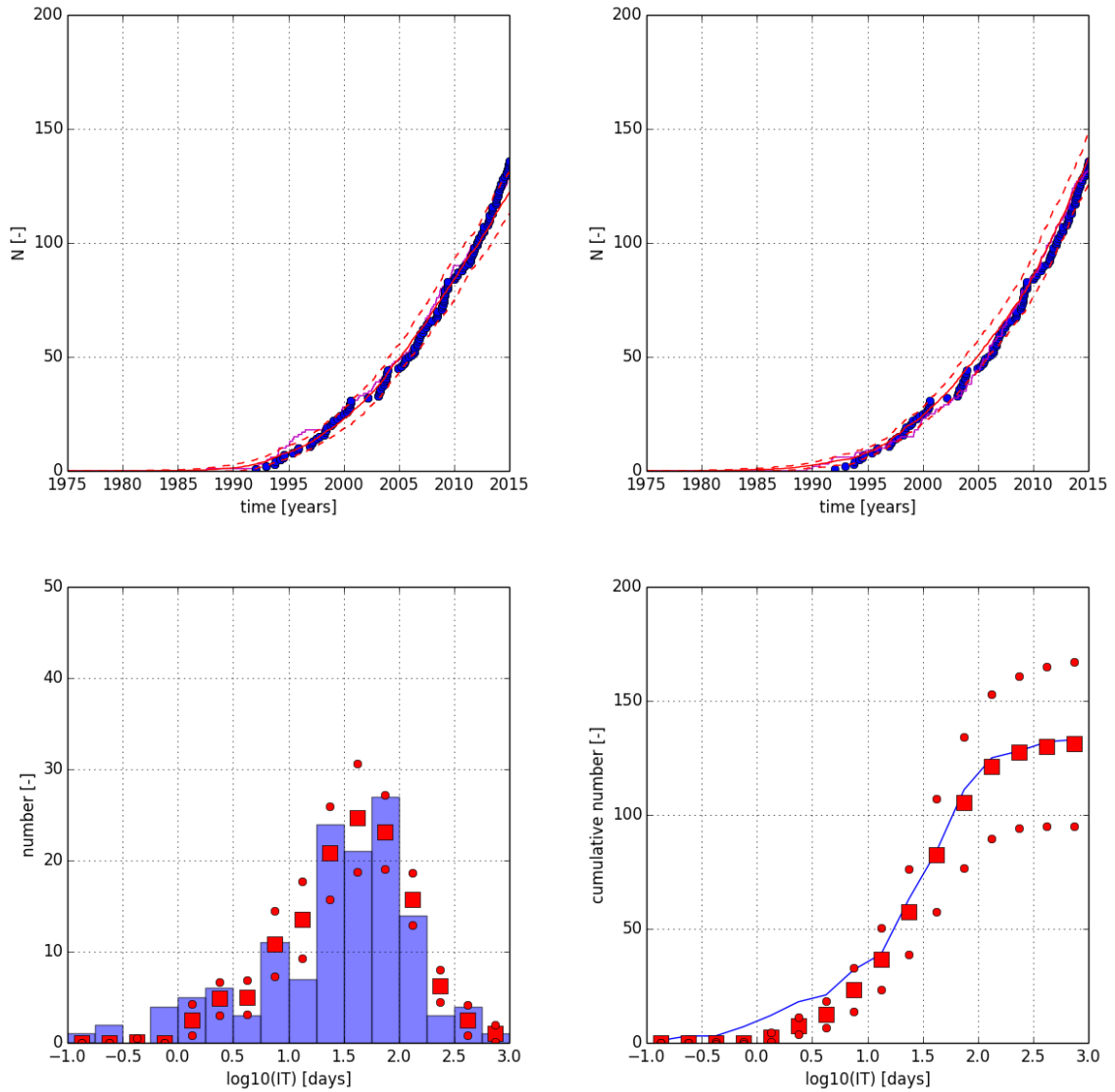


Figure A.2 : Number of observed and modelled tremors in the Loppersum region,  $M_{min} = 1.0$ ,  $c_{M_0} = 0$ . Top: The red solid line shows the mean value of 20 simulations. The red dashed lines show  $\pm 1$  standard deviation from the mean value. The purple solid line shows one simulation.

The top left figure shows the fits for the simple reservoir pressure proxy. The top right figure shows the fit for the improved, and more realistic, reservoir pressure proxy.

Bottom: Histograms of the logarithm of the interevent times of the observed tremors (blue bars) and simulated tremors for the improved, and more realistic, reservoir pressure proxy (red squares, mean value; red dots above and below  $\pm 1$  standard deviation from the mean value). The sum of the numbers in the 16 bins of the histograms is equal to the total number of tremors.

The observed and simulated interevent time distributions somewhat differ for short interevent times of 0.5 - 5 days. This difference does not disappear by taking 100000 smaller time steps of about 0.25 day.

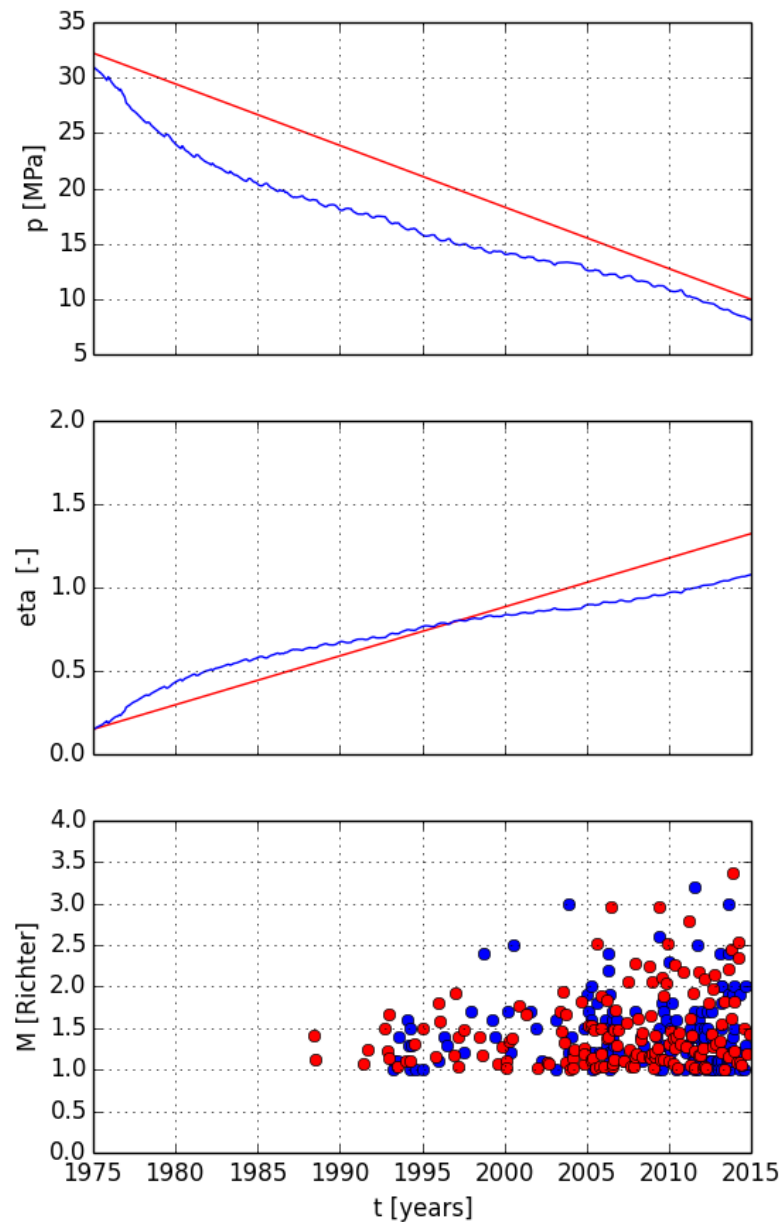


Figure A.3 : Reservoir pressure, failure criterion variable  $\eta$  and observed and modelled tremors in the Ten Boer region.  $M_{min} = 1.0$ ,  $c_{M_0} = 0$ . The top and centre figures show the simple linear reservoir pressure proxy and resulting failure criterion variable  $\eta$  (red lines) used in Wentinck (2015) and the improved, more realistic, reservoir pressure proxy and failure criterion variable  $\eta$  (blue lines). The bottom figure shows the observed (blue dots) and modelled tremors (red dots) using the improved, and more realistic, reservoir pressure proxy.

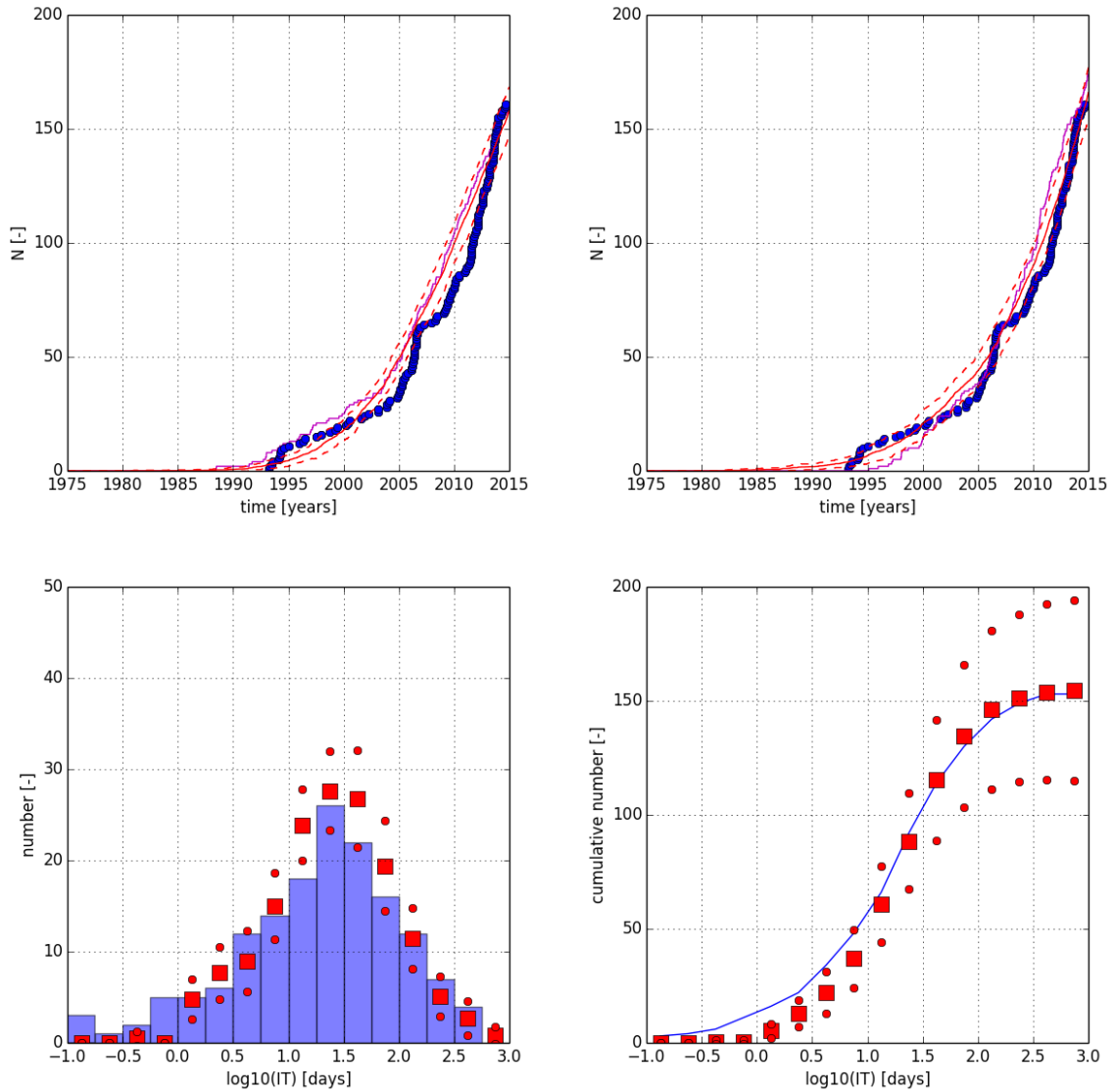


Figure A.4 : Number of observed and modelled tremors in the Ten Boer region,  $M_{min} = 1.0$ ,  $c_{M_0} = 0$ . Top: The red solid line shows the mean value of 20 simulations. The red dashed lines show  $\pm 1$  standard deviation from the mean value. The purple solid line shows one simulation.

The top left figure shows the fits for the simple reservoir pressure proxy. The top right figure shows the fit for the improved, and more realistic, reservoir pressure proxy.

Bottom: Histograms of the logarithm of the interevent times of the observed tremors (blue bars) and simulated tremors for the improved, and more realistic, reservoir pressure proxy (red squares, mean value; red dots above and below  $\pm 1$  standard deviation from the mean value). The sum of the numbers in the 16 bins of the histograms is equal to the total number of tremors.

The observed and simulated interevent time distributions somewhat differ for short interevent times of 0.5 - 5 days. This difference does not disappear by taking 100000 smaller time steps of about 0.25 day.

## Appendix A.2 Modified models M1 and M2

For all simulations, the period 1960 - 2020 is discretised in 50000 time steps of about 0.5 day. For model M2, we have used the reservoir pressure intervals  $\delta p_{int} = 0.005$  MPa and  $\delta p_{int} = 0.01$  MPa. In both cases, the number of tremors over time can be well reproduced with  $\lambda_{PS}$  almost in proportion to  $\delta p_{int}$ . The tables and figures show the results for  $\delta p_{int} = 0.005$  MPa. For the catalogues with  $M_{min} = 1.0$  and  $M_{min} = 1.5$ .

Also, the interevent time distribution is reasonably well reproduced albeit that the simulated distributions have a small discontinuity around  $^{10} \log(IT) \sim 0.5$ . This is a numerical artifact due to the pressure interval chosen. This discontinuity increases for larger pressure steps and time steps. Other effects of the chosen reservoir pressure interval and the number of time steps on the fit parameters are discussed in Appendix B. For the catalogue with  $M_{min} = 1.5$ ,  $\delta p_{int} = 0.01$  MPa would small enough to reproduce the observed interevent time distribution.

The improved reservoir pressure proxy used is shown in Appendix D, §D.1, Figure D.1 , red curve. It follows from the simulated reservoir pressure in the Leermens gas production well cluster. This data has been smoothened with a moving average filter. The moving average is over 20 data points taken each month, i.e. over a period of about 1.5 year.

Figures A.5 and A.6 show the number of tremors and the histograms of the interevent times of model M1 for all regions in the Groningen field for  $M_{min} = 1.0$ . The values for the typical failure pressure  $\delta p_{fail}$  are slightly smaller than for model M2, see Table A.2 for the fit parameters used.

Figures A.7 - A.8 show the number of tremors and the interevent times of model M2 for all regions in the Groningen field for  $M_{min} = 1.5$ . Only the normalisation parameters  $c_{PS}$  and  $\lambda_{PS}$  have been adjusted.

Figures A.9 - A.10 compare the fits one-to-one for the regions around Loppersum and Ten Boer for models M1 (left side) and M2 (right side) for  $M_{min} = 1.0$ . The fit parameters are listed in Table A.3 .

Table A.2 : Fit parameters for the regions in the Groningen field for modified models M1 and M2 for  $M_{min} = 1.0$  and for modified model M2 for  $M_{min} = 1.5$ . The radius of the regions is 5 km. The Weibull distribution shape parameter  $k_W = 13$ . The stress relaxation parameter  $c_{M_0} = 0$ .

Property	Symbol	Unit			
.....	.....	.....	.....	.....	.....
<i>M<sub>min</sub> = 1.0 - models M1 and M2</i>					
region			Lop	TenB	Mee
number of observed tremors	$N_{obs}$	-	142	171	72
Gutenberg-Richter b-value	$b$	-	0.82	1.0	2.1
min. magn. to fit GR law	$M_{min,GR}$	Richter	1.5	1.5	1.4
max. magn. to fit GR law	$M_{max,GR}$	Richter	3.5	3.3	2.3
Poisson distr. shape parameter (M1)	$c_{PS}$	MPa <sup>-1</sup>	0.019	0.033	0.017
typ. pressure change for fault failure (M1)	$\delta p_{fail}$	MPa	21	23	24
Poisson distr. shape parameter (M2)	$\lambda_{PS}$	Pa <sup>-1</sup>	0.11	0.18	0.10
typ. pressure change for fault failure (M2)	$\delta p_{fail}$	MPa	20	22	23
region			Lag	Wou	Hel
number of observed tremors	$N_{obs}$	-	74	69	80
Gutenberg-Richter b-value	$b$	-	1.2	1.2	0.9
min. magn. to fit GR law	$M_{min,GR}$	Richter	1.6	1.4	1.5
max. magn. to fit GR law	$M_{max,GR}$	Richter	2.8	2.8	3.2
Poisson distr. shape parameter (M1)	$c_{PS}$	MPa <sup>-1</sup>	0.017	0.014	0.022
typ. pressure change for fault failure (M1)	$\delta p_{fail}$	MPa	24	24	24
Poisson distr. shape parameter (M2)	$\lambda_{PS}$	Pa <sup>-1</sup>	0.10	0.085	0.10
typ. pressure change for fault failure (M2)	$\delta p_{fail}$	MPa	21	23	23
<i>M<sub>min</sub> = 1.5 - model M2</i>					
region			Lop	TenB	Mee
number of observed tremors	$N_{obs}$	-	85	67	21
Poisson distr. shape parameter (M2)	$\lambda_{PS}$	Pa <sup>-1</sup>	0.068	0.067	0.028
typ. pressure change for fault failure (M2)	$\delta p_{fail}$	MPa	20	22	23
region			Lag	Wou	Hel
number of observed tremors	$N_{obs}$	-	23	29	21
Poisson distr. shape parameter (M2)	$\lambda_{PS}$	Pa <sup>-1</sup>	0.030	0.032	0.030
typ. pressure change for fault failure (M2)	$\delta p_{fail}$	MPa	21	23	23

Table A.3 : Fit parameters for the Loppersum and Ten Boer regions for the modified models M1 and M2. The radius of the regions is 5 km. The Weibull distribution shape parameter  $k_W = 13$ . The stress relaxation parameter  $c_{M_0} = 0$ .

Property	Symbol	Unit		
.....	.....	.....	.....	.....
region			Lop	TenB
typ. pressure change for fault failure (M1)	$\delta p_{fail}$	MPa	21	23
typ. pressure change for fault failure (M2)	$\delta p_{fail}$	MPa	20	22
$M_{min} = 1.0$				
- number of observed tremors	$N_{obs}$	-	141	171
- Poisson distr. shape parameter (M1)	$c_{PS}$	MPa <sup>-1</sup>	0.019	0.033
- Poisson distr. shape parameter (M2)	$\lambda_{PS}$	Pa <sup>-1</sup>	0.10	0.18
$M_{min} = 1.5$				
- number of observed tremors	$N_{obs}$	-	84	67
- Poisson distr. shape parameter (M1)	$c_{PS}$	MPa <sup>-1</sup>	0.011	0.014
- Poisson distr. shape parameter (M2)	$\lambda_{PS}$	Pa <sup>-1</sup>	0.068	0.067

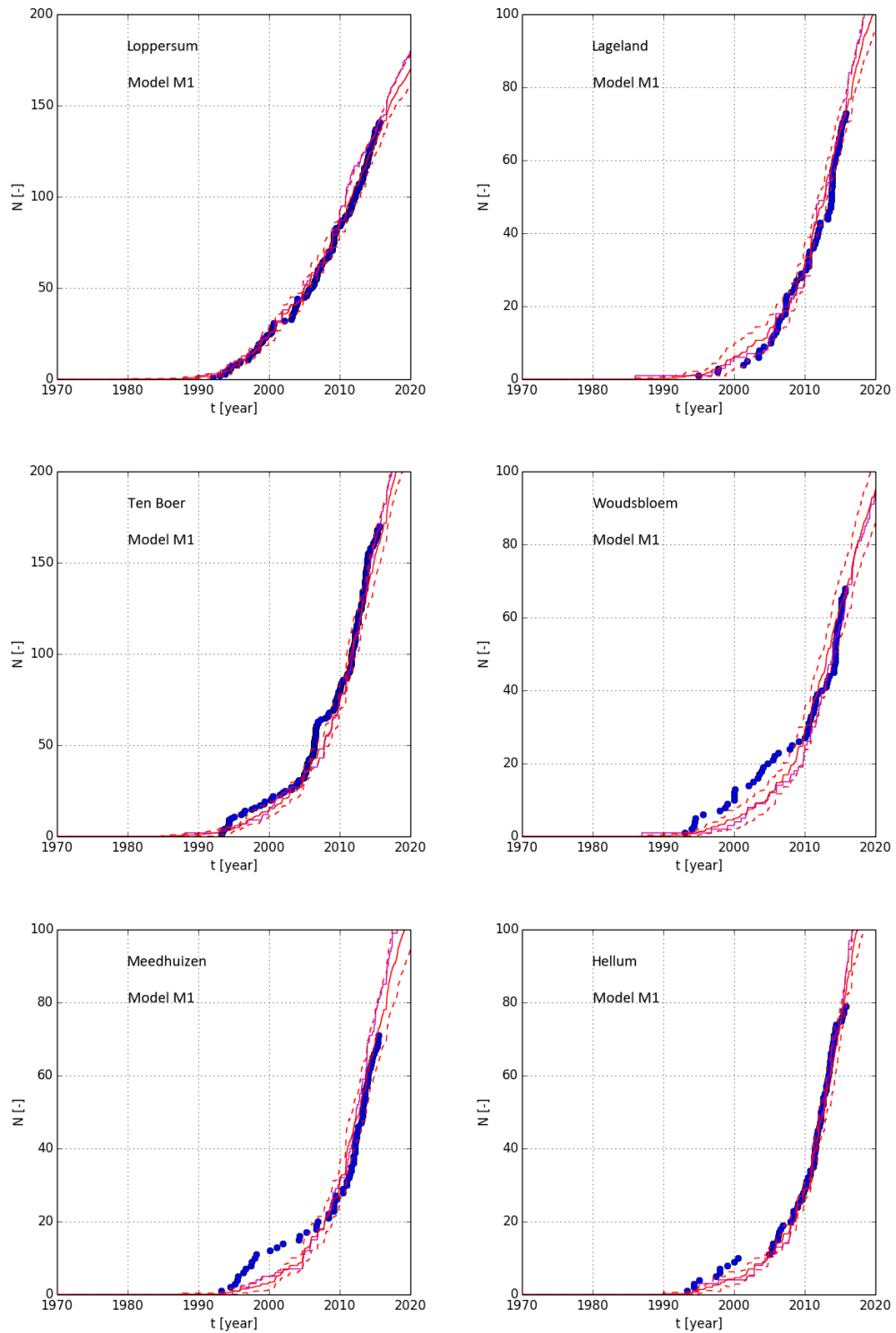


Figure A.5 : Number of observed and modelled tremors in the various regions in the Groningen field, using model M1.  $M_{min} = 1.0$ ,  $c_{M_0} = 0$ . Period of simulation 1960 - 2020. The number of observed tremors are given by the blue dots. The red solid line shows the mean value of 20 simulations. The red dashed lines show  $\pm 1$  standard deviation from the mean value. The purple solid line shows one simulation. Note that the vertical scale of the top and centre left figures is twice as large as of the other figures.

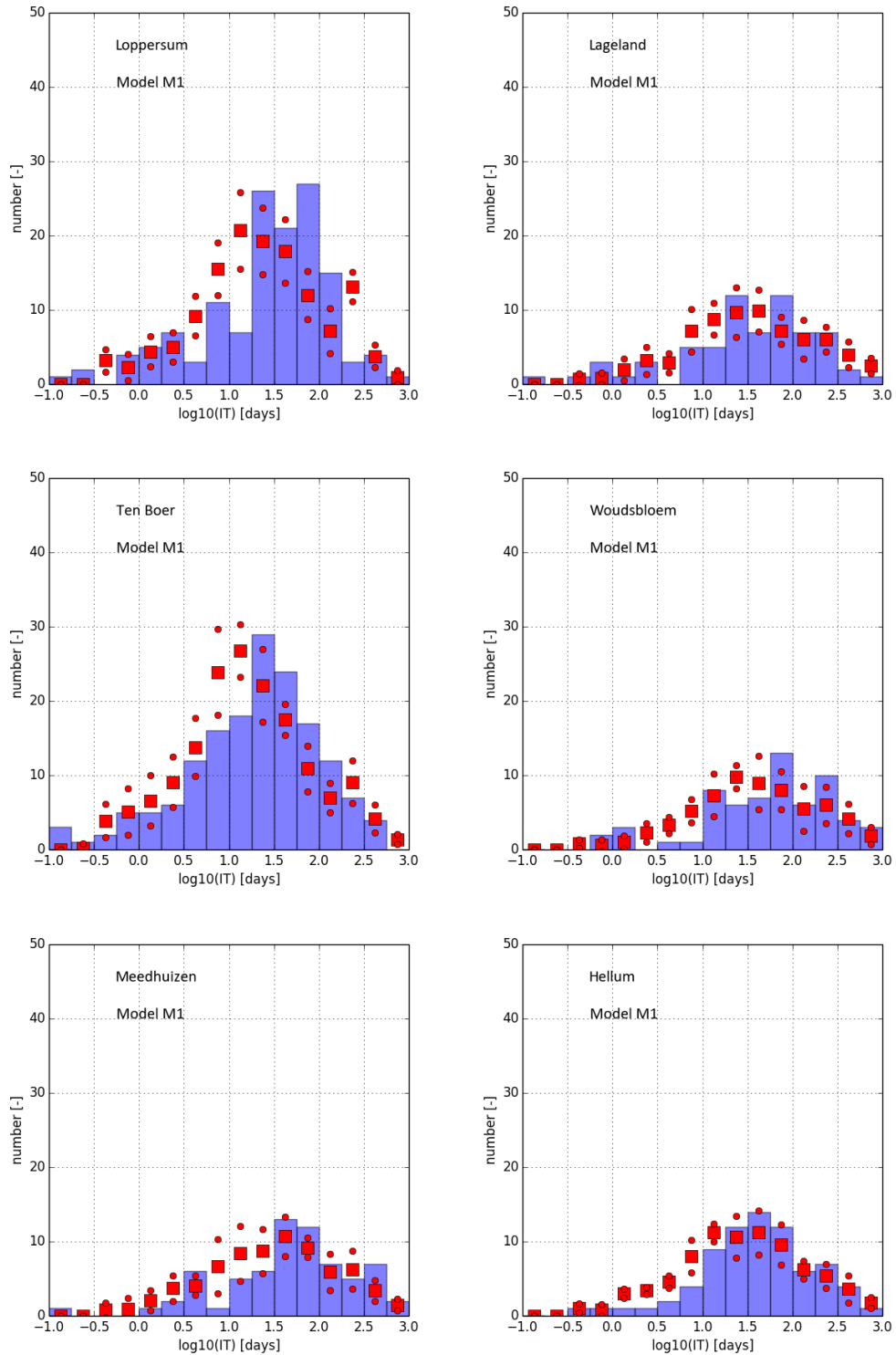


Figure A.6 : Observed and modelled interevent time distributions in the various regions in the Groningen field, using model M1.  $M_{min} = 1.0$ ,  $c_{M0} = 0$  in the period 1960 - 30 September 2015. Histograms of the logarithm of the interevent times of the observed tremors (blue bars) and the simulated tremors (red squares, mean value; red dots above and below  $\pm 1$  standard deviation from mean the value). The sum of the numbers in the 16 bins of the histograms is equal to the total number of tremors.

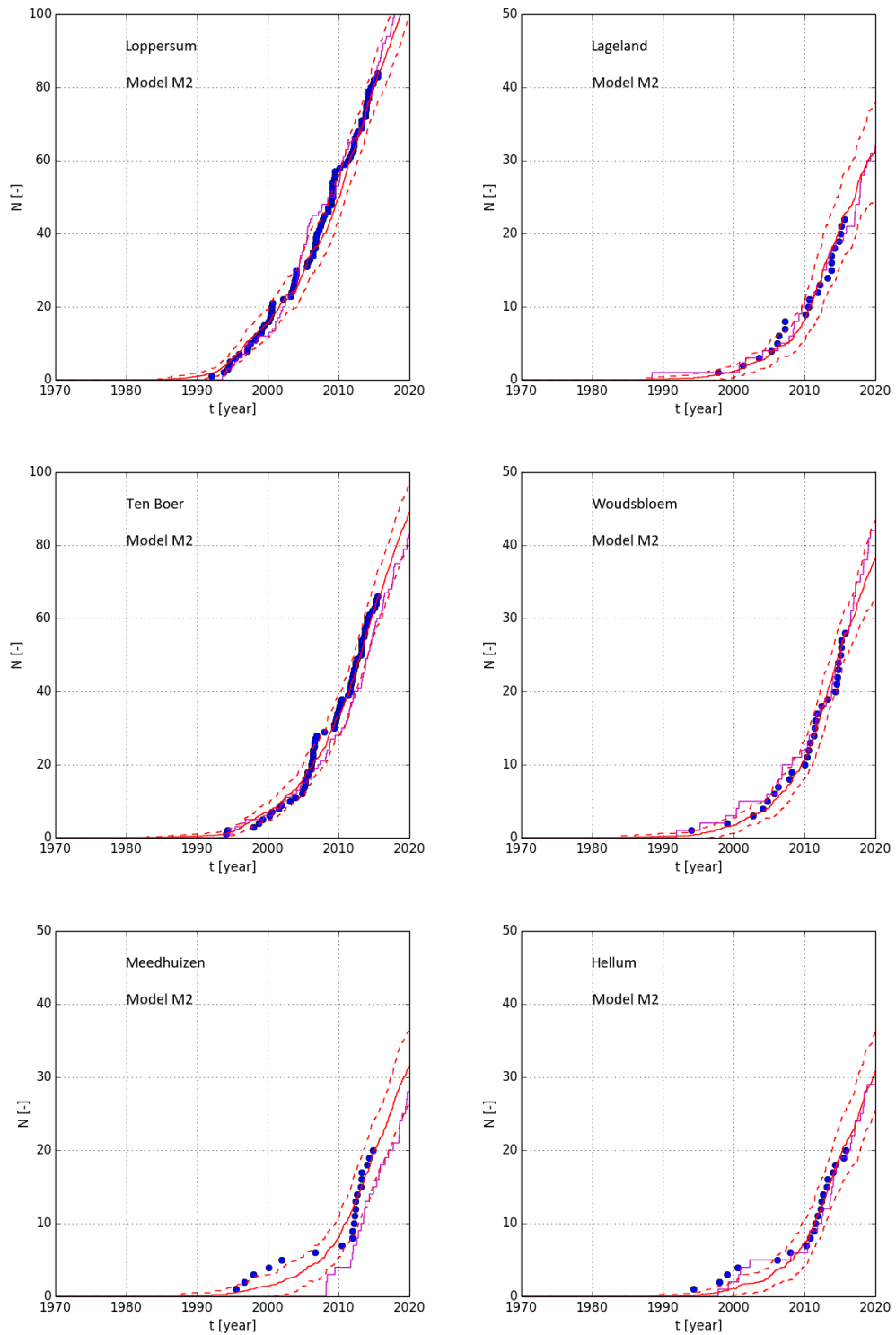


Figure A.7 : Number of observed and modelled tremors in the various regions in the Groningen field, using model M2.  $M_{min} = 1.5$ ,  $c_{M_0} = 0$ . Period of simulation 1960 - 2020. The number of observed tremors are given by the blue dots. The red solid line shows the mean value of 20 simulations. The red dashed lines show  $\pm 1$  standard deviation from the mean value. The purple solid line shows one simulation. Note that the vertical scale of the top and centre left figures is twice as large as of the other figures.

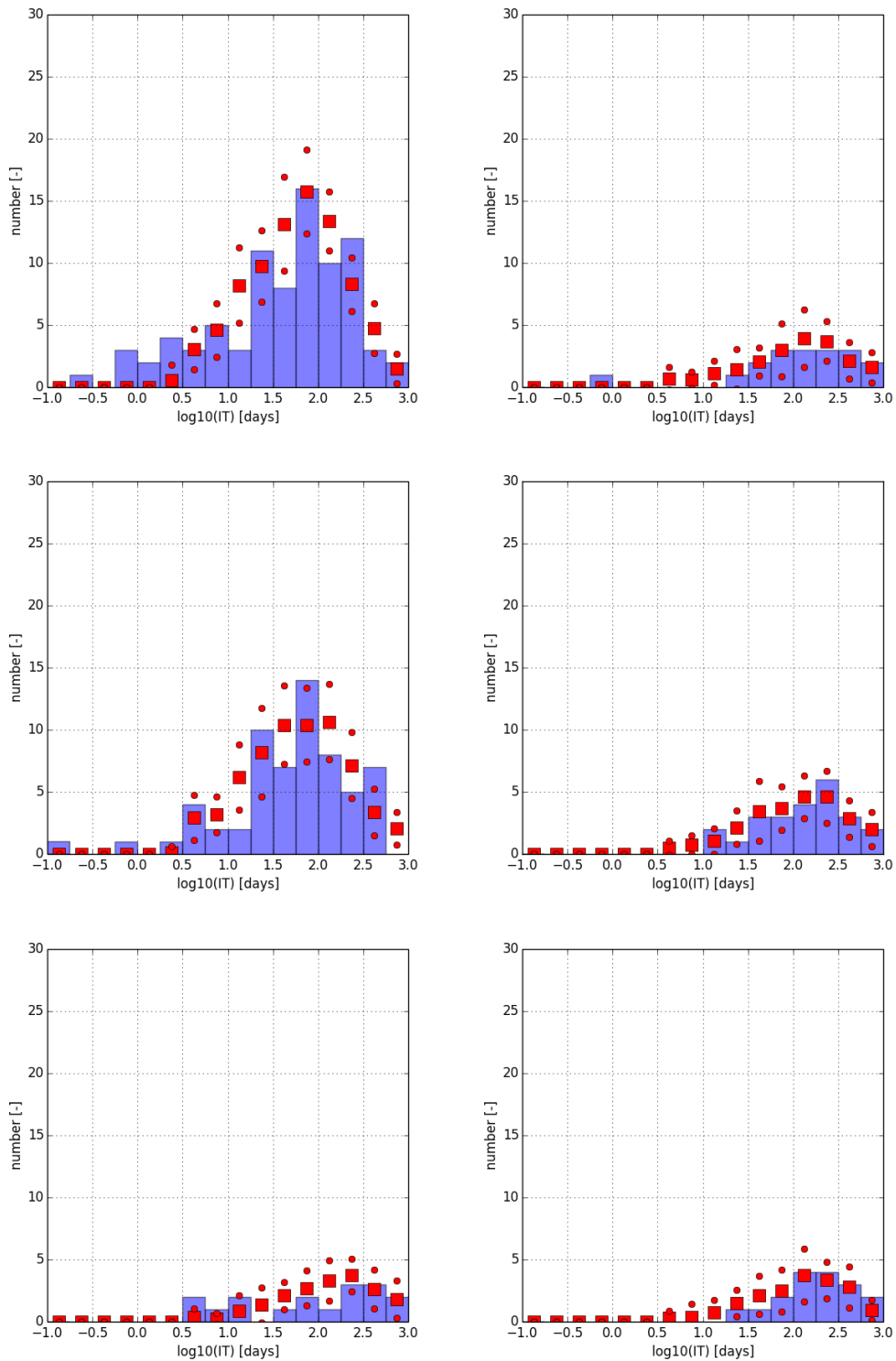


Figure A.8 : Observed and modelled interevent time distributions in the various regions in the Groningen field, using model M2.  $M_{min} = 1.5$ ,  $c_{M_0} = 0$  in the period 1960 - 30 September 2015. Histograms of the logarithm of the interevent times of the observed tremors (blue bars) and the simulated tremors (red squares, mean value; red dots above and below  $\pm 1$  standard deviation from the mean value). The sum of the numbers in the 16 bins of the histograms is equal to the total number of tremors.

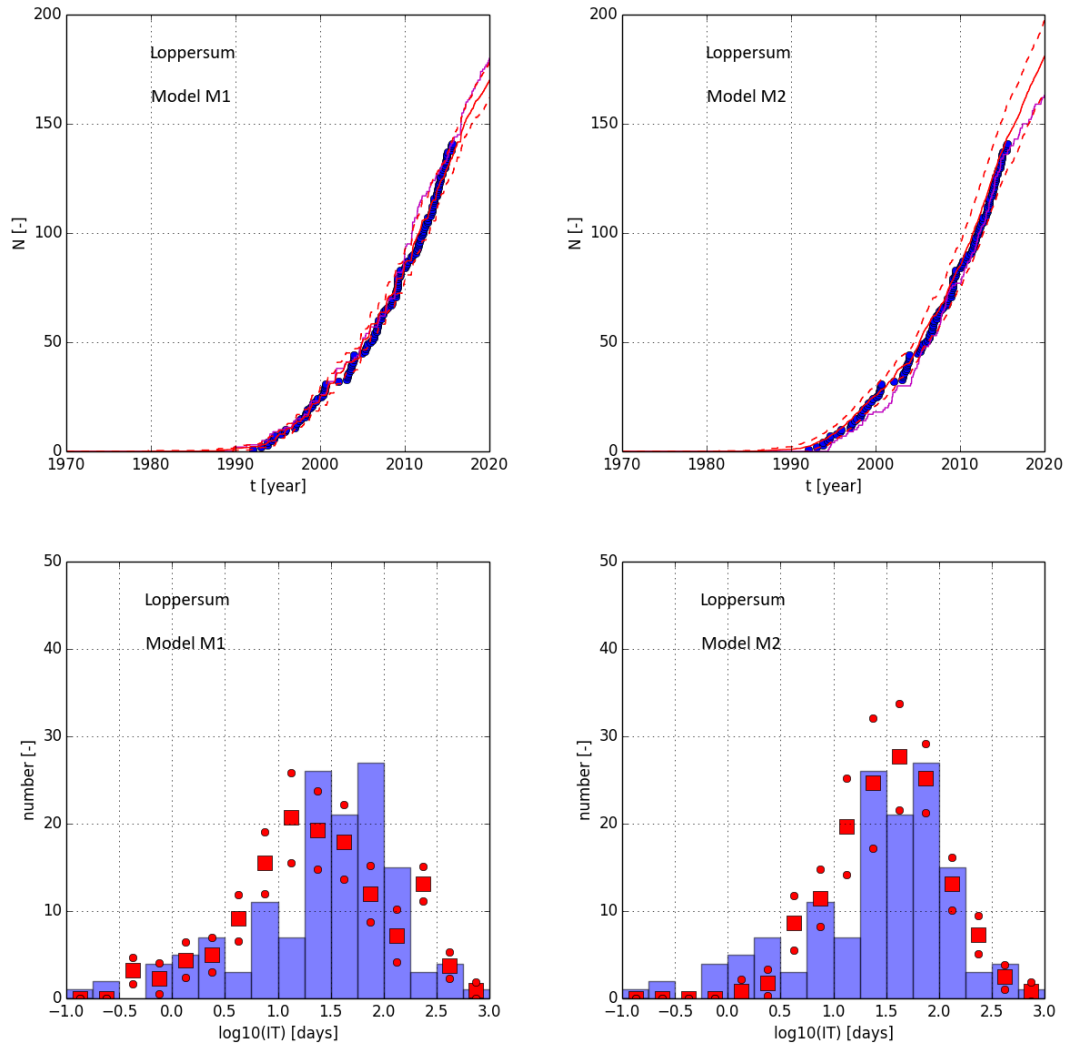


Figure A.9 : Region around Loppersum.  $M_{min} = 1.0$ ,  $c_{M_0} = 0$ . Period of simulation 1960 - 2020. Comparison between Model M1 (left figures) and model M2 (right figures).

Top: number of observed (blue dots) and modelled tremors. The red solid line shows the mean value of 20 simulations. The red dashed lines show  $\pm 1$  standard deviation from the mean value. The purple solid line shows one simulation.

Bottom: observed and modelled interevent times in the period 1960 - 30 September 2015. Histograms of the logarithm of the interevent times of the observed tremors (blue bars) and the simulated tremors (red squares, mean value; red dots above and below  $\pm 1$  standard deviation from mean the value). The sum of the numbers in the 16 bins is equal to the total number of tremors.

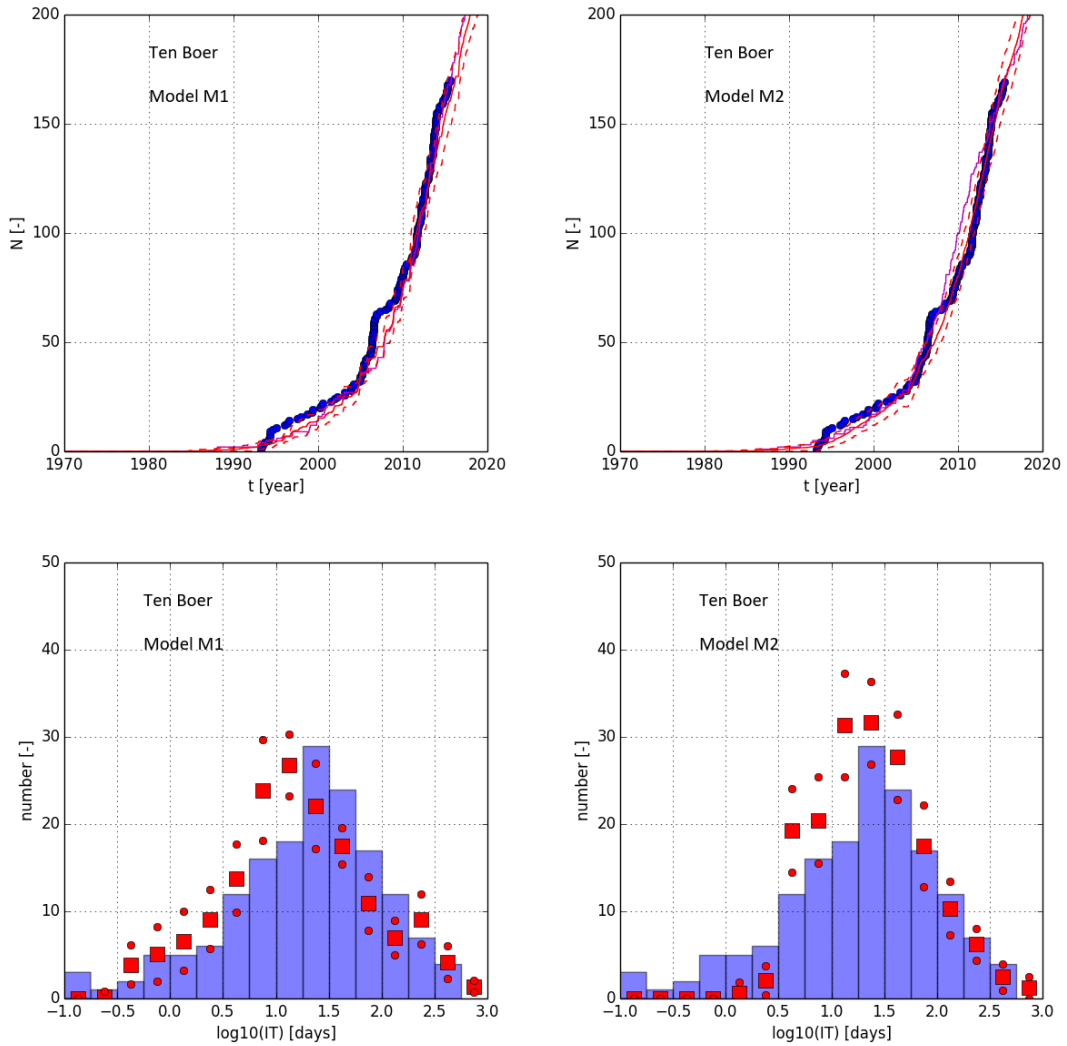


Figure A.10 : Region around Ten Boer.  $M_{min} = 1.0$ ,  $c_{M_0} = 0$ . Period of simulation 1960 - 2020. Comparison between Model M1 (left figures) and model M2 (right figures).

Top: number of observed (blue dots) and modelled tremors. The red solid line shows the mean value of 20 simulations. The red dashed lines show  $\pm 1$  standard deviation from the mean value. The purple solid line shows one simulation.

Bottom: observed and modelled interevent times in the period 1960 - 30 September 2015. Histograms of the logarithm of the interevent times of the observed tremors (blue bars) and the simulated tremors (red squares, mean value; red dots above and below  $\pm 1$  standard deviation from the mean value). The sum of the numbers in the 16 bins is equal to the total number of tremors.

The modelled distribution for model M2 shows a discontinuity around  $^{10}\log(IT) \sim 0.5$ . This is a numerical artifact due to the pressure interval chosen.

## Appendix A.3 Modified model M2 applied to the entire Groningen field

Figure A.11 shows the selected area as defined by the blue ellipse, which covers almost the entire Groningen field. Figure A.12 shows the number of tremors and histograms of the interevent times of model M2 for  $M_{min} = 1.0$  and  $M_{min} = 1.5$ . Table A.4 shows the fit parameters used. The number of steps and the reservoir pressure intervals have been varied.

For the same typical pressure change for fault failure  $\delta p_{fail}$  and Weibull distribution shape parameter  $k_W$ , we obtain good fits for the tremors as a function of time in all cases. Small steps are needed to reproduce the short interevent times. For these small steps, the shape factor  $\lambda_{PS}$  reduces less than proportional to the intervals taken.

Figure A.13 shows the dip and throw of the fault segments nearest to the hypocentres of the tremors or in the distance between subsequent tremors over time. We don't see a systematic change in these variables over time. Similar figures are obtained for the regions in the Groningen field.

Table A.4 : Fit parameters for the entire Groningen field for modified model M2. The Weibull distribution shape parameter and the stress relaxation parameter are for all simulations  $k_W = 13$  and  $c_{M_0} = 0$ , respectively. The number of time steps and reservoir pressure intervals have been varied. The  $M_{min} = 1.5$  catalogue contains about 50 tremors more than the one used by Bourne and Oates (2014).

Property	Symbol	Unit				
.....	.....	.....	.....	.....	.....	.....
number of time steps	$n_{step}$	-	50000	100000	200000	200000
pressure interval	$\delta p_{int}$	MPa	0.0002	0.0002	0.0002	0.0001
$M_{min} = 1.0$						
- number of observed tremors	$N_{obs}$	-	613			
- Poisson distr. shape parameter	$\lambda_{PS}$	Pa <sup>-1</sup>	0.11	0.060	0.042	0.028
- typ. pressure change for fault failure	$\delta p_{fail}$	MPa	22			
$M_{min} = 1.5$						
- number of observed tremors	$N_{obs}$	-	258			
- Poisson distr. shape parameter	$\lambda_{PS}$	Pa <sup>-1</sup>	0.047	0.026	0.017	0.012
- typ. pressure change for fault failure	$\delta p_{fail}$	MPa	22			

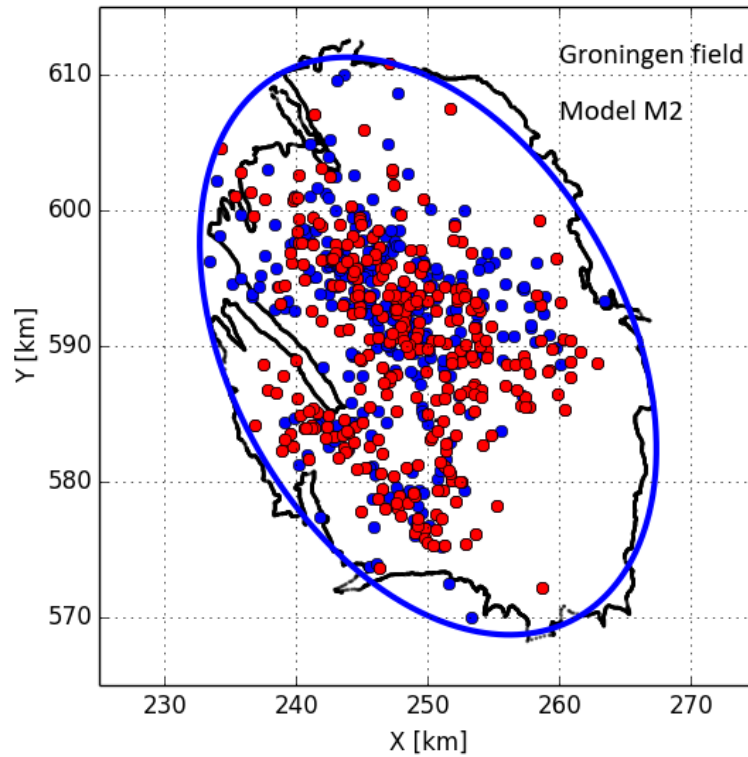


Figure A.11 : Selected area as defined by the blue ellipse (black contour), which covers almost the entire Groningen field. Tremors in the Groningen field for  $M_{min} = 1.5$  in this area. The X and Y coordinates of the centre of the ellipse are 250 and 590 km, respectively. The large and small radii of the ellipse are 23 and 15 km, respectively. The angle between the long axis and the north direction is -30 degrees. The blue and red dots show the observed tremors in the periods before and after 1 January 2010, respectively.

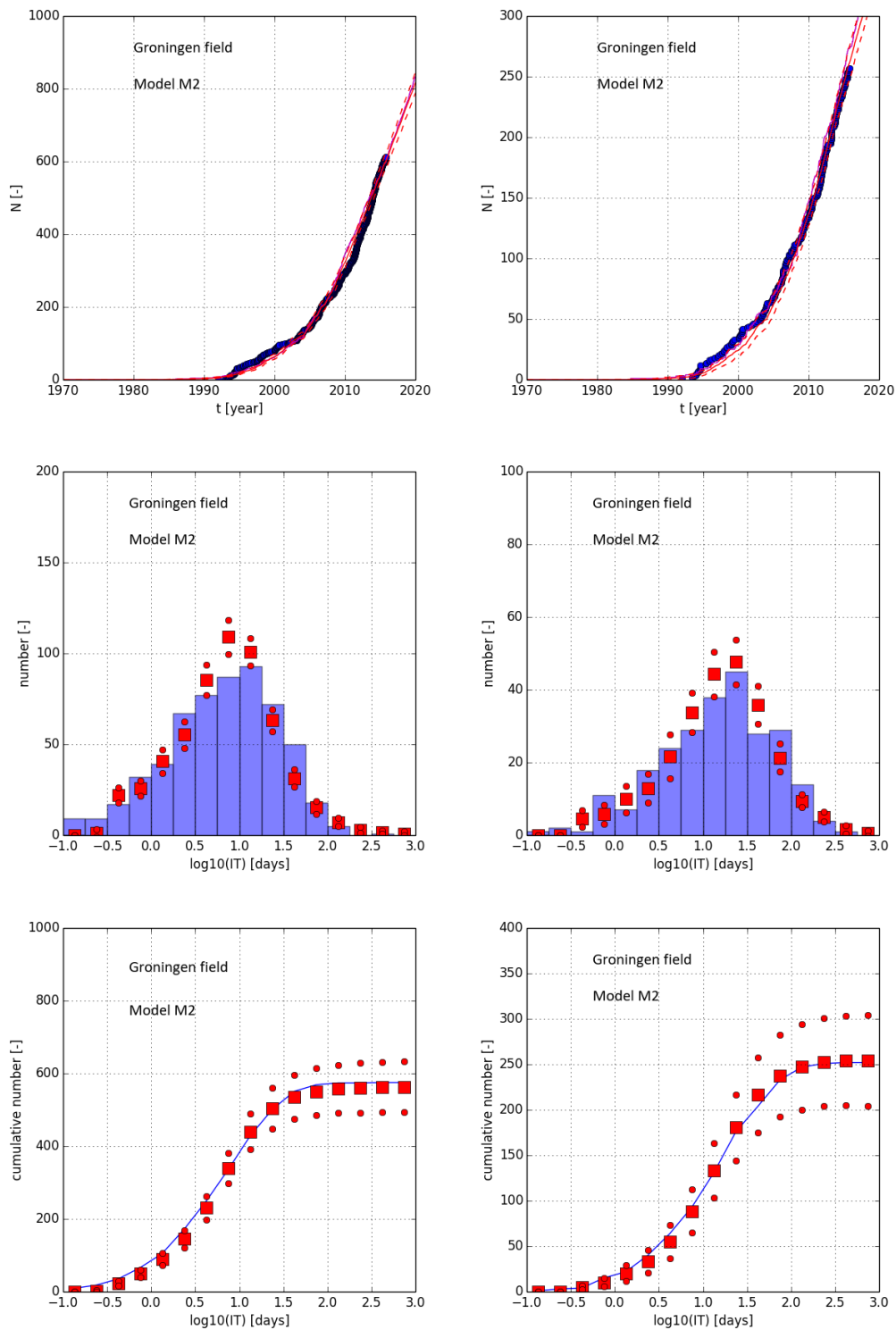


Figure A.12 : Top figures: number of observed (blue dots) and modelled tremors in the entire Groningen field for  $M_{min} = 1.0$  (left) and  $M_{min} = 1.5$  (right). Period of simulation 1960 - 2020 in 100000 timesteps. The red solid line shows the mean value of 20 simulations. The red dashed lines show  $\pm 1$  standard deviation from the mean value. The purple solid line shows one simulation.

Centre and bottom figures: observed and modelled interevent time distributions of the observed tremors for  $M_{min} = 1.0$  (left) and  $M_{min} = 1.5$  (right) in the period 1960 - 30 September 2015. Histograms of the logarithm of the interevent times of the observed tremors (blue bars) and the simulated tremors (red squares, mean value; red dots above and below  $\pm 1$  standard deviation from the mean value). The sum of the numbers in the 16 bins is equal to the total number of tremors.

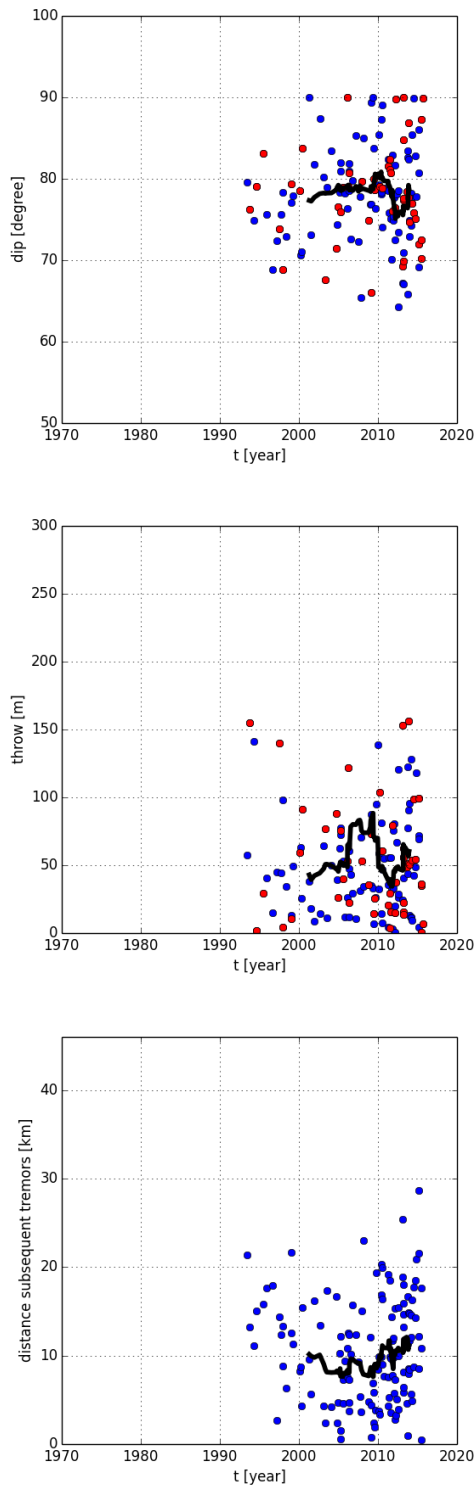


Figure A.13 : Dip (top) and throw (center) of faults most close to the hypocentres of the tremors and the distance between subsequent tremors (bottom) over time for the Groningen field. Period of simulation 1960 - 2020. In the top and center figures, the blue dots are for the range  $1.0 \leq M < 2.5$ , the red dots are for the range  $2.5 \leq M < 4.0$ . All hypocentres farther away than 0.3 km from a fault have been rejected. The black lines show moving averages of 20 data points using all data. We don't see systematic changes in the moving averages. Similar figures can be produced when rejecting hypocentres away from a fault segment, farther than 0.1 km or 0.5 km.

## Appendix A.4 Fit function for $c_{PS}$

For a Probabilistic Seismic Hazard Analysis (PSHA), the area of interest is divided into regions or zones where the distribution of events and their characteristics is assumed to be uniform. The resulting tremor density map is sometimes called a ‘heat map’. For the Groningen field, this non-uniform density map is rather smooth, see Dost and Spetzler (2015). Comparing this map with those of the observed ground subsidence or underlying reservoir compaction, the local tremor rate has been correlated to the local reservoir compaction, see Bourne et al. (2014).

Like model M2, model M1 can reproduce the total observed tremors as a function of time and the observed interevent time distribution in the entire field or in regions of interest. In the following we show whether we can also reproduce the spatial distribution of the tremors over the Groningen field with model M1 by choosing a fit function for  $c_{PS}(x)$  [ $\text{Pa}^{-1}$ ] which depends on the reservoir compaction in the field.

The reservoir compaction data used is over the period between 1972 and 2015. It is shown in Appendix C, §C.1, Figure C.11. It is calculated from subsidence data by Bierman and Kraaijeveld (2015). Assuming that the Weibull distribution shape parameter  $k_W$  and the typical change in reservoir pressure for seismic fault failure  $\delta p_{fail}$  are constant over the Groningen field, the number of tremors in a small subregion of the field is now proportional to the Poisson distribution shape parameter  $\lambda_{PS}(x)$  and herewith to  $c_{PS}(x)$ .

Dividing the Groningen field in square cells of  $2 \times 2$  km, we calculate for each cell the mean reservoir compaction in this cell and populate the entire field with tremors, see Figure A.14. The total number of modelled tremors is equal to the total number of observed number of tremors in the selected catalogue. The probability that a tremor occurs in a certain cell is only a function of the reservoir compaction. The hypocentres of the tremors in a cell are uniformly distributed over the cell area. Finally, we calculate for the modelled tremors the spatial distribution function and compare this with the observed one.

To obtain a reasonable correspondence between the modelled and observed spatial distributions,  $c_{PS}(x)$  must be a steep function of the reservoir compaction  $c(x)$ . For example, Figure A.15 shows the result of using a power law function  $c_{PS}(x) \propto c(x)^n$  where<sup>3</sup>  $n = 6$ . The modelled spatial distribution of tremors over the field differs from the observed distribution. In particular, the model systematically overpopulates the regions south-west and north-east of Loppersum. Note that the calculated compaction in the north-east part

---

<sup>3</sup>Another option to generate a similar spatial distribution would follow from using  $\delta p_{fail}$  as a function of  $c$  and  $c_{PS} \propto c$  (or constant). Since the Weibull distribution shape parameter  $k_W$  is large, the relative likelihood of a tremor following from the Weibull distribution function depends strongly on the failure criterion variable  $\eta = \delta p / \delta p_{fail}$  and herewith on  $\delta p_{fail}$ . Using this option, the functional form for the probability of a tremor gets a similar appearance as the expression that follows from the model of Bourne et al. (2014).

of the field is not well constrained by subsidence data.

We have not been able to resolve the differences between modelled and observed tremor distributions by using another function for  $c_{PS}(c(x))$ . Without improving the results, we have repeated this exercise using subsidence data instead of the compaction data and including the reservoir thickness in a function for  $c_{PS}$ . Likely, other field or fault properties influence the spatial distribution of the tremors in the Groningen field.

Bourne and Oates (2015) have included the reservoir offset (or fault throw data) in the activity rate model to improve the spatial distribution of modelled tremors in the Groningen field<sup>4</sup>. So far, we have not included local averages of fault offsets or other fault properties in  $c_{PS}(c(x))$  since we don't observe clear differences in the histograms for fault density, fault dip and fault throw for the different regions of interest, see Wentinck (2015), Appendix C.

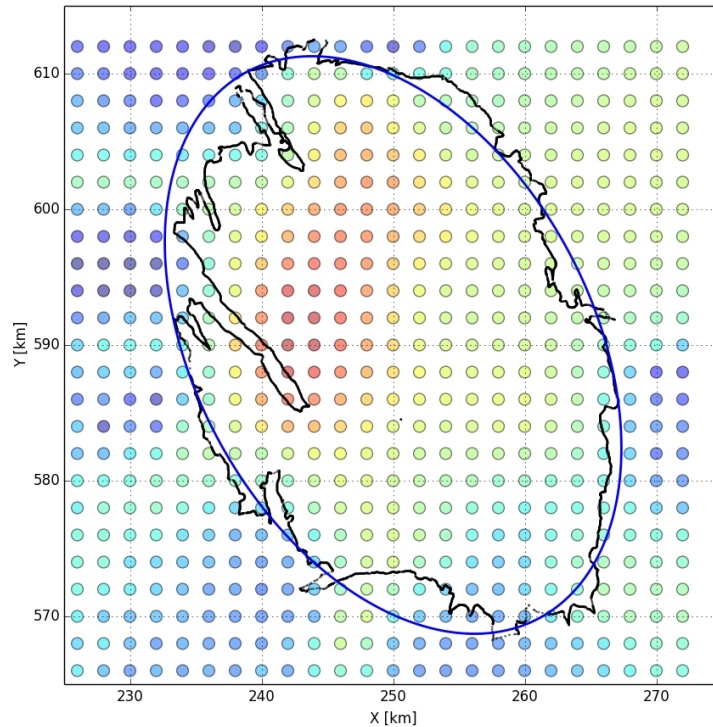


Figure A.14 : Mean reservoir compaction in the  $2 \times 2$  km square grid cells over the Groningen field over the period 1972 - 2015. The black contour line shows the Groningen field. The blue ellipse shows the part of the Groningen field used in the calculations.

<sup>4</sup>Actually, they have used the local gradient of the top of the reservoir.

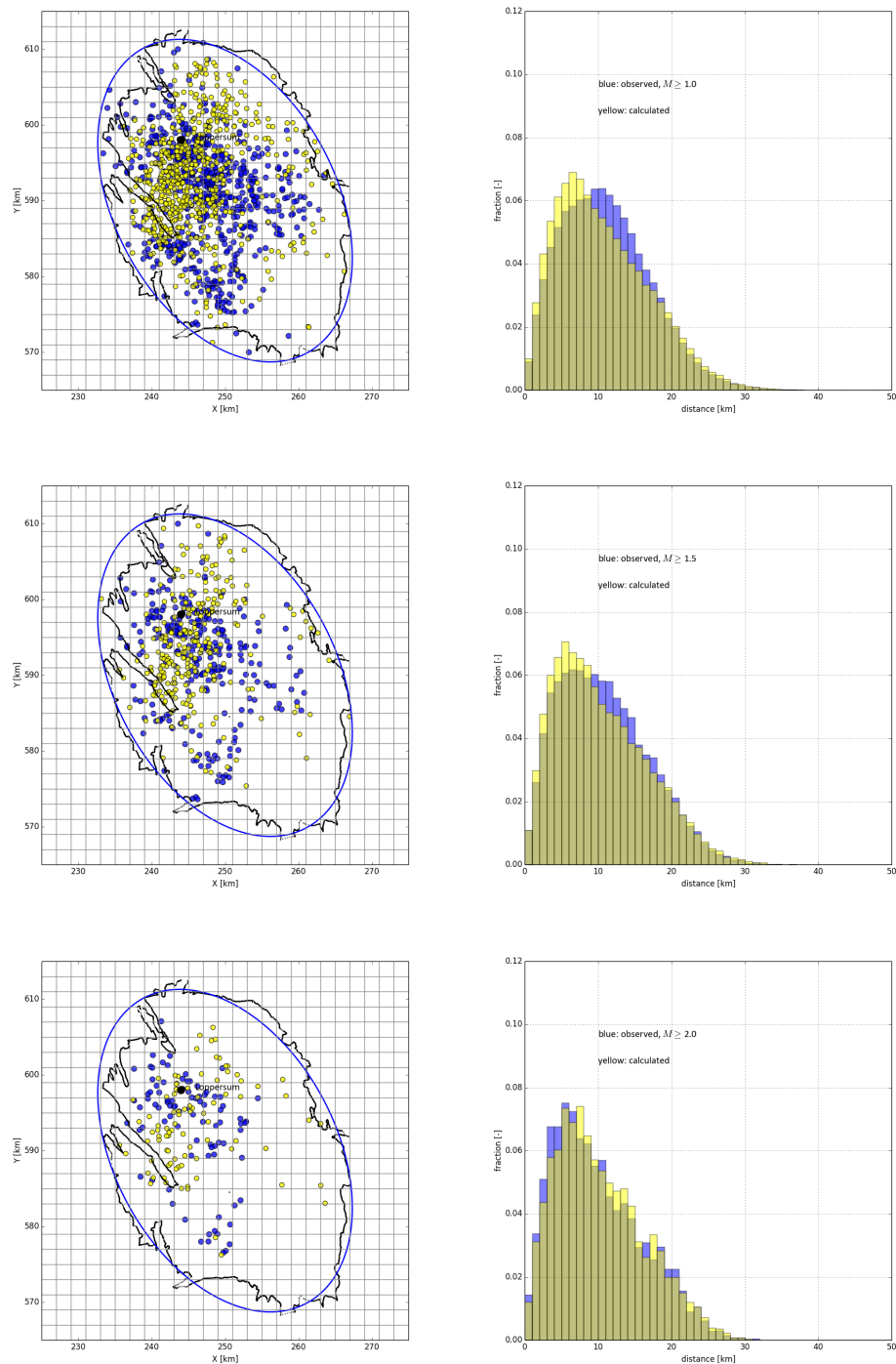


Figure A.15 : Spatial distribution of observed and modelled tremors (left figures) and histograms of these distributions (right figures) in the Groningen field for  $M_{min} = 1.0$  (top, 612 tremors),  $M_{min} = 1.5$  (center, 257 tremors) and  $M_{min} = 2.0$  (bottom, 89 tremors). The blue and yellow dots show the observed and modelled tremors, respectively. The black dot shows the center of the Loppersum region. Similar results are obtained using square grid cells of  $3.3 \times 3.3$  km. In the histograms: the blue bars show the normalised spatial distribution of all observed tremors; the yellow bars show the normalised spatial distribution of modelled tremors. The brown colour appears where the yellow bars overlay the blue bars.

The regions south-west and north-east of Loppersum are systematically overpopulated with tremors by this model.

## Appendix A.5 Additional simulations for the Roswinkel field

Since the fundamental mismatch between the modelled and observed tremor rate is not relieved by using catalogues with  $M_{min} = 1.5$  or  $M_{min} = 2.0$ , we only show additional modelled data for the catalogue with  $M_{min} = 1.0$ . Also, the mismatch cannot be solved by using a non-zero stress relaxation parameter  $c_{M_0}$  or using a smaller pressure interval  $\delta p_{int}$ . So, we keep  $c_{M_0} = 0$  and  $\delta p_{int} = 0.01$  MPa.

Table A.5 shows the fit parameters of additional simulations for the Roswinkel field using modified model M2. Figure A.16 shows the results. Reducing the parameter for the typical change in the reservoir pressure for failure  $\delta p_{fail}$ , this leads to more tremors but also to an earlier onset of the sharp rise of tremors than observed. It is uncertain how much this onset would cover possibly undetected tremors prior to 1995.

Figure A.17 shows the cdf of the log of number of tremors versus the lower limiting magnitude  $M_{lim}$ . A line through the data points would show a clear kink around  $M = 2.5$ , which is an indication for an incomplete catalogue with  $M_{min} = 1.0$ . The few data points for larger tremors suggest a b-value of about 1.

It is questionable whether the original model, as explained in Wentinck (2015), would perform better. Although this model generates tremors once a critical stress state is reached, it must also incorporate a non-zero stress relaxation parameter  $c_{M_0}$  to explain a reduction of the tremor rates when production stops like in the Annerveen and Eleveld fields. To reproduce to some extent the Roswinkel tremor rate, one needs to tune  $c_{M_0}$  unnaturally precisely to stop the tremor rate after 2006.

Table A.5 : Fit parameters for the Roswinkel for the modified model M2 for  $M_{min} = 1.0$ . The radius of the region is 5 km. The Weibull distribution shape parameter  $k_W = 13$ . Mean stress relaxation by tremors is disregarded. Hence, the stress relaxation parameter  $c_{M_0} = 0$ .

Property	Symbol	Unit	case I	case II	case III
.....	.....	.....	.....	.....	.....
Poisson distr. shape parameter	$\lambda_{PS}$	Pa <sup>-1</sup>	0.07	0.07	0.21
typ. pressure change for fault failure	$\delta p_{fail}$	MPa	31.5	28.7	28.7

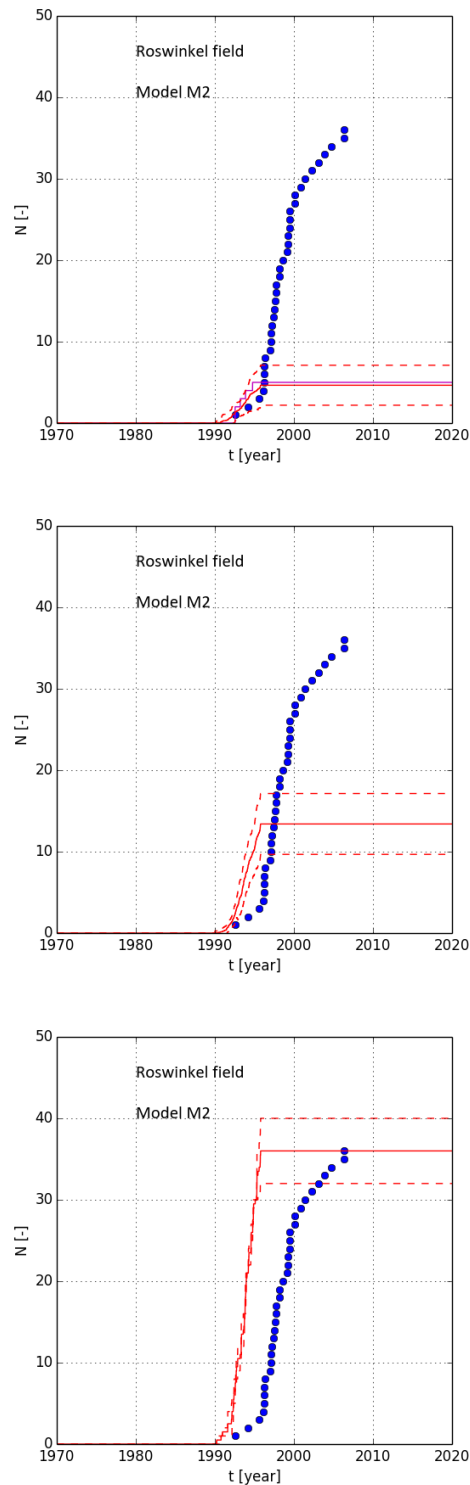


Figure A.16 : Number of observed and modelled tremors in the Roswinkel field, using model M2.  $M_{min} = 1.0$ ,  $c_{M_0} = 0$ . From top to bottom: case I, II and III.

The number of tremors can only be increased by increasing the value of  $\lambda_{PS}$  or by decreasing the value of  $\delta p_{fail}$ . The consequence is that the sharp increase of the tremor rate starts years earlier than observed.

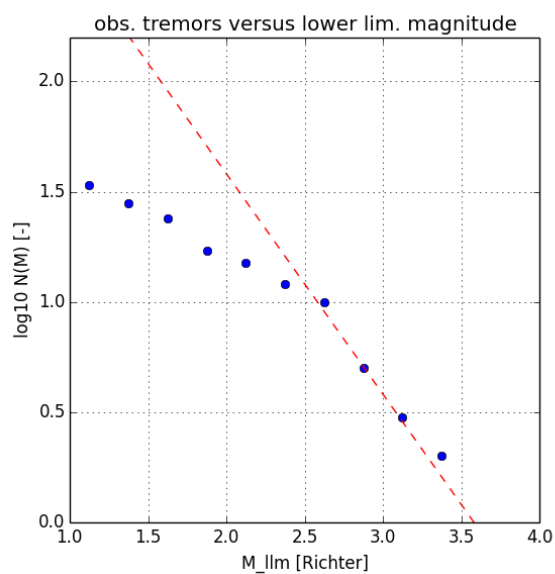


Figure A.17 : Cdf of log of number of tremors versus lower limiting magnitude  $M_{lim}$  for the Roswinkel field catalogue  $M_{min} = 1.0$ . The bins are  $0.25 M$ . Dashed line  $b = 1$ . A line through the data points would show a clear kink around  $M = 2.5$ , an indication for an incomplete catalogue with  $M_{min} = 1.0$ .

# Appendix B

## Reservoir pressure interval and time step

Too large pressure intervals or time steps lead to unrealistic interevent time distributions. Due to the numerical implementation of the Monte Carlo simulation<sup>1</sup>, interevent times of more than one tremor in a single small pressure interval are equally distributed over this interval instead of randomly distributed. Depending on the number of tremors and reservoir pressure transient, it must be verified whether the pressure interval or time step is adequate.

For modified model M2, Table B.1 shows the effect of the time step and reservoir pressure interval on  $\lambda_{PS}$  for the region around Loppersum. For a substantial range of reservoir pressure intervals,  $\lambda_{PS}$  is proportional to the chosen reservoir pressure interval, as expected. This proportionality holds over a larger range the time steps are smaller.

Figure B.1 shows the effect of the pressure interval on the interevent time histograms. The reproduction of the distribution for short interevent times clearly improves with a smaller pressure interval while the curves of the number of tremors over time are the same for all cases.

For modified model M1, the fit parameter  $c_{PS}$  is proportional to the number of time steps in a certain period or inversely proportional to the time step in the same range as for the modified model M2.

The reservoir pressures in the gas production well clusters includes small seasonal variations. In the surrounding area these fluctuations smooth out by pressure diffusion. At this stage, it is not clear how much these fluctuations influence the tremor rate in the regions of interest. For this reason we have smoothened the raw reservoir pressure data with a moving average filter. The moving average is over 20 data points taken each month, i.e. over a period of about 1.5 year. The effect of smoothening these seasonal pressure fluctuations have an effect on the distribution of interevent times. For modified model M2,

---

<sup>1</sup>The simulation is done in Python. We make use of arrays of fixed length.

this is shown in Figure B.1 . A small seasonal peak appears in the simulated histogram.

Table B.1 : Effect of the reservoir pressure interval on the fit parameter  $\lambda_{PS}$  for the region around Loppersum for modified model M2. Three different time steps are used over the period 1960 - 2020. The reservoir pressure data has been smoothened using a moving average over a number of data in proportion to the time steps taken. The fit parameters  $k_W = 13$  and  $\delta p_{fail} = 20$  MPa yield acceptable fits for all reservoir pressure intervals and time steps. The stress relaxation parameter  $c_{M_0} = 0$ .

$M_{min}$ Richter	$\delta p_{int}$ MPa	$\lambda_{PS}$ -
.....		
100000 time steps		
1.0	0.001	0.027
1.0	0.01	0.19
1.0	0.1	1.9
1.0	0.5	9.5
1.0	1.0	19
50000 time steps		
1.0	0.001	0.032
1.0	0.002	0.053
1.0	0.01	0.20
1.0	0.02	0.40
1.0	0.1	1.9
1.0	0.5	9.4
1.0	1.0	16
1.5	0.001	0.021
1.5	0.01	0.13
1.5	0.1	1.2
1.5	0.5	6.3
1.5	1.0	13
10000 time steps		
1.0	0.001	0.16
1.0	0.01	0.32
1.0	0.1	2.3
1.0	0.5	9.1
1.0	1.0	17

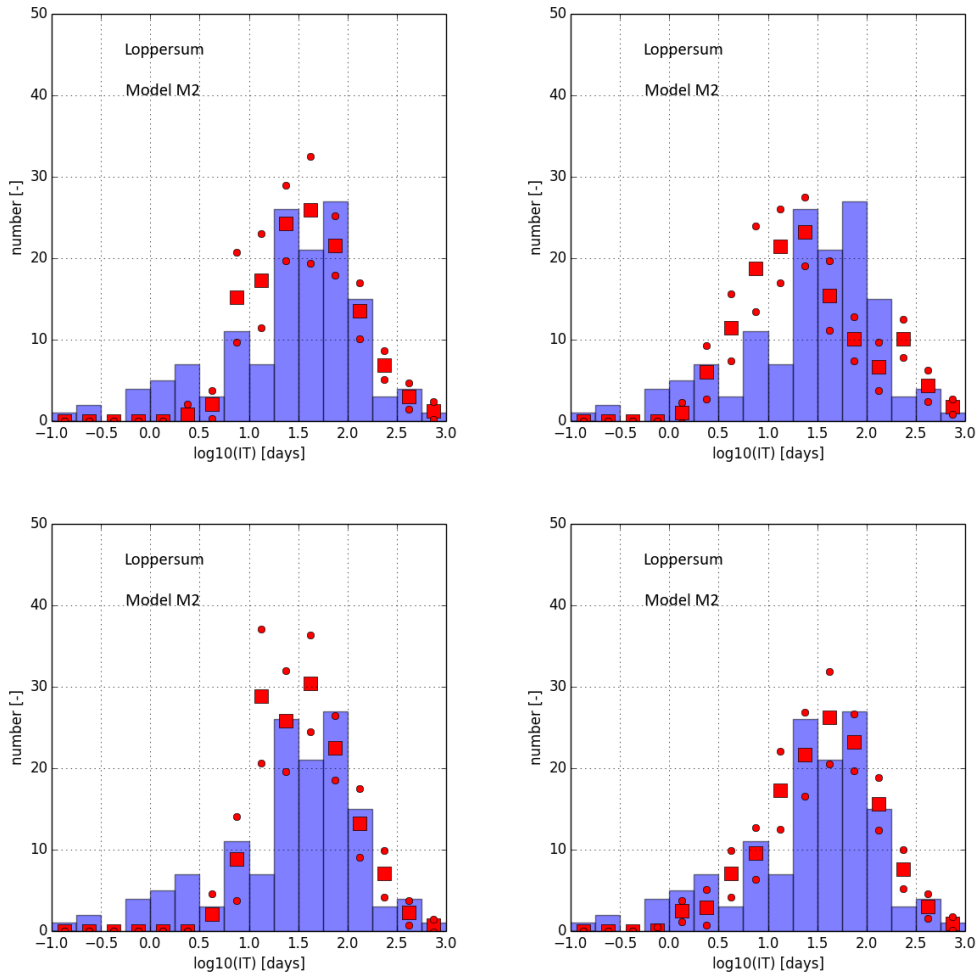


Figure B.1 : Region around Loppersum.  $M_{min} = 1.0$ ,  $c_{M_0} = 0$ . Effect of the size of the pressure interval and smoothness of the reservoir pressure proxy on the histograms of the interevent times of the observed tremors (blue bars) and the simulated tremors (red squares, mean value; red dots above and below  $\pm 1$  standard deviation from mean the value). The number of time steps (of about 0.5 day) is 50000.

The top figures are for a pressure interval of 0.01 MPa. The left top figure is for the actual reservoir proxy. The right top figure is for a smoothed reservoir proxy using a moving average of 20 time steps (of 10 days). The bottom figures are for a pressure interval of 0.02 and 0.002 MPa, respectively. The sum of the numbers in the 16 bins is equal to the total number of tremors.

When the pressure interval is too large, the left bottom figure shows that the simulated interevent time distribution does not capture the observed short interevent times. The top right figure shows a small seasonal peak in the histogram when the reservoir pressure proxy in the Leermens gas production well cluster is not filtered as is shown by the black curve in Appendix D, Figure D.1 .

# Appendix C

## Field data

### Appendix C.1 Detailed maps

The  $\sim 40 \times 40$  km Groningen field has numerous faults with various reservoir offsets and fault dips. The reservoir thickness varies from about 100 m in the south-east to about 350 m in the north-west and the reservoir compaction has varied over the period 1964 - 2008 from 0.15 m in the south-east of the field to about 0.30 m in the centre of the field. The mean uniaxial compression coefficient  $C_m$  is of the order  $10^{-4}$  MPa $^{-1}$ . The well cluster and fault data used originates from NAM.

Figures C.1 - C.8 below show detailed maps of the faults and hypocentres of the tremors in the Groningen field and of the hypocentres in the other fields. The mean distance between the faults in the Groningen field is of the order of 1 km $^1$ .

For a number of tremors, the hypocentres are not mapped on the plotted faults. Still, we assume that most if not all tremors originate from fault failure for the following reasons. Firstly, the shown set of faults is incomplete. Likely, a number of faults have not been identified by seismics. From a statistical analysis of the number of faults with different fault throws, it can be expected that a considerable number of faults with throws in the range 30 - 70 m have not been found, see Mallik (2015). Further, not all the faults that could have been derived from seismics have been included in the fault data file $^2$ . The second reason is that the location of the observed tremors is not accurately known. It may even exceed the 500 m uncertainty circle around the location designated by the KNMI $^3$ .

---

$^1$ The typical fault distance in a region  $D_f$  [m] can be calculated from  $D_f = c_f S_{area} / L_f$  where  $c_f$  [-] is a geometric constant depending on the azimuth angle and the distribution of the faults and  $S_{area}$  [m $^2$ ] is the surface area of the region, see Wentinck (2015), Appendix D. For  $c_f = 2$  and  $S_{area} = 78$  km $^2$ ,  $D_f$  1 - 2 km.

$^2$ Another processing of the top reservoir horizon PETREL $^{TM}$  data shows a much higher density of faults with small throws which could be mapped on the tremors, according to Energiebeheer Netherlands, EBN, presentation to NAM october 2015.

$^3$ According to Kraaijpoel and Dost (2013), the typical accuracy of the tremor hypocentre location is in the order of 1 km in the horizontal plane.

Histograms for fault dip, throw and azimuth angle for the regions of interest in the Groningen field can be found in Wentinck (2015), Appendix C. There are no significant differences in these histograms for tremor-rich and tremor-poor regions.

We have reprocessed two histograms in this report because of a more accurate transformation of the longitude and latitude data to the  $X$  and  $Y$  coordinates used for the tremors after 11 February 2014, see also Appendix. Figure C.9 shows the histograms for the fault dip and fault throw of fault segments which are closest to the hypocentres of the strongest tremors with  $M \geq 2.5$ . Uncertainty in the location of the tremors is included by adding to the  $X$ - and  $Y$ -coordinates of the locations of the tremors a random number from a normal distribution with a mean value and standard deviation of 0 km and 0.5 km, respectively.

Again, according to these histograms, strong tremors evolve from areas close to or along fault segments with a throw of about 100 m and a dip angle of about  $65^\circ$ . Repeating this exercise for a lower limiting magnitude for the ‘strongest’ tremors, the peaks in the histograms become less pronounced. Remarkable is that the strong tremors near West-eremden at 8 August 2006 with magnitude 3.5 and near Huizinge in the Loppersum region at 14 April 2009 and 16 August 2014 with magnitudes  $M = 2.6$  and  $M = 3.6$  are in an area where faults have a small throw of less than 50 m, see also Dost and Kraaijpoel (2013).

Figure C.10 shows subsidence data over the period 1972 - 2008 determined from ground level meters. In this period, the reservoir pressure decreased from about 35 MPa to about 12 MPa, almost uniformly over the field. Figure C.11 shows the reservoir compaction data. The reservoir compaction has been calculated from the subsidence data by Bierman and Kraaijeveld (2015). Because of little subsidence data in the north-east part of the Groningen field, the calculated reservoir compaction in this part of the field is not well constrained. The ‘bowl’ of reservoir compaction is more pronounced than the ‘bowl’ of subsidence. Figure C.12 shows the reservoir thickness which gradually increases from about 100 m in the south-east to about 350 m in the north-west. The data in these figures originates from the Nederlandse Aardolie Maatschappij (NAM).

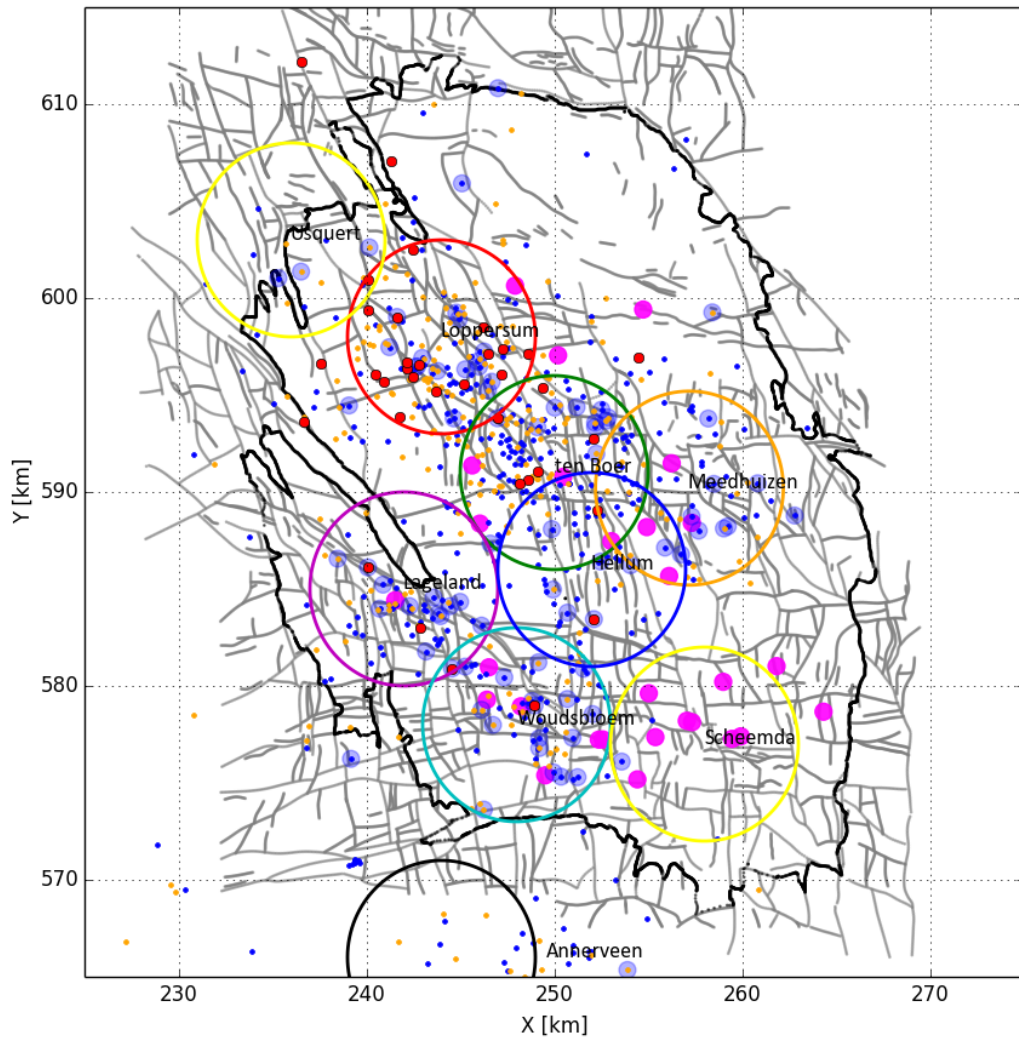


Figure C.1 : Overview of faults and hypocentres of tremors in the Groningen field according to KNMI and NAM data. The faults are shown as grey lines. The regions of interest in the Groningen field are shown by circles of 5 km radius. They are around Loppersum (red), Ten Boer (green), Lageland (magenta), Woudsbloem (cyan), Meedhuizen (orange) and Hellum (blue). The regions around Scheemda and Usquert (yellow circles) have almost no tremors.

The hypocentres of the tremors are shown by the coloured dots. The colours correspond to the magnitude of the tremors in the following ranges on the scale of Richter: blue for  $1.0 \leq M < 1.5$ , orange for  $1.5 \leq M < 2.5$  and red for  $2.5 \leq M < 4$ . Note that not all faults with throws less than about 80 m and tremors below  $M = 1.5$  have been captured. The light-blue dots show the tremors that have been measured after 23 March 2014. This date has been considered by the Centraal Bureau for Statistics (CBS), Netherlands as a trend break in subsidence and tremor rate, see Pijpers (2014a) and Pijpers (2014b). The magenta dots show the gas production well cluster locations according to Table D.1 in Appendix D.

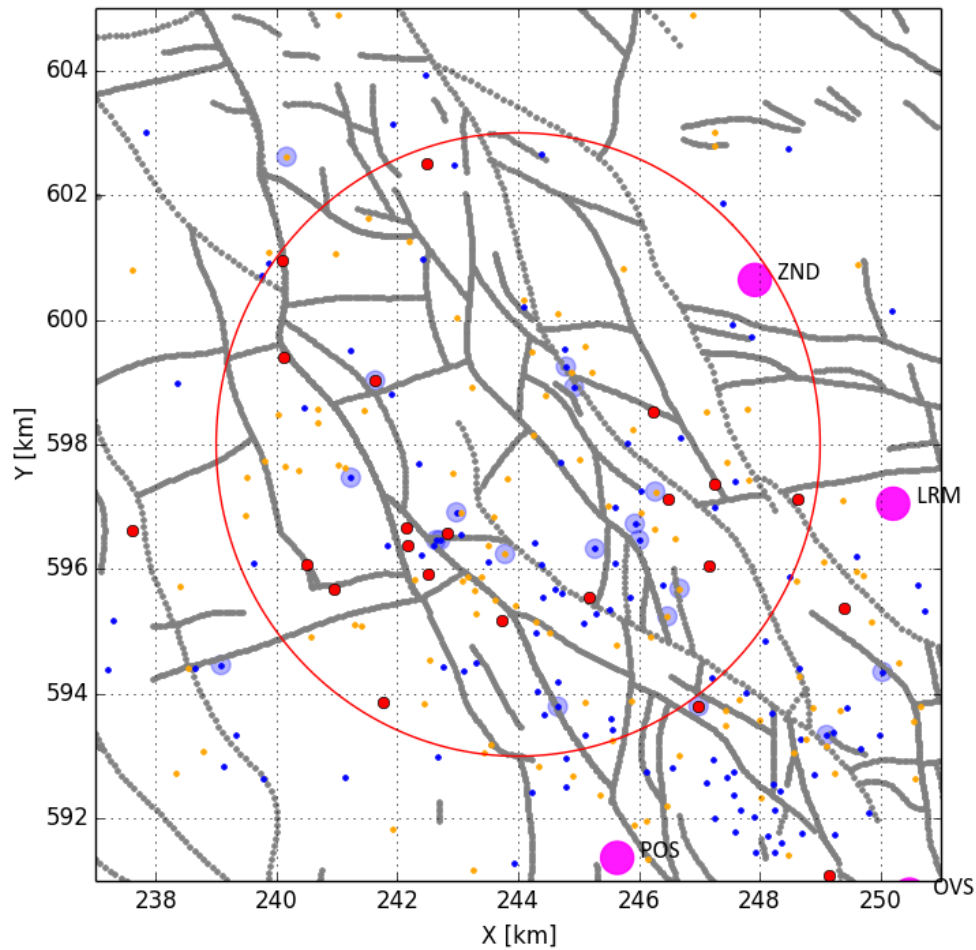


Figure C.2 : Faults and hypocentres of tremors around Loppersum according to KNMI and NAM data. The grey lines show the faults. The region of interest is shown by the circle of 5 km radius. The hypocentres of the tremors are shown by the coloured dots. The colours correspond to the magnitude of the tremors in the following ranges on the scale of Richter: blue for  $1.0 \leq M < 1.5$ , orange for  $1.5 \leq M < 2.5$  and red for  $2.5 \leq M < 4$ . The light-blue dots show the tremors that have been measured after 23 March 2014. The magenta dots show the production well cluster locations.

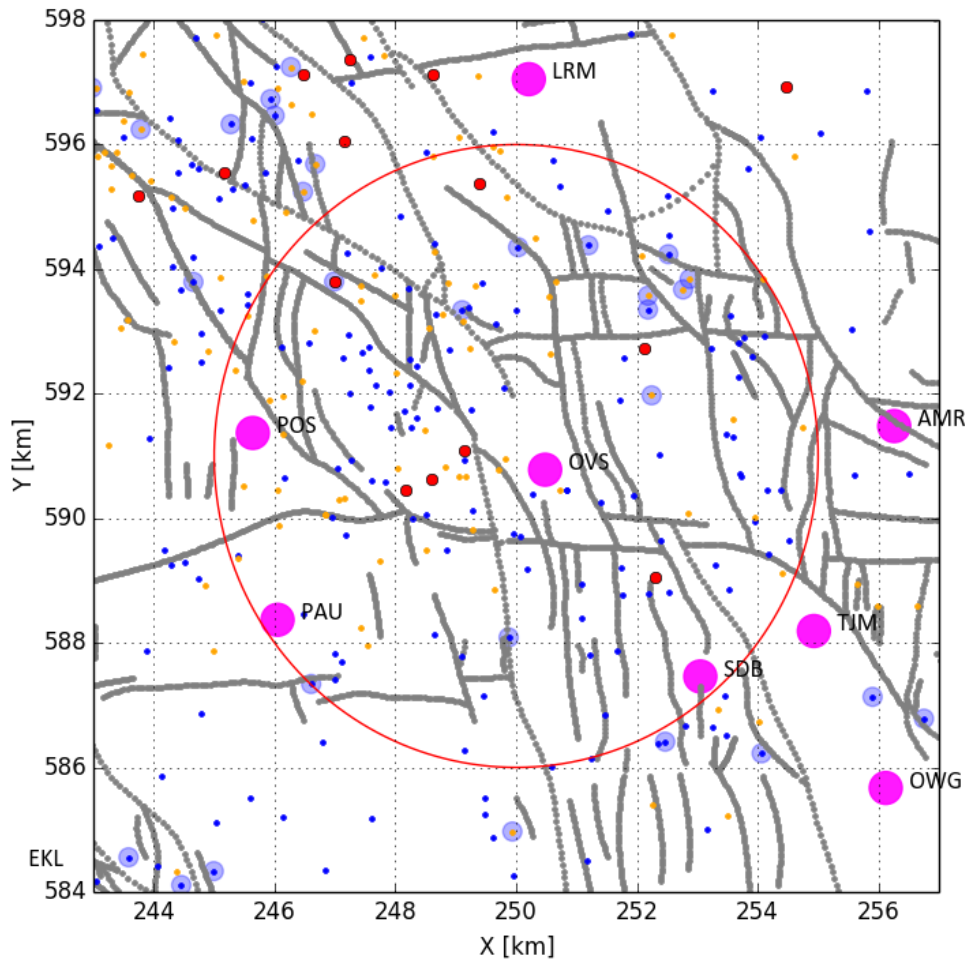


Figure C.3 : Faults and hypocentres of tremors around Ten Boer according to KNMI and NAM data. The grey lines show the faults. The region of interest is shown by the circle of 5 km radius. The hypocentres of the tremors are shown by the coloured dots. The colours correspond to the magnitude of the tremors in the following ranges on the scale of Richter: blue for  $1.0 \leq M < 1.5$ , orange for  $1.5 \leq M < 2.5$  and red for  $2.5 \leq M < 4$ . The light-blue dots show the tremors that have been measured after 23 March 2014. The magenta dots show the production well cluster locations.

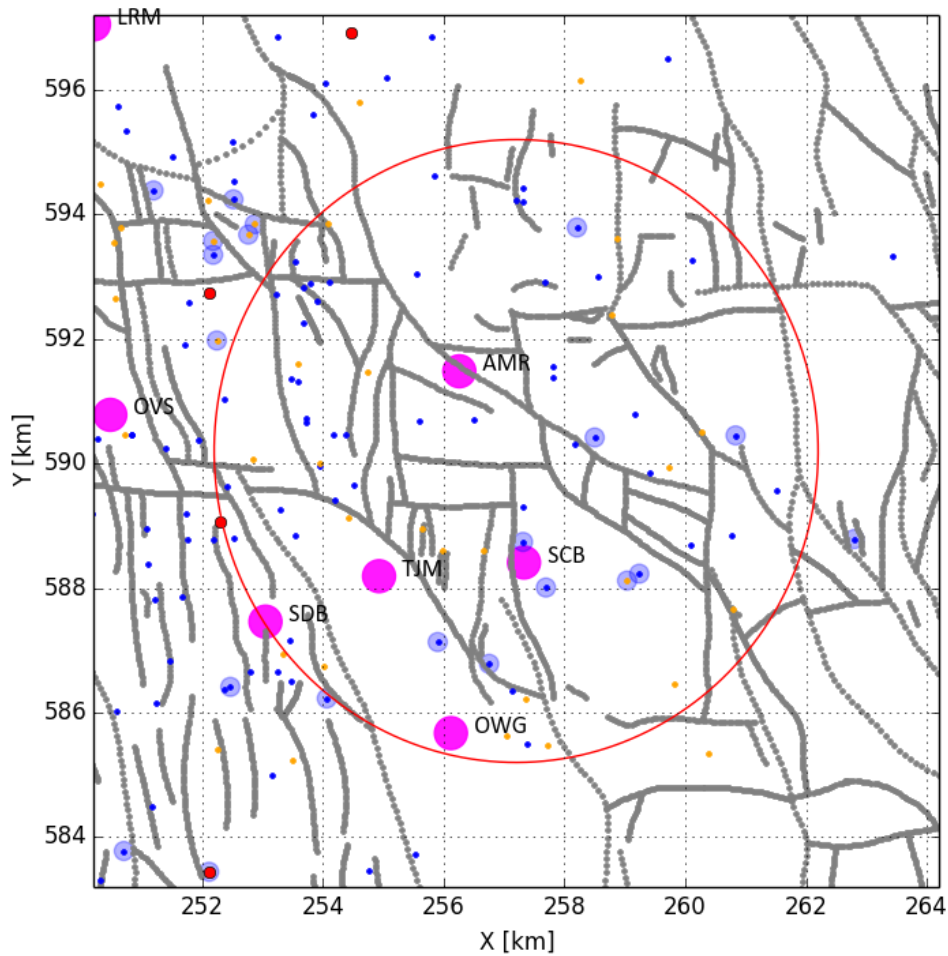


Figure C.4 : Faults and hypocentres of tremors around Meedhuizen according to KNMI and NAM data. The grey lines show the faults. The region of interest is shown by the circle of 5 km radius. The hypocentres of the tremors are shown by the coloured dots. The colours correspond to the magnitude of the tremors in the following ranges on the scale of Richter: blue for  $1.0 \leq M < 1.5$ , orange for  $1.5 \leq M < 2.5$  and red for  $2.5 \leq M < 4$ . The light-blue dots show the tremors that have been measured after 23 March 2014. The magenta dots show the production well cluster locations.

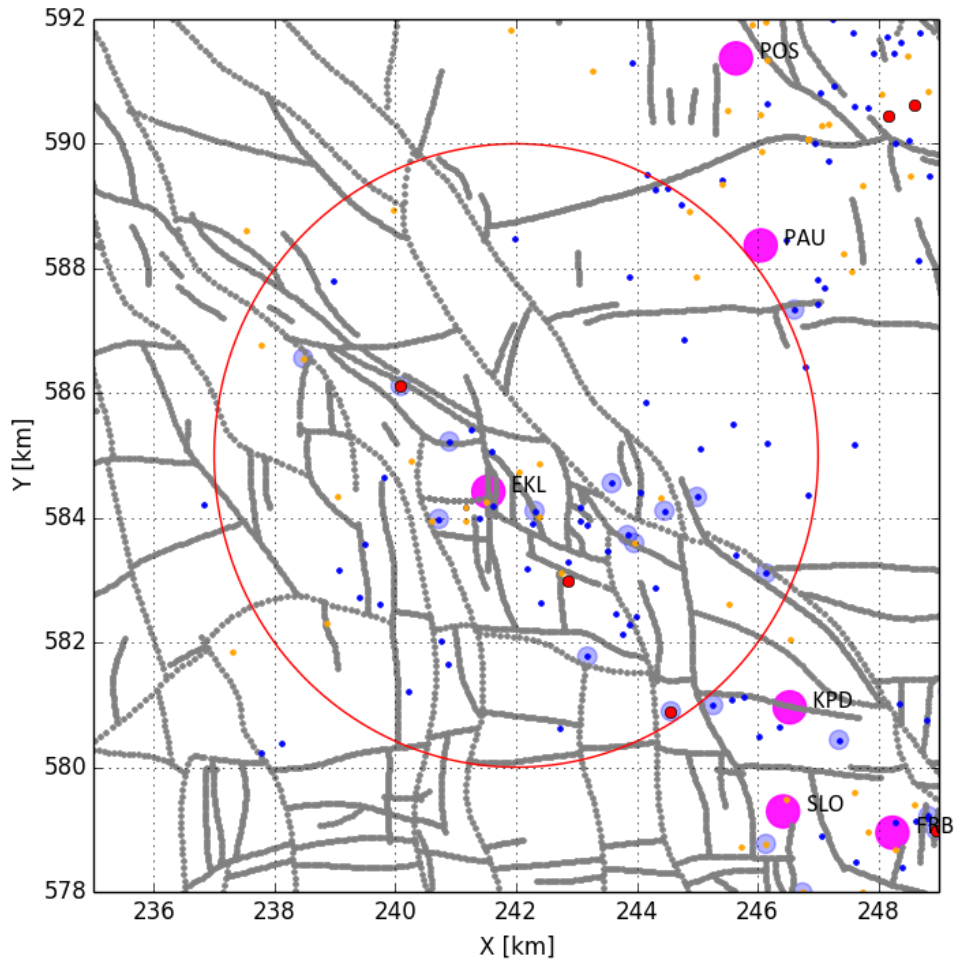


Figure C.5 : Faults and hypocentres of tremors around Lageland according to KNMI and NAM data. The grey lines show the faults. The region of interest is shown by the circle of 5 km radius. The hypocentres of the tremors are shown by the coloured dots. The colours correspond to the magnitude of the tremors in the following ranges on the scale of Richter: blue for  $1.0 \leq M < 1.5$ , orange for  $1.5 \leq M < 2.5$  and red for  $2.5 \leq M < 4$ . Not all faults with throws less than about 80 m and tremors below  $M = 1.5$  have been captured.

The light-blue dots show the tremors that have been measured after 23 March 2014. The magenta dots show the production well cluster locations.

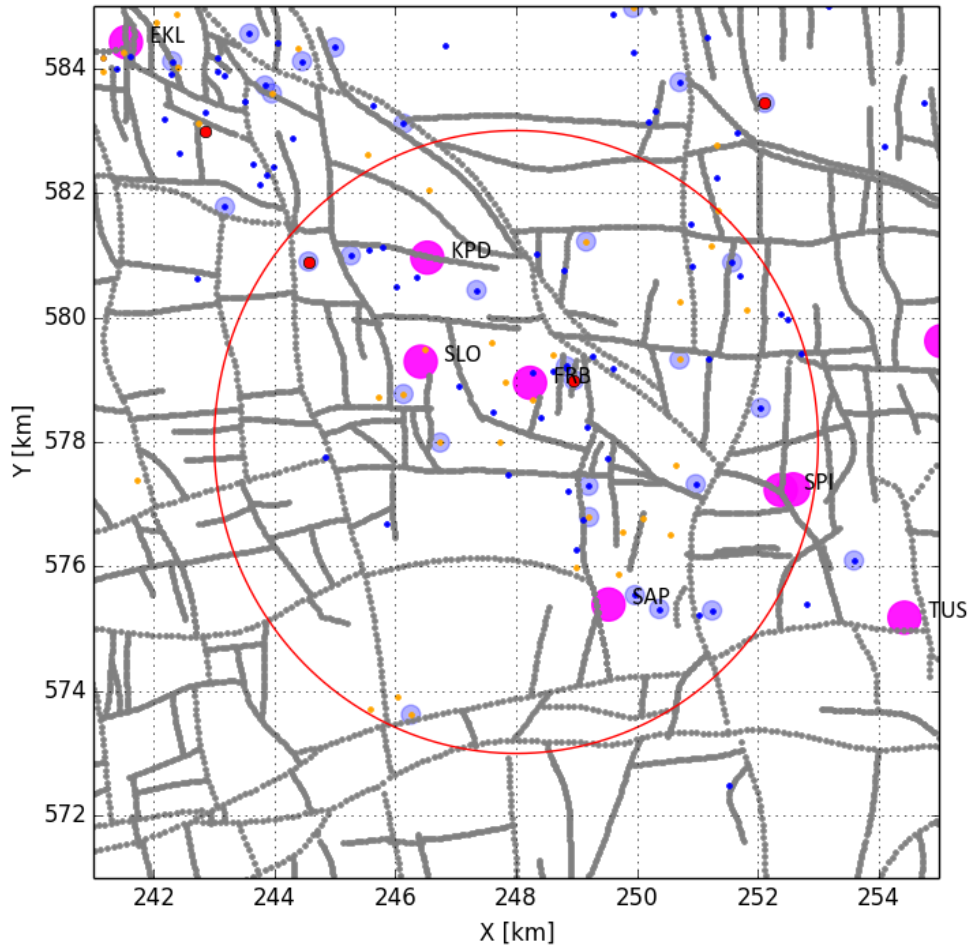


Figure C.6 : Faults and hypocentres of tremors around Woudsbloem according to KNMI and NAM data. The grey lines show the faults. The region of interest is shown by the circle of 5 km radius. The hypocentres of the tremors are shown by the coloured dots. The colours correspond to the magnitude of the tremors in the following ranges on the scale of Richter: blue for  $1.0 \leq M < 1.5$ , orange for  $1.5 \leq M < 2.5$  and red for  $2.5 \leq M < 4$ . The light-blue dots show the tremors that have been measured after 23 March 2014. The magenta dots show the production well cluster locations.

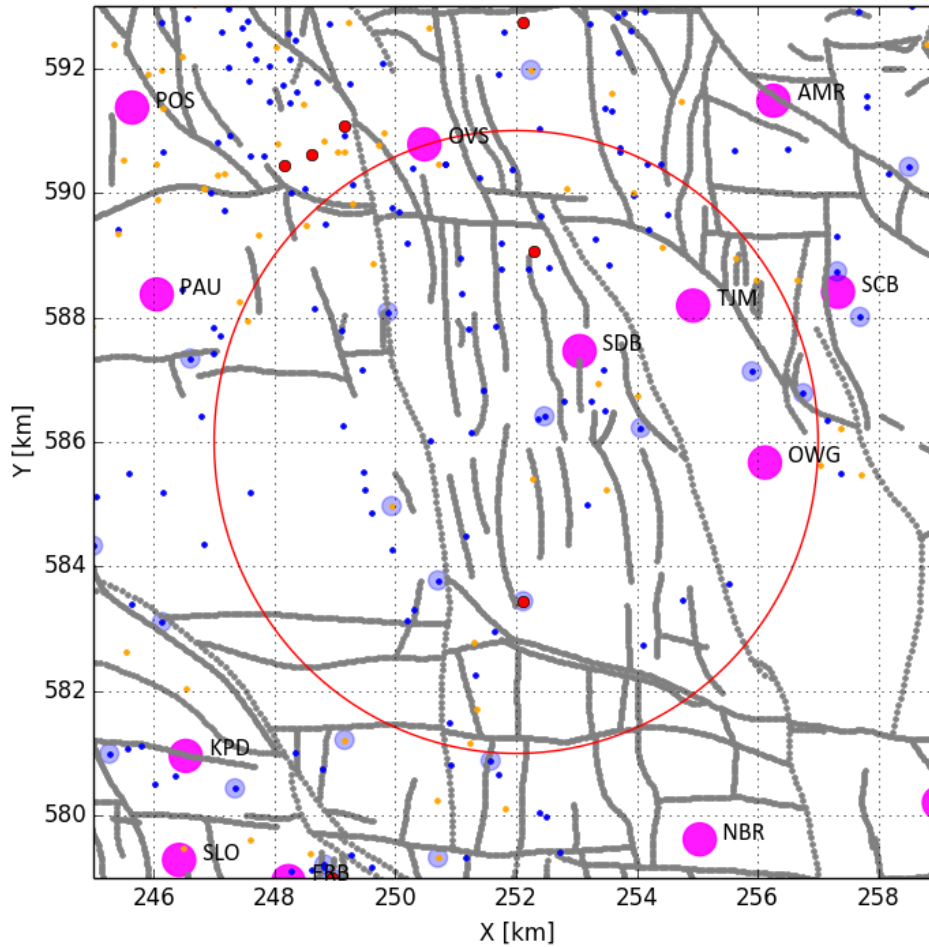


Figure C.7 : Faults and hypocentres of tremors around Hellum according to KNMI and NAM data. The grey lines show the faults. The region of interest is shown by the circle of 5 km radius. The hypocentres of the tremors are shown by the coloured dots. The colours correspond to the magnitude of the tremors in the following ranges on the scale of Richter: blue for  $1.0 \leq M < 1.5$ , orange for  $1.5 \leq M < 2.5$  and red for  $2.5 \leq M < 4$ . The light-blue dots show the tremors that have been measured after 23 March 2014. The magenta dots show the production well cluster locations.

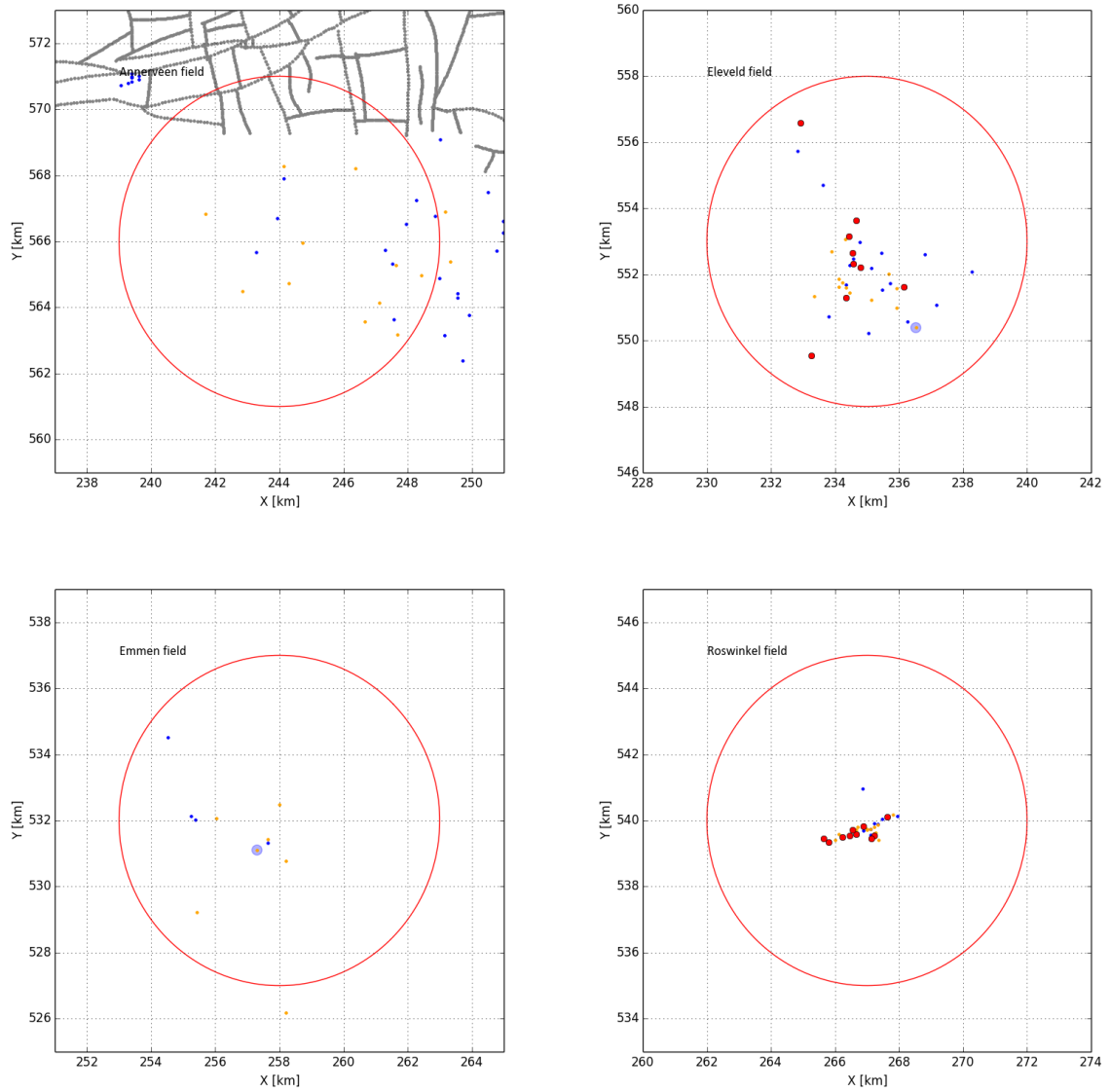


Figure C.8 : Hypocentres of tremors in the Annerveen, Eleveld, Emmen and Roswinkel fields according to KNMI data. The Roswinkel field has a few dominant faults which may explain the concentration of tremors along a few lines. The colours correspond to the magnitude of the tremors in the following ranges on the scale of Richter: blue for  $1.0 \leq M < 1.5$ , orange for  $1.5 \leq M < 2.5$  and red for  $2.5 \leq M < 4$ .

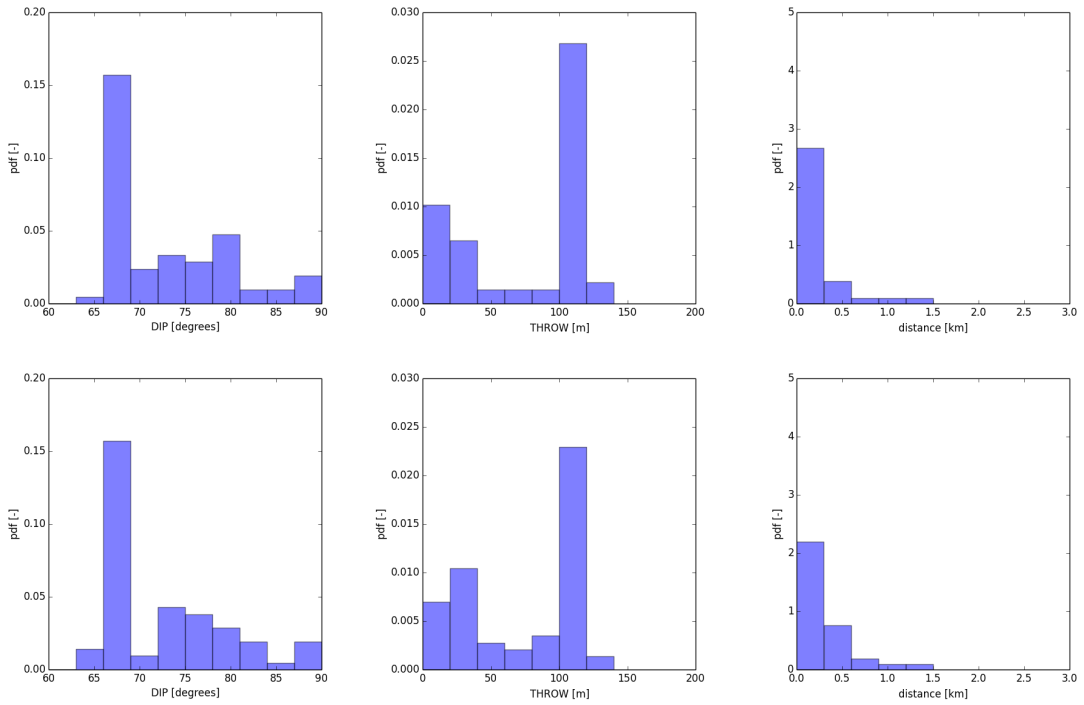


Figure C.9 : Histograms of the distribution of dip angles  $\delta$  (left) and fault throws  $t_{res}$  (centre) of fault segments most close to the hypocentres of the 65 largest tremors with a magnitude  $M \geq 2.5$ . The right figures show the histogram of the distances between the hypocentres of the largest tremors and these fault segments.

For the top figures, we have used the hypocentre coordinates from the KNMI data, see Appendix E. For the bottom figures, we have added to the coordinates of these hypocentres a random number from a normal distribution, accounting for the uncertainty in the location of the hypocentres.

Strong tremors evolve from areas close to or along fault segments with a throw of about 100 m and a dip angle of about  $65^\circ$ . According to the right figures, most of the hypocentres of these tremors are in a distance less than 0.5 km away from these fault segments.

Note that the strong tremors near Westeremden at 8 August 2006 with magnitude 3.5 and near Huizinge in the Loppersum region at 14 April 2009 and 16 August 2014 with magnitudes  $M = 2.6$  and  $M = 3.6$  are in an area where faults have a small throw of less than 50 m.

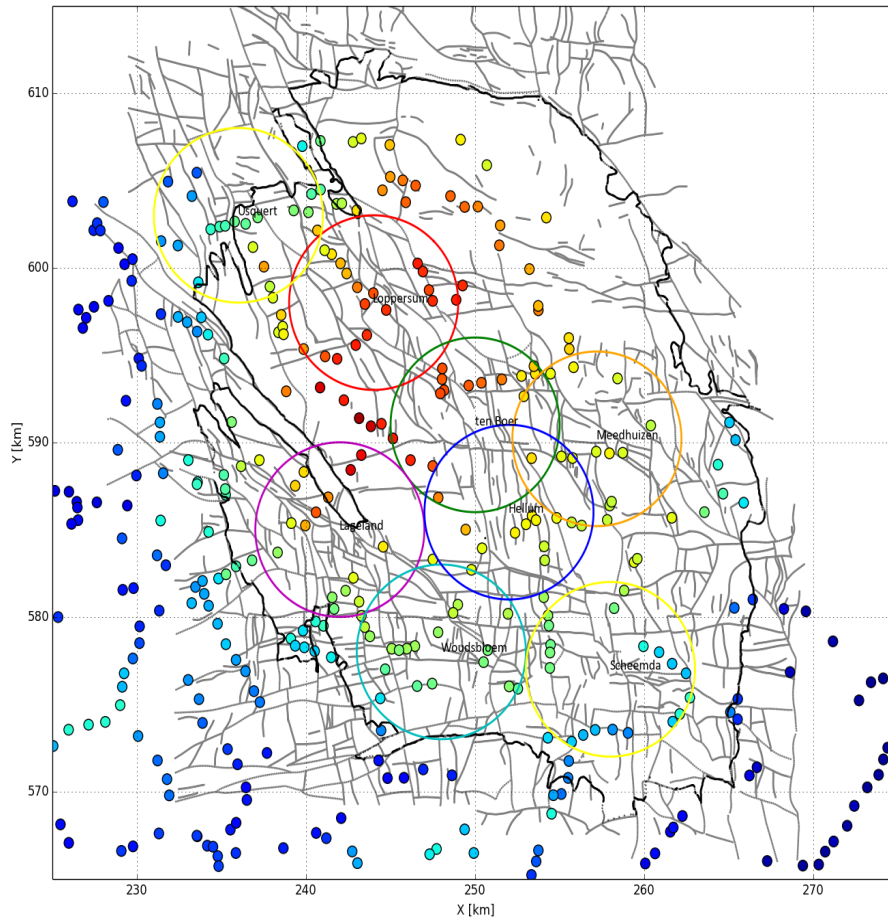


Figure C.10 : Faults and subsidence of the ground surface above the Groningen reservoir over the period 1972 - 2008 according to processed ground level measurements by NAM. The regions of interest are shown by circles of 5 km radius. They are around Loppersum (red), Ten Boer (green), Lageland (magenta), Woudsbloem (cyan), Meedhuizen (orange) and Hellum (blue). The regions around Scheemda and Usquert (yellow circles) have almost no tremors.

The rainbow colour scale for the subsidence data is linear. It ranges from 0 m (dark blue) to 0.32 m (red).

Note that subsidence data in the north-east part of the Groningen field is scarce.

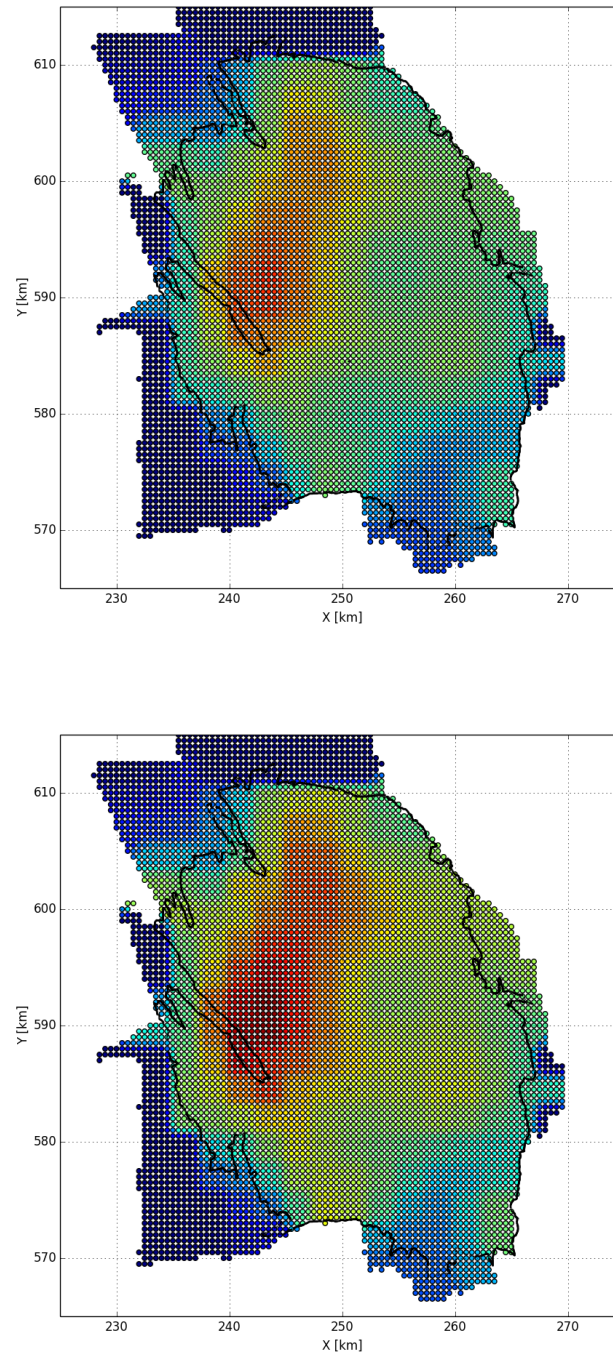


Figure C.11 : Reservoir compaction calculated from the subsidence data over the period 1962 - 2008 (top) and 1972 - 2015 (bottom). Data from Bierman and Kraaijeveld (2015). The rainbow colour scale for the reservoir compaction is linear. It ranges from 0 m (dark blue) to 0.32 m (red). Because of little subsidence data in the north-east part of the Groningen field, the calculated reservoir compaction is in this part less well constrained.

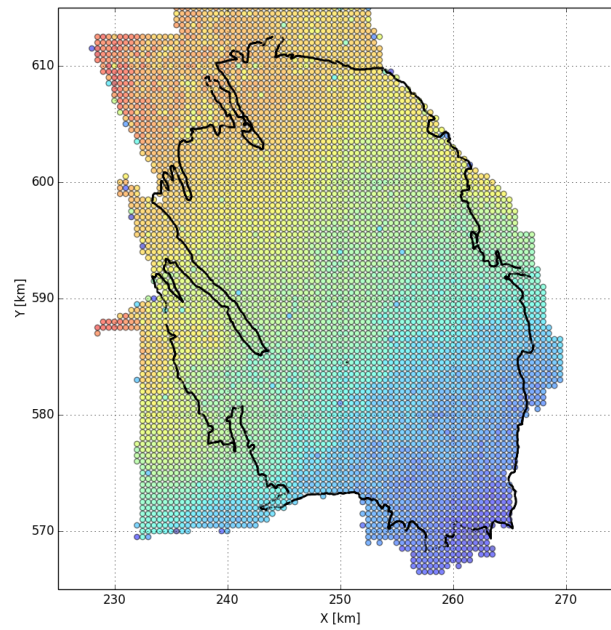


Figure C.12 : Reservoir thickness. Data from NAM.  
The rainbow colour scale for the reservoir thickness is linear. It ranges from 50 m (dark blue) to 400 m (red).

## Appendix C.2 Cumulative fault slip area of the observed tremors

The slip area  $S$  [m<sup>2</sup>] of a tremor can be estimated as follows. According to Leonard (2010), it is generally accepted that the seismic moment  $M_0$  of natural earthquakes scales with the slip area as  $M_0 \propto S^{3/2}$ . This holds even for considerable aspect ratio's  $L/W$  where  $L$  [m] and  $W$  [m] are the length and the width of the slip plane, respectively. The seismic moment is given by  $M_0 = \mu DS$  where  $\mu$  [Pa] is the shear modulus of the rock and  $D$  [m] is the relative displacement along the fault. This implies that the relative displacement along the fault scales as  $D \propto S^{1/2}$ .

For small tremors with a circular slip plane, the radius of the slip plane  $R$  [m] is given by, see Scholz (2002), Eq. 4.30,

$$R \sim \left( \frac{7 M_0}{16 \Delta\tau} \right)^{1/3}. \quad (\text{C.1})$$

$M_0$  is the seismic moment of the tremor and  $\Delta\tau$  [Pa] is the stress reduction over the slip plane caused by the tremor. Vice versa,  $M_0 \propto R^3 \propto S^{3/2}$  in accordance with Leonard (2010). For a rectangular slip plane with length  $L$  [m] and width  $W$  [m] with the slip parallel to  $L$ , according to Stein and Wysession (2003), §4.6.3, Eq. 20,

$$L \sim \left( \frac{8 M_0}{3\pi c_{WL} \Delta\tau} \right)^{1/3}, \quad (\text{C.2})$$

where  $c_{WL} = W/L$  [-]. For a square slip plane  $c_{WL} = 1$ . According to Eq. (C.2), for the same seismic moment  $M_0$ , the length of the square plane  $L$  is about 0.7 times smaller than the diameter of the circular plane  $2R$  from Eq. (C.1).

Combining Eq. (C.2) with the relation between the seismic moment and the mean relative displacement or slip length  $D$  [m] in the slip plane,  $M_0 = \mu DS$  where  $S = WL$  [m<sup>2</sup>] is the surface area of the slip plane,

$$D = \frac{3\pi \Delta\tau}{8 \mu} SL. \quad (\text{C.3})$$

For small tremors and for constant  $S$ ,  $D \propto L$ , as noted before.

The seismic moment for the largest circular or square slip plane, which resides in a fault plane with throw  $t_{res}$  in a reservoir with reservoir height  $h_{res}$ , follows from these expressions by inserting  $R = W_{res}/2$  or  $L = W_{res}$  and  $c_{WL} = 1$  where  $W_{res} = h_{res} + t_{res}$  into Eqs. (C.1) and (C.2), i.e.,

$$M_0 \sim \Delta\tau \frac{2}{7} W_{res}^3 \quad \text{and} \quad M_0 \sim \Delta\tau \frac{3\pi}{8} W_{res}^3. \quad (\text{C.4})$$

In the following, we assume  $\Delta\tau = 2$  MPa, which is in the range of expected values for the

Groningen field, see e.g. Kraaijpoel and Dost (2013). For  $h_{res} = 200$  m,  $t_{res} = 100$  m,  $\mu = 6.2$  GPa (using a typical Young modulus  $E = 15$  GPa and Poisson ratio  $\nu = 0.2$  for the Groningen reservoir rock) we obtain from these expressions  $M_0 = 15$  TJ and  $M_0 = 64$  TJ, respectively. Using the relation between seismic moment and seismic magnitude from Hanks and Kanamori (1979),  $M = 2/3 \log M_0 - 6.1$ , the corresponding seismic magnitudes are  $M = 2.7$  and  $M = 3.1$  on the scale of Richter, respectively.

According to Eq. (C.2), for large tremors with seismic slip parallel to the largest dimension  $L$  (or parallel to fault strike), i.e. for a rectangular slip plane with  $c_{W_{res}L} = W_{res}/L = 0.2$  and  $W_{res} = 300$  m,  $M_0 \propto L^2$  and is 25 times larger. However, from rupture modelling we expect that most of the seismic slip is parallel to the fault dip. In this case, we expect that  $M_0 \propto L$  and  $M_0$  is 5 times larger. Bounded by these extremes, we expect that the largest dimension of the slip plane scales as  $L^* \propto M_0^n$  with  $n$  in the range  $1/2 - 1$  if  $L^*$  is larger than the reservoir thickness.

If the dimension of the slip plane along fault strike would be proportional to  $M_0$  for seismic magnitudes above  $M \sim 3$ ,  $L^*$  is  $\sim 10$  km for a magnitude  $M = 4.1$  and the slip plane has the form of a long ribbon. On the other hand, if the slip plane of these tremors would penetrate into the carboniferous underburden and remains more or less circular,  $L^* \propto M_0^{1/3}$ . For  $M = 4.1$ , the diameter of the slip plane would be about 2 km, according to Eq. (C.1).

For the observed tremors, we have calculated the cumulative slip area of all tremors in the catalogue in the region of interest. It appears that the cumulative length of the slip planes is small compared to available fault length along strike in the regions investigated. Assuming circular slip planes, the radius of the slip plane is given by Eq. (C.1), i.e.,

$$R \sim \left( \frac{7}{16} \frac{M_0}{\Delta\tau} \right)^{1/3}. \quad (C.5)$$

Using  $\Delta\tau = 2$  MPa as a typical stress drop during rupture, Figures C.13 and C.14 show the diameter of the slip plane of the observed tremors and the cumulative diameter of the slip planes over time in the regions in the Groningen field and in the other fields of interest.

For the selected regions in the Groningen field, the cumulative fault length  $L_f$  is in the range 75 - 150 km according to the fault data shown in Figures C.2 - C.7 in §C.1. According to Figure C.13, the cumulative slip diameter of the observed tremors is only a small fraction of the potential fault length for seismic slip  $L_f$ .

Taking that the stress redistribution along the fault plane takes place over a distance of a few times the cumulative slip diameter and that some of the larger tremors could be non-circular and elongated along fault strike, it is not likely that a substantial number of tremors have been triggered by static or quasi-static redistribution of stress caused by preceding tremors<sup>4</sup>.

---

<sup>4</sup>In general, static stress increase in the fault plane around a slip area is predominantly within a distance of about the largest dimension of the slip area  $L^*$ , see e.g. Pilkey and Pilkey (2008). Away

On the other hand, the cumulative slip diameter of the observed tremors in the Roswinkel field is comparable with the length of the fault over which these tremors occur, see Figure C.8 in §C.1. Unless the stress drop during rupture  $\Delta\tau$  is much larger than 2 MPa and the slip planes are much smaller, it may well be that the static stress redistribution around the slip planes have influenced the probability of other tremors along this fault.

---

from the fault plane, the stress field is predominantly disturbed within a distance of about one reservoir thickness. This distance is less than the mean distance between the fault segments in the field. Hence, we expect that the main effect of static stress redistribution takes place in the fault plane of the tremor and, more specifically, around the plane of seismic slip. Most of the stress is redistributed within a distance equal to the largest dimension of the slip area. Whether seismic waves from tremors can cause fatigue-type damage in nearby fault planes and/or trigger other tremors is another question which is not answered here.

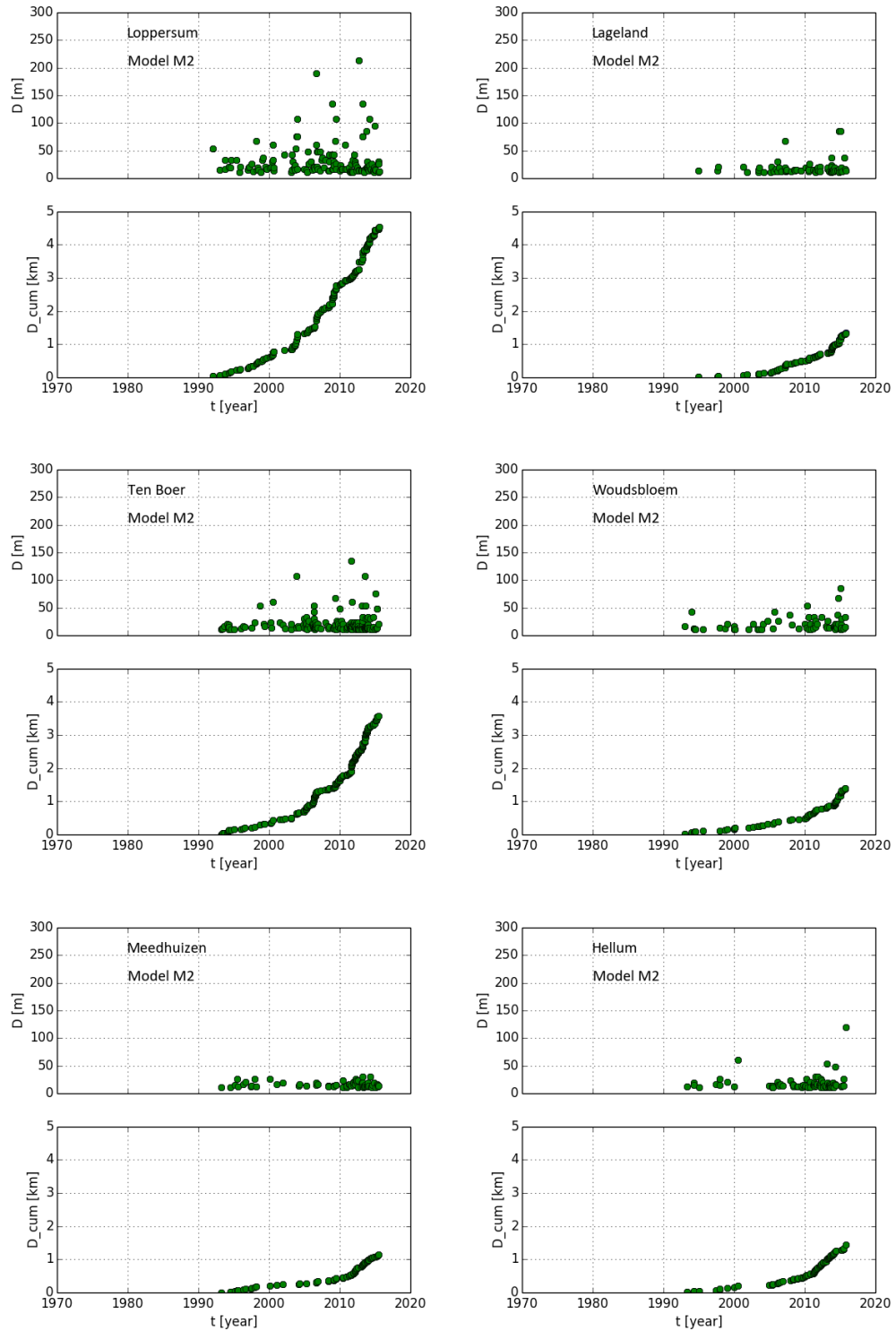


Figure C.13 : Slip diameter and cumulative slip diameter of the observed tremors in the regions of interest for the catalogue with  $M_{min} = 1.0$ .

Period of simulation 1960 - 30 september 2015 according to Eq. (C.5), using  $\Delta\tau = 2$  MPa. We disregard that the moment magnitudes  $M$  are on average 0.2 units smaller than local magnitude  $M_L$  for local magnitudes of 2.5 and greater and reported in the tables.

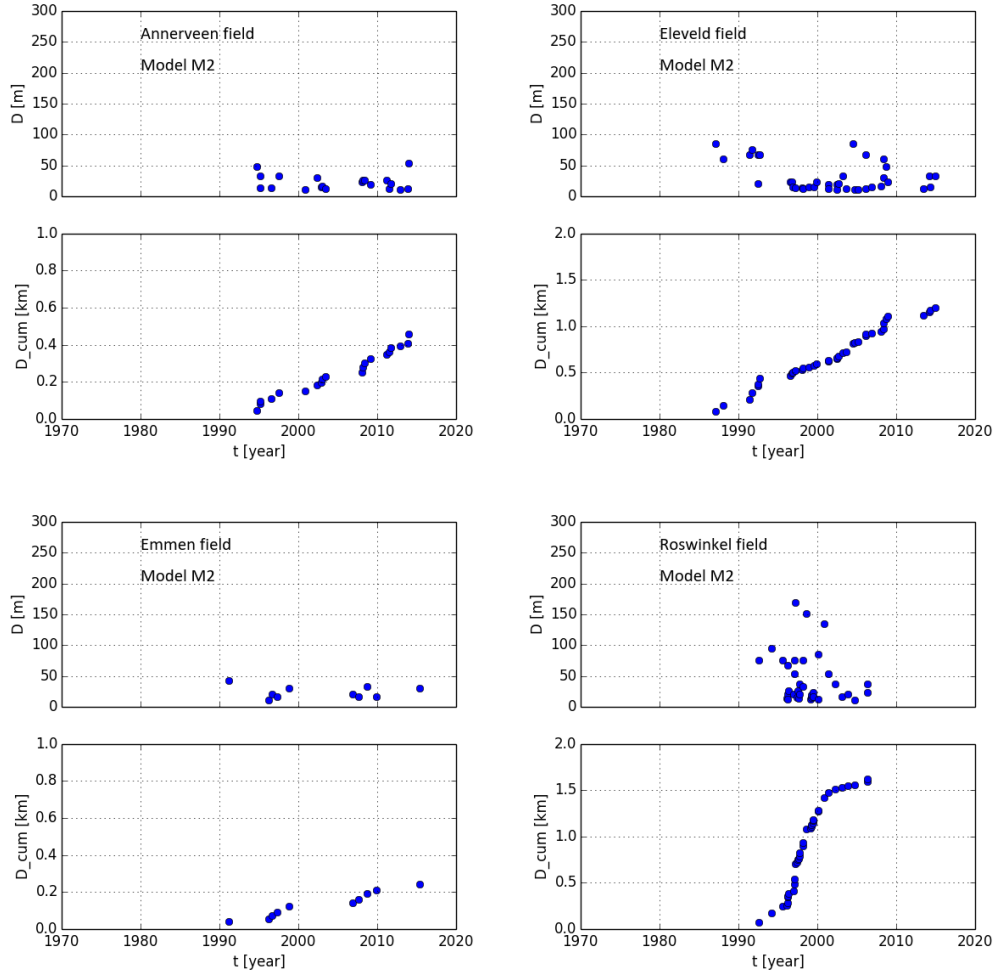


Figure C.14 : Slip diameter and cumulative slip diameter of the observed tremors in the regions of interest for the catalogue with  $M_{min} = 1.0$ .

Period of simulation 1960 - 30 september 2015 according to Eq. (C.5), using  $\Delta\tau = 2$  MPa.

We disregard that the moment magnitudes  $M$  are on average 0.2 units smaller than local magnitude  $M_L$  for local magnitudes of 2.5 and greater and reported in the tables.

The cumulative slip diameter in the Roswinkel field is comparable with the length over which the tremors are spread, see Figure C.8 in §C.1. It is not unlikely that stress redistribution around the slip planes in the related fault may have an influence on the probability of another tremor along that fault.

# Appendix D

## Reservoir pressures, gas production and tremors

### Appendix D.1 Reservoir pressure

The names, abbreviations and locations of the observation wells and gas production well clusters in the Groningen field are given in Table D.1 . The data originates from NAM EXCEL files. Figure D.6 shows the observation wells, gas production well clusters and faults in the Groningen field. Figure D.1 shows the measured reservoir pressures in the gas production well clusters and observation wells of the Groningen field. Because of good pressure communication in a large part of the field and the gas production strategy over many years, the reservoir pressure has been practically uniform over the main part of the field and over an extended period of time.

The proxy used follows the reservoir gas pressure of the Leermens well cluster. For the future, it is based on reservoir simulations by NAM for a 33 Bcm/year senario<sup>1</sup>.

Because of seasonal variations in the gas production, the reservoir pressure proxy for the Groningen field includes a small seasonal effect at the production well clusters. In the surrounding area these pressure fluctuations smooth out by pressure diffusion. At this stage, it is not clear how much these pressure fluctuations at the production well clusters influence the tremor rate. For this reason we have smoothed the raw reservoir pressure data with a moving average filter. The moving average is over 20 data points taken each month, i.e. over a period of about 1.5 year.

Figures D.2 - D.5 show the reservoir pressures in the Annerveen, Eleveld, Emmen and Roswinkel fields.

---

<sup>1</sup>The associated gas flow to the production well clusters and reservoir pressure diffusion fronts are very complex. They depend on the locations and production rates of these clusters, topology, variations in reservoir thickness and in fault geometry and flow transmissivity, and local variations in reservoir porosity, permeability and water leg.

Table D.1 : Names and Dutch Rijksdriehoeksstelsel coordinates of the observation wells in the Groningen field.

Name	Abbreviation	X	Y
		km	km
.....	.....	.....	.....
observation wells			
Bolderij	BOL	257.8	582.7
Barnheem	BRH	241.1	592.3
Delfzijl	DZL	260.7	592.0
Farmsum	FRM	258.3	594.2
Heiligerlee	HGL	261.9	575.6
De Hond	HND	256.9	602.5
Harkstede	HRS	239.8	582.6
Kolham	KHM	244.4	577.8
Meeden	MDN	258.3	574.8
Oldorp	ODP	238.6	601.8
Oostwold	OLD	265.2	582.8
Roode Til	ROT	258.0	579.6
Stedum	SDM	242.5	595.0
Schildmeer	SMR	253.6	589.5
Schaaphok	SPH	244.1	582.9
Schildwolde	SWO	250.3	584.8
Ten Boer	TBR	238.9	586.7
Uithuizermeeden	UHM	249.3	607.9
Uithuizen	UHZ	242.6	605.8
Zuidbroek	ZBR	255.1	576.0
Zeerijp	ZRP	245.0	596.4
Zuidwending	ZWD	259.6	571.4
production wells			
Amsweer	AMR	256.3	591.5
Bierum	BIR	254.7	599.4
Eemskanaal	EKL	241.5	584.4
De Eeker 1	EKR-1	259.5	577.3
De Eeker 2	EKR-2	259.9	577.4
Froombosch	FRB	248.2	579.0
Kooipolder	KPD	246.5	581.0
Leermens	LRM	250.2	597.1
Midwolda	MWD	264.3	578.7
Noordbroek	NBR	255.0	579.6
Nieuwscheemda	NWS	259.0	580.2
Overschild	OVS	250.5	590.8
Oudeweg	OWG	256.1	585.7
De Paauwen	PAU	246.1	588.4
Ten Post	POS	245.6	591.4
Sappemeer	SAP	249.5	575.4
Schaapbulten	SCB	257.3	588.4
Siddeburen	SDB	253.1	587.5
Slochteren	SLO	246.4	579.3
Spitsbergen 1	SPI-1	252.4	577.2
Spitsbergen 2	SPI-2	252.6	577.2
Scheemderzwaag 1	SZW-1	257.1	578.2
Scheemderzwaag 2	SZW-2	257.3	578.1
Tjuchem	TJM	254.9	588.2
Tusschenklappen	TUS	254.4	575.2
Uiterburen	UTB	255.4	577.4
Zuiderpolder	ZDP	261.8	581.0
t Zandt	ZND	247.9	600.6

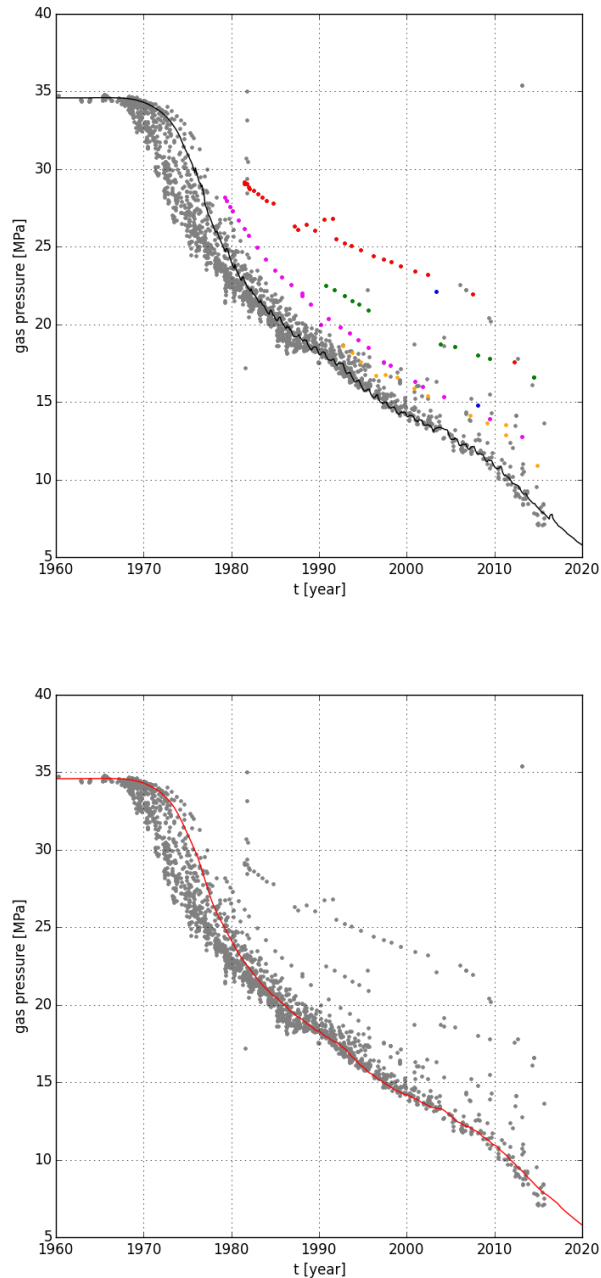


Figure D.1 : Reservoir pressure in the Groningen field as measured at the well production clusters and observation wells (dots). The observed reservoir pressures in a few observation wells deviates from the major trend. The blue, green, red, orange and magenta dots represent measurements in the Farmsum (FRM), Kolham (KHM), Harkstede (HRS), Zuidwending (ZWD) and Oldorp (ODP) observation wells, respectively.

The solid black line in the top figure shows the reservoir pressure in the Leermens gas production well cluster under a 33 Bcm/year scenario as calculated from reservoir simulations. It holds for approximately most of the well locations in the Groningen field, and in particular around Loppersum.

The solid red line in the bottom figure is the moving average of the pressure in this cluster. The moving average is over 20 data points taken each month, i.e. over a period of about 1.5 year. It is used as a proxy for the reservoir pressure in all the regions of the Groningen field.

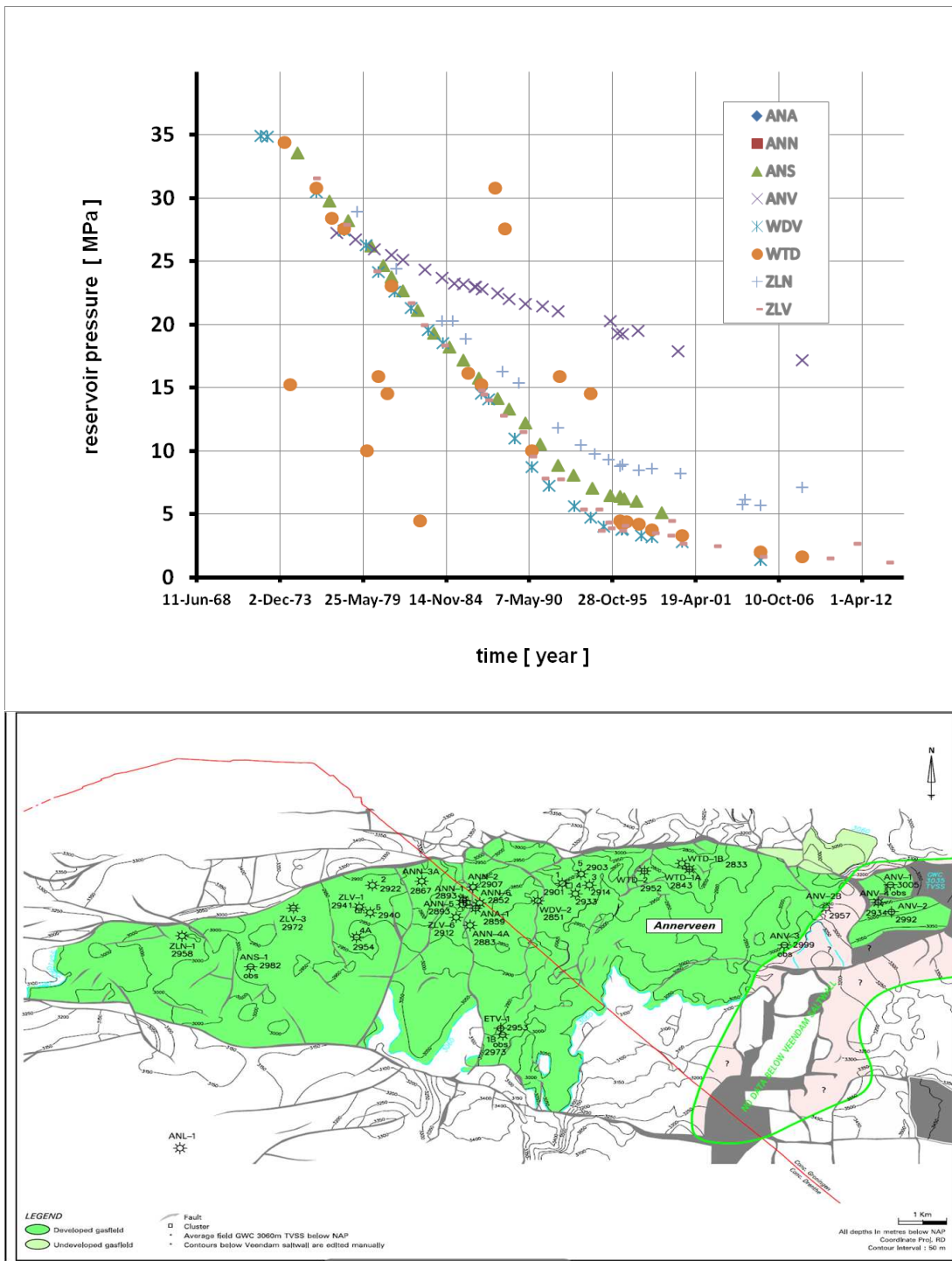


Figure D.2 : Reservoir pressures in gas production wells in the Annerveen field and map of the Annerveen field.

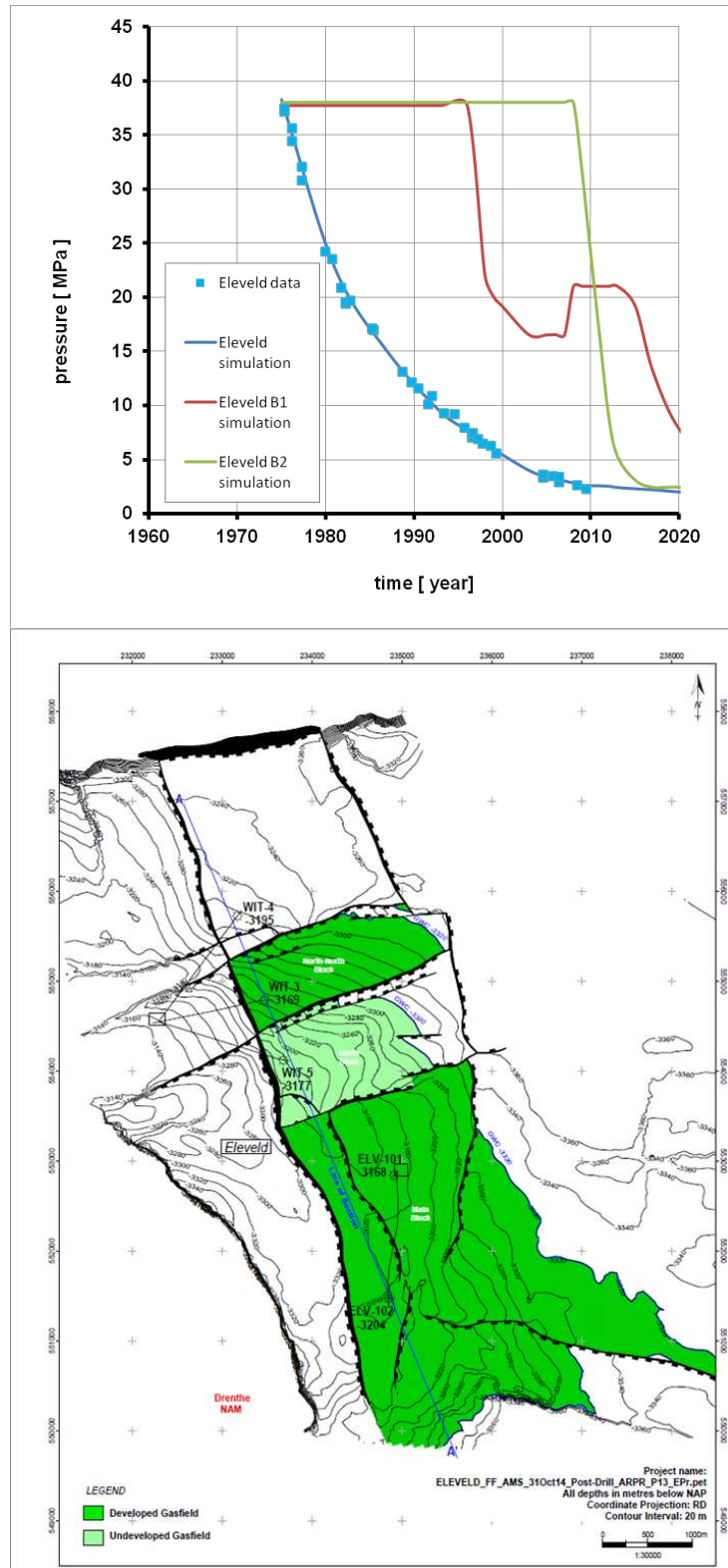


Figure D.3 : Reservoir pressures in gas production wells in the Eleveld field and map of the Eleveld field.

According to NAM ELV-101 and ELV-102 well data, the reservoir pressure in the south and largest  $4 \times 3 \text{ km}^2$  B block decreased from about 38 MPa to about 3 MPa over the period 1975 - 2005, initially at a somewhat higher rate. In June 2009, the reservoir pressure in the ELV-101 well was about 2 MPa.

The reservoir pressure in the centre block B1 of about  $2 - 3 \text{ km}^2$  reduced from 1996 - 2014 from 38 MPa to 20 MPa. The reservoir pressure in the north block B2 of about  $2 - 3 \text{ km}^2$  reduced from 2008 - 2014 from 38 MPa to 5 MPa.

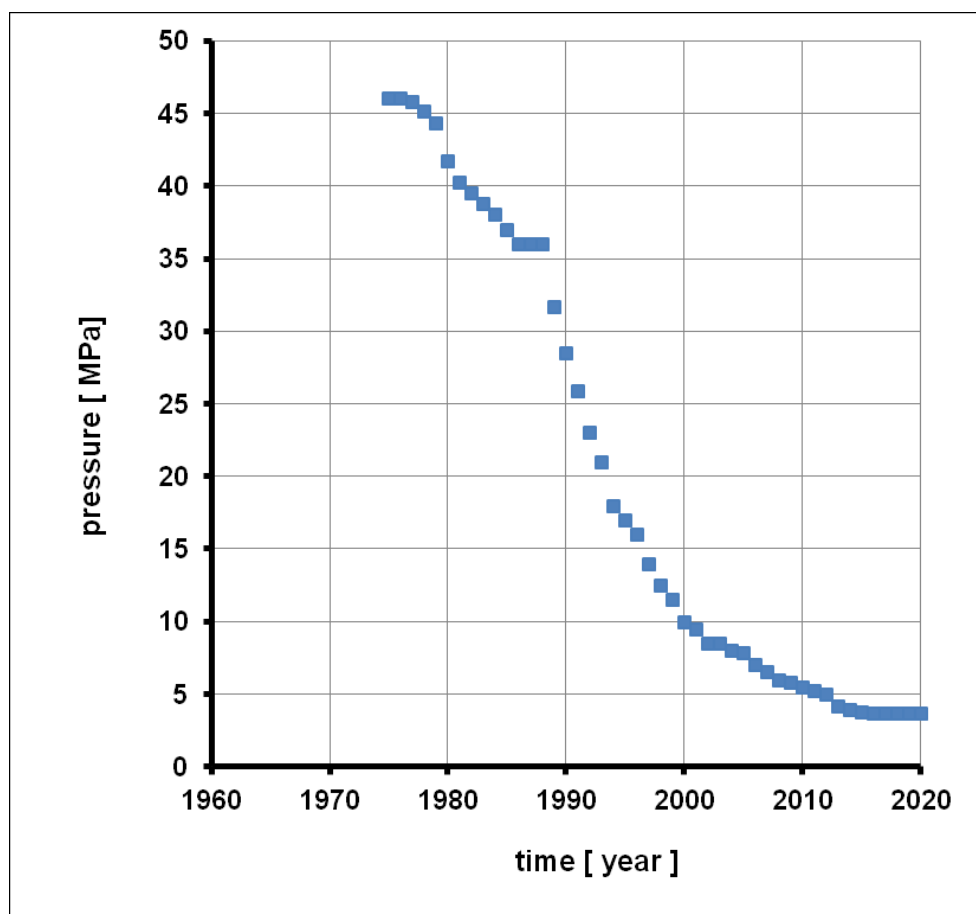


Figure D.4 : Reservoir pressure in gas production well EMM-ZEZ2C-W in the Emmen field.

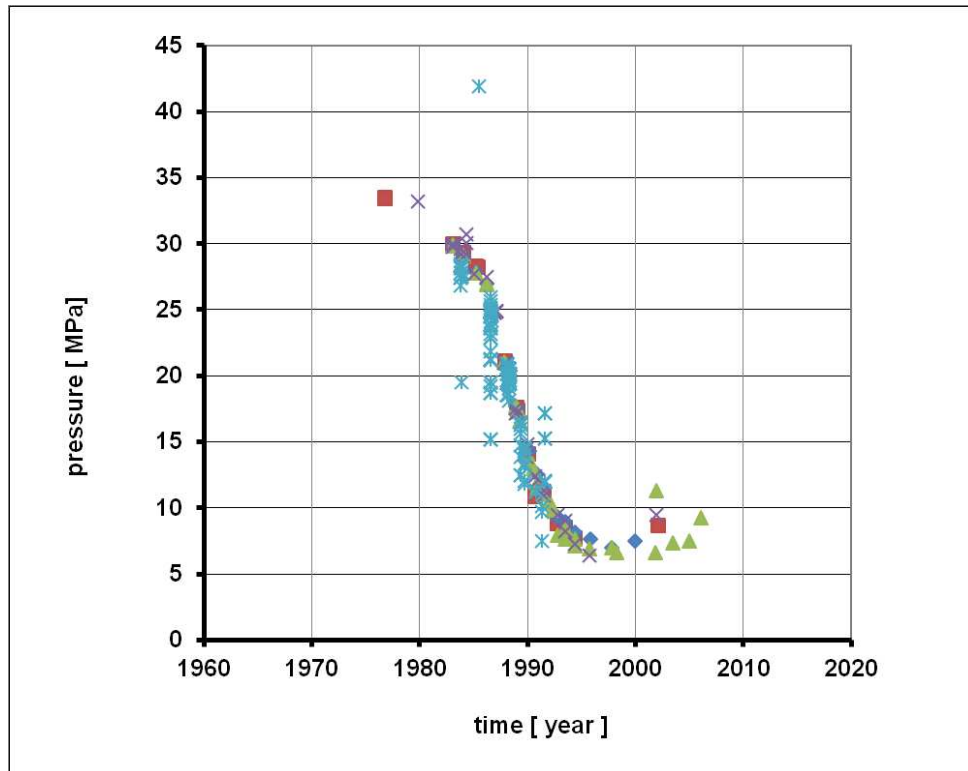


Figure D.5 : Reservoir pressures in gas production wells in the Roswinkel field. In the period between 1995 and 2007, the Roswinkel field shows a more or less stable pressure level while gas was produced. The gas production in the Roswinkel field has been stopped in 2007. The gas production in the Roswinkel field has been supported by an active aquifer. Water infill from this aquifer leads to a small increase in the reservoir pressure after the gas production had declined.

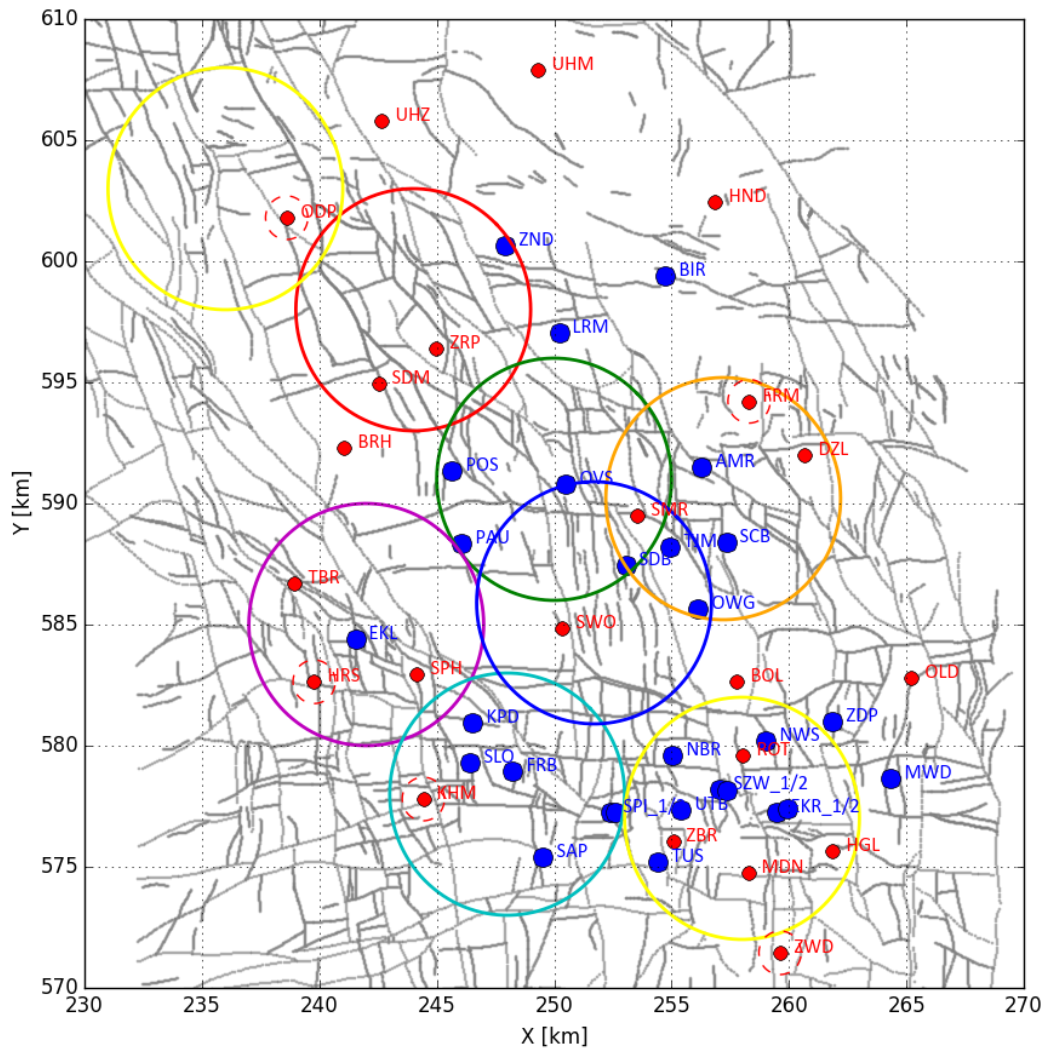


Figure D.6 : Locations of the gas production well clusters (blue) and observation wells (red) in the Groningen field. The regions of interest in the Groningen field are shown by circles of 5 km radius. They are around Loppersum (red), Ten Boer (green), Lageland (magenta), Woudsbloem (cyan), Meedhuizen (orange) and Hellum (blue). The regions in the Groningen field around Scheemda and Usquert (yellow circles) have almost no tremors.

The Farmsum (FRM), Kolham (KHM), Harkstede (HRS), Zuidwending (ZWD) and Oldorp (ODP) observation wells with gas pressures significantly deviating from the main trend, see Figure D.1 below, have a small dashed red circle around them. These wells are along the circumference of the Groningen field.

## Appendix D.2 Gas production and tremors

Figures D.7 - D.8 show the number of observed tremors and cumulative gas production of nearby production well clusters over time for the regions of interest in the Groningen field.

The figures show also a ‘weighted’ cumulative gas production of these clusters for each region. The weight of each production well cluster decreases with the distance between the cluster and the centre of the region considered. Ad hoc, the weighted cumulative gas production is calculated by multiplying the gas production with the weight function  $f(r_{ij}) = \exp(-(r_{ij}/r_c)^2)$ .  $r_{ij}$  is the distance between the centre of the region  $j$  and the location of the production well cluster  $i$ .  $r_c$  [m] is a characteristic distance. We take  $r_c = 3$  km, which is of the order of the pressure diffusion distance in a year time.

The figures show no clear correlation between changes in the gas production and changes in the tremor rate in a certain region other than one resulting from a resulting change in the reservoir pressure. More or less prominent deviations in the tremor rate from a smooth curve are difficult to explain from changes in the gas production.

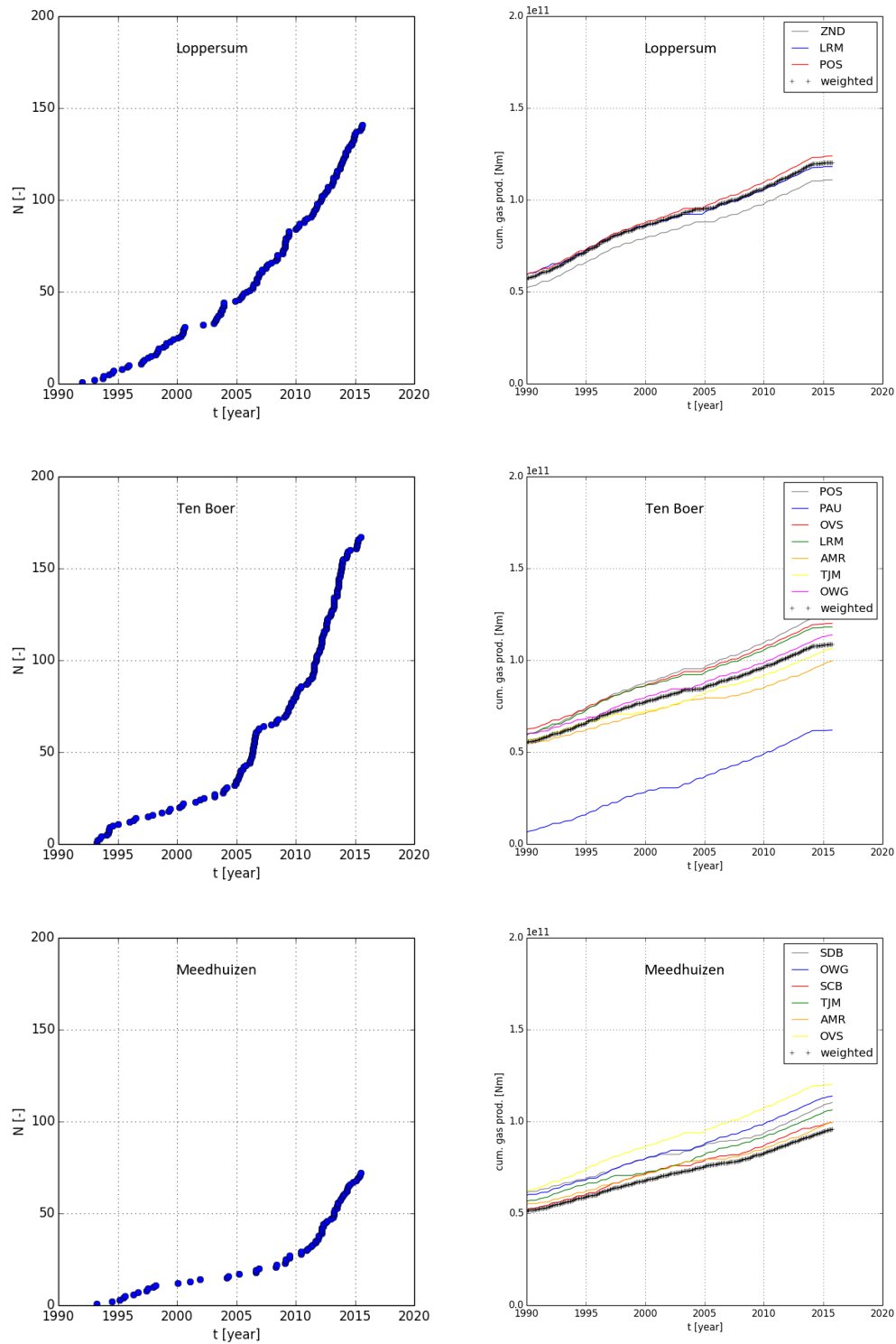


Figure D.7 : Number of observed tremors (left) and cumulative gas production in nearby well clusters (right) in the selected regions in the Groningen field.  $M_{min} = 1.0$ . The weighted cumulative gas production curve has another scale (not shown) than the scale on the vertical axis used for the cumulative gas production of the well clusters.

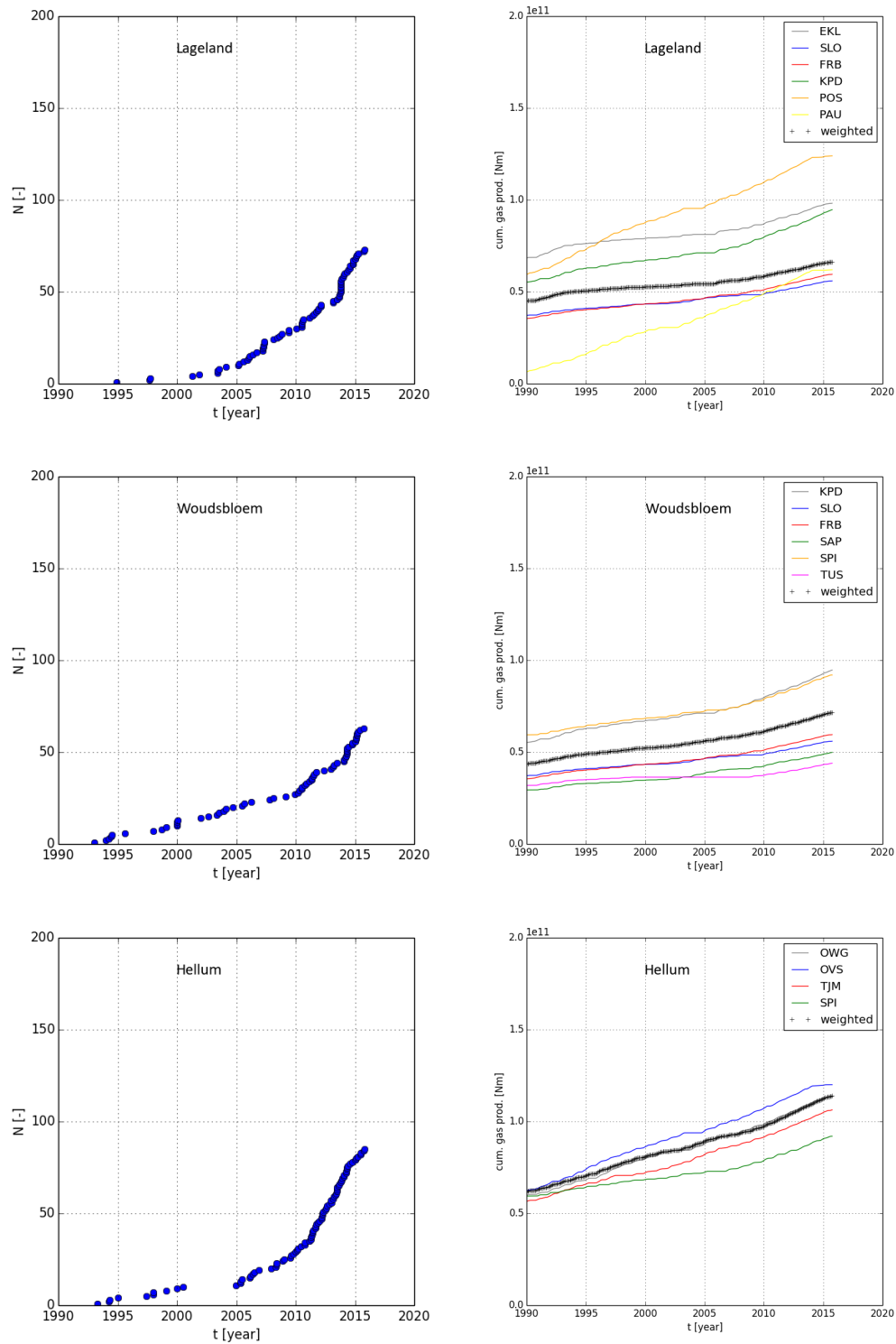


Figure D.8 : Number of observed tremors (left) and cumulative gas production in nearby well clusters (right) in the selected regions in the Groningen field.  $M_{min} = 1.0$ . The weighted cumulative gas production curve has another scale (not shown) than the scale on the vertical axis used for the cumulative gas production of the well clusters.

# Appendix E

## Tremor data

The tremor data originates from the Koninklijke Nederlands Meteorologisch Instituut in the Netherlands (KNMI) and can be found in tables available from the [www.knmi.nl](http://www.knmi.nl) website. These tables contain about 1200 tremors, also outside the regions of interest. Tables E.1 - E.3 contain the name of the town/village, the  $X$  and  $Y$  [m] Dutch Rijksdriehoeksstelsel coordinates of the hypocentres, the date/time and the local magnitude of the tremors in the Netherlands between 1 January 2014 and 30 September 2015. According to Bernard Dost from KNMI, the moment magnitudes  $M$  are on average 0.2 units smaller than local magnitude  $M_L$  for local magnitudes of 2.5 and greater and reported in these tables.

For the period before 11 February 2014, the coordinates have been provided by KNMI. For the period after 11 February 2014, they have been calculated from the latitude and longitude data provided by KNMI.

We have used  $X = 67.198LO - 207.116$  and  $Y = 111.300LA - 5341.500$  where  $LO$  is the longitude and  $LA$  is the latitude of the tremor location in degrees<sup>1</sup>.

The elapsed time in terms of days has been calculated from the data by taking that the average year has 365.25 days, starting 1<sup>st</sup> of January 1960. We refer to Wentinck (2015), Appendix D for the tremor data used before 1<sup>st</sup> of January 2014.

In general, the distribution of tremors is not uniform over the Groningen field and the other fields. Also, the frequency-magnitude relationship derived from this data varies over the regions of interest. Note that the network of seismometers has been designed to de-

---

<sup>1</sup>These relations follow from linear fits from the relations between the  $X$  and  $Y$  coordinates in kilometres and the latitude and longitude tremor location data prior to 11 February 2014.

In Wentinck (2015), Appendix D, less accurate relations have been used for the tremor locations after 11 February 2014,  $X = 67.060LO - 206.600$  and  $Y = 111.300LA - 5339.000$ . The main effect of this inaccuracy is that the calculated  $Y$  coordinate in this reference is about 1.5 km north from the location calculated by the relations in this report.

Because of this mapping the coordinates of some tremors in the catalogue used in this report may somewhat differ from other catalogues. These small differences will hardly change the results of this report.

tect and locate tremors in the Groningen field above magnitudes of 1.5 and was only fully operational after 1994. Tremors below a magnitude of 1.5 may have been undetected, especially in seasons of the year when seismic noise has been relatively strong.

The tables have been compared with a recent ArcGIS file used by NAM. They contain a few tremors less than the ArcGIS file. Some tremors are assigned to other village names. For the data in the period from February 2014 until September 2015, the easting and northing  $X$  and  $Y$  coordinates of the hypocentres of the tremors have been calculated from the longitude and latitude data provided by KNMI.

Table E.1 : Observed tremors in the Netherlands since 1 January 2014.

Location	$t$	$t$	$X$	$Y$	$M_L$
	y/m/d	days	m	m	Richter
Woudbloem	20140102	19756.7	246348	580636	1.4
Garmerwolde	20140104	19758.7	239065	583155	1.1
Rottum	20140109	19763.6	236670	599568	1.0
Garrelsweer	20140112	19766.1	247160	590575	0.9
Nieuwolda	20140116	19770.8	260759	588834	1.2
Zuidwolde	20140121	19775.0	233760	587665	1.0
Garsthuizen	20140123	19777.3	244767	599657	0.6
Noordbroek	20140123	19777.1	255197	578233	1.1
Zevenhuizen	20140126	19780.5	241166	583953	1.5
Loppersum	20140203	19787.8	246188	594916	1.5
Luddeweer	20140205	19789.5	248368	585572	0.9
Geelbroek	20140205	19790.2	234326	553064	2.0
Froombosch	20140206	19791.1	248396	578393	1.3
Meedhuizen	20140211	19795.4	259382	590770	0.8
Leermens	20140213	19797.5	248622	597134	3.0
Winneweer	20140217	19801.6	245934	591235	0.8
Westerwijtwerd	20140218	19802.6	240558	594908	1.7
Woltersum	20140228	19812.6	246471	588453	1.2
Annerveenschekanaal	20140304	19819.0	251847	565970	1.1
Annerveenschekanaal	20140304	19819.0	251713	566861	0.8
Annerveenschekanaal	20140304	19818.9	251713	566638	0.8
Zeerijp	20140310	19825.0	247681	596466	0.9
Schildwolde	20140311	19826.2	251310	582776	2.3
Froombosch	20140311	19826.2	251175	579326	1.1
Eleveld	20140312	19826.8	235720	551724	1.3
Appingedam	20140314	19829.7	251713	591903	1.0
Waterhuizen	20140314	19829.0	239886	580884	0.8
Appingedam	20140315	19830.6	254737	591458	1.9
Rottum	20140318	19833.7	237601	600807	2.1
Slochteren	20140321	19836.5	251713	580662	1.1
Sappemeer	20140323	19838.2	249697	575876	1.6
Siddeburen	20140327	19842.2	254065	586227	1.4
Eemshaven	20140328	19843.7	247009	610824	1.3
Borgsweer	20140330	19845.7	262801	588787	1.4
Zevenhuizen	20140331	19846.6	241230	583889	0.7
Sappemeer	20140402	19847.5	249966	575542	1.2
Sappemeer	20140402	19847.5	250369	575319	1.1
Sappemeer	20140403	19848.3	250974	577323	1.0
Zevenhuizen	20140404	19849.6	240894	585225	1.2
Meedhuizen	20140409	19854.4	256753	586783	1.1
Loppersum	20140417	19863.1	244657	593795	1.3
Zeerijp	20140420	19865.6	246001	596466	1.4
Schildwolde	20140426	19871.6	250705	583778	1.3
Westerbroek	20140427	19873.2	243246	577879	0.5
Woudbloem	20140512	19888.6	245262	580996	1.3
Westerwijtwerd	20140513	19889.4	239080	594463	1.4
Kolham	20140517	19892.8	246135	578770	1.6
Meedhuizen	20140519	19895.4	259239	588230	1.0
Kolham	20140612	19919.0	246606	578658	0.8
Woudbloem	20140612	19918.4	247345	580439	1.2
Westerenden	20140616	19922.8	243783	596244	1.8
Slochteren	20140629	19935.7	251310	581107	0.7
Meedhuizen	20140702	19938.9	257693	588008	1.3
Slochteren	20140702	19939.3	249159	581218	2.1
Haren	20140706	19942.7	237601	577991	0.9
Zevenhuizen	20140707	19944.4	242305	584112	1.2
Woltersum	20140707	19944.5	246606	587340	1.0
Lageland	20140708	19945.0	243582	584557	1.2
Slochteren	20140715	19952.2	251646	581330	0.7
Siddeburen	20140722	19959.3	253998	585114	0.9

Table E.2 : Observed tremors in the Netherlands, continued.

Location	$t$	$t$	$X$	$Y$	$M_L$
	y/m/d	days	m	m	Richter
Oosterwijtwerd	20140809	19976.7	252183	593350	1.3
Oosterwijtwerd	20140809	19976.7	252183	593573	2.0
Garsthuizen	20140819	19986.8	244791	599249	1.2
Garsthuizen	20140821	19988.5	244926	598915	1.2
Slochteren	20140825	19992.4	248622	582999	0.8
Garmerwolde	20140901	19998.5	238072	583667	0.5
Froombosch	20140901	19998.7	248958	578992	2.6
Froombosch	20140901	19998.8	250705	579326	1.6
Lageland	20140923	20021.1	244455	584112	1.4
Lageland	20140923	20021.2	244993	584335	1.0
Huizinge	20140924	20022.4	242641	596466	1.0
Meedhuizen	20140925	20023.3	259037	588119	1.5
Ten-Boer	20140930	20027.9	240088	586115	2.8
Zeerijp	20141021	20049.2	246270	597245	1.5
Zandeweer	20141105	20063.4	241633	599026	2.9
Amen	20141111	20069.9	236526	550388	2.0
Hellum	20141116	20074.3	254065	582776	0.9
Woudbloem	20141116	20075.1	247278	582776	0.6
Huizinge	20141122	20080.5	242977	596912	1.3
Oosterwijtwerd	20141129	20088.2	252519	594240	1.0
Huizinge	20141130	20088.4	241230	597468	1.4
Noordbroek	20141203	20091.9	252049	578547	1.0
Zevenhuizen	20141205	20094.0	240720	583982	1.1
Zeerijp	20141228	20117.7	245932	596729	1.3
Woudbloem	20141230	20119.4	244561	580898	2.8
Luddeweer	20141230	20119.2	246166	584379	0.8
Wirdum	20150106	20125.4	246987	593800	2.7
Farmsum	20150106	20125.3	258206	593788	1.0
Sappemeer	20150111	20130.7	249208	576795	1.5
Steendam	20150114	20134.1	252468	586413	1.1
Lageland	20150118	20137.4	243955	583596	1.5
Schildwolde	20150122	20141.7	250713	585154	0.6
Sappemeer	20150122	20141.3	251244	575295	1.0
Sappemeer	20150123	20142.5	249198	577296	1.2
Wirdum	20150126	20146.2	249106	593340	1.1
Sappemeer	20150127	20147.0	248968	577643	0.5
Sappemeer	20150131	20150.8	248870	576954	0.8
Waddenzee	20150131	20151.1	258421	599264	1.6
Woltersum	20150202	20152.4	245438	587575	0.9
Wildervank	20150203	20153.2	253901	565350	1.6
Oosterwijtwerd	20150204	20154.3	251196	594383	1.1
Noordzee	20150205	20155.1	78339	545713	1.8
Westermeden	20150210	20159.7	244271	596513	0.9
Godlinze	20150211	20161.4	249542	599415	0.4
Kropswolde	20150212	20162.6	246258	573622	1.9
Steendam	20150213	20162.9	251190	589151	0.8
Steendam	20150222	20172.0	252897	587201	0.8
Sappemeer	20150222	20172.3	249738	578178	0.6
Meedhuizen	20150222	20172.4	258501	590417	1.4
Schildwolde	20150224	20173.6	250621	584187	0.8
Appingedam	20150225	20175.5	252873	593843	2.3
Overschild	20150301	20181.5	249876	588087	1.2
Houwerzijl	20150301	20181.5	218659	594435	1.4
Kommerzijl	20150301	20181.1	217838	589286	1.5
Onnen	20150314	20194.8	240525	576150	0.7
Overschild	20150316	20196.5	248528	588784	0.6
Lageland	20150324	20205.1	243841	583723	1.1
Appingedam	20150324	20204.8	252765	593674	2.3
Uithuizermeeden	20150325	20206.0	245092	605915	1.2
Emmen	20150405	20216.2	257302	531105	1.9
Borgsweer	20150406	20217.1	260834	590450	1.3
Harkstede	20150406	20217.0	240093	581690	0.7
Appingedam	20150415	20226.2	254799	592008	0.9

Table E.3 : Observed tremors in the Netherlands, continued.

Location	$t$	$t$	$X$	$Y$	$M_L$
	y/m/d	days	m	m	Richter
Hellum	20150415	20226.0	254084	583571	0.8
Slochteren	20150422	20233.3	249543	582404	0.8
Meedhuizen	20150503	20244.4	257314	588740	1.1
Froombosch	20150507	20247.9	248826	579217	1.1
Zeerijp	20150507	20248.9	245273	596327	1.0
Waterhuizen	20150508	20249.1	239186	576238	1.1
Tjuchem	20150513	20254.6	255902	587133	1.2
Appingedam	20150516	20257.1	252244	591974	1.6
Schildwolde	20150521	20262.6	249938	584971	1.8
Uithuizen	20150527	20268.0	240166	602616	2.0
Appingedam	20150602	20274.4	252116	592237	0.7
Zuidbroek	20150604	20276.2	253594	576098	1.0
Loppersum	20150606	20278.4	246471	595242	1.9
Garrelsweer	20150607	20279.0	246942	592905	0.5
Zeerijp	20150610	20281.5	246673	595687	1.8
Westeremden	20150610	20281.8	243985	595576	0.4
Westeremden	20150610	20282.0	243985	595799	0.8
Zandweer	20150610	20282.0	241566	598804	0.8
Anna Paulowna	20150623	20294.4	116846	541595	1.5
Anna Paulowna	20150623	20294.4	115905	541039	2.3
Harkstede	20150626	20298.3	244523	582554	0.0
Harkstede	20150629	20300.9	245329	582665	0.6
Ten Boer	20150630	20301.4	242104	588119	0.5
Harkstede	20150702	20304.5	244455	580662	0.5
Hoogezand/Sappemeer	20150704	20306.0	249966	574206	0.5
Zuidwolde (Gr.)	20150704	20306.3	237534	586449	0.6
Westeremden	20150704	20306.6	242708	596466	1.1
Zuidbroek	20150706	20308.0	251914	577768	0.5
Thesinge	20150707	20308.9	238475	586561	2.1
Appingedam	20150708	20309.9	252183	590790	0.4
Zuidbroek	20150710	20312.5	254266	576655	0.5
Garrelsweer	20150716	20317.9	250974	590234	0.8
Westeremden	20150716	20318.2	244119	595353	0.4
Siddeburen	20150718	20320.1	254199	587228	0.7
Froombosch	20150718	20320.8	247211	578881	0.5
Appingedam	20150719	20321.7	253258	593350	0.6
Thesinge	20150720	20322.7	240424	588675	0.4
Oosterwijtwerd	20150721	20322.9	250033	594352	1.3
Garmerwolde	20150721	20323.2	240155	584335	0.6
Noordzee	20150724	20325.9	95074	632416	2.5
Froombosch	20150730	20332.5	247950	577879	0.7
Thesinge	20150802	20334.3	238878	588230	0.6
Zeerijp	20150807	20339.8	247076	595131	0.8
Harkstede	20150811	20343.7	245060	580217	0.9
Oosterwijtwerd	20150812	20345.2	250638	594018	0.3
Oosterwijtwerd	20150813	20345.5	251041	594463	0.6
Zeerijp	20150817	20349.3	247211	596355	0.6
Kolham	20150818	20350.5	246740	577991	2.0
Harkstede	20150822	20354.3	246135	583110	1.4
Usquert	20150822	20354.7	236526	601364	1.6
Froombosch	20150823	20355.5	250302	576989	0.3
Wirdum (Gr.)	20150824	20357.1	248958	593461	0.5
Hellum	20150826	20359.0	252385	581663	0.4
Harkstede	20150827	20359.4	245867	583110	0.2
Meedhuizen	20150828	20360.4	259373	590122	0.8
Slochteren	20150828	20360.6	251578	580884	1.3
Warffum	20150828	20361.0	235316	601030	1.3
Kolham	20150905	20367.8	244926	576210	0.5
Harkstede	20150909	20372.5	243179	581775	1.2
Garsthuizen	20150910	20373.4	243985	598804	0.8
Hellum	20150930	20393.4	252116	583444	3.1

Copyright Shell Global Solutions International B.V., Rijswijk International, B.V., 2016.

Neither the whole nor any part of this document may be reproduced, stored in any retrieval system or transmitted in any form or by any means (electronic, mechanical, reprographic, recording or otherwise) without the prior written consent of the copyright owner.